

การศึกษาในรายละเอียดของการสังเคราะห์เส้นใยไทเทเนียม (IV) ออกไซด์ ขนาดนาโน
ด้วยเทคนิคโซลเจลผสมกับการปั่นเส้นใยด้วยไฟฟ้าสถิต



นายจตุรนต์ ศุภผล

สถาบันวิทยบริการ

วิทยานิพนธ์นี้เป็นส่วนหนึ่งของการศึกษาตามหลักสูตรปริญญาวิศวกรรมศาสตรมหาบัณฑิต

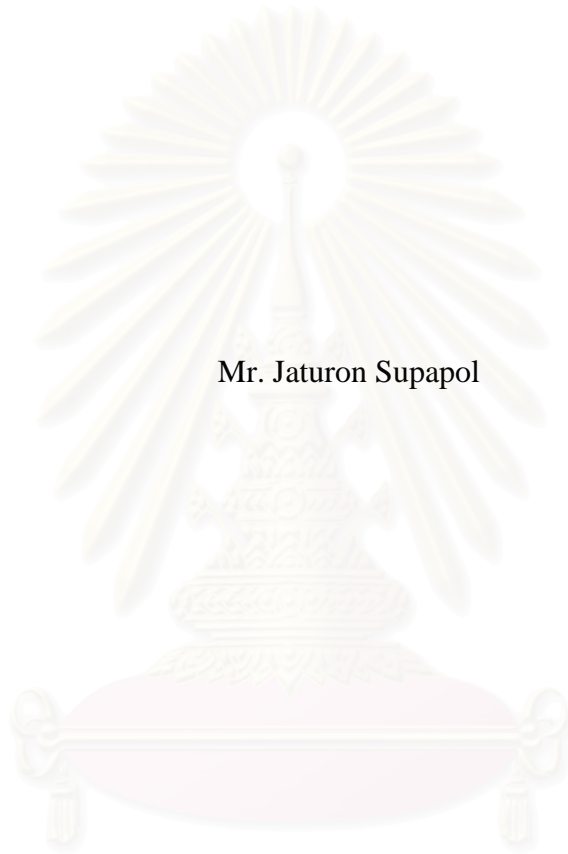
สาขาวิชาวิศวกรรมเคมี ภาควิชาวิศวกรรมเคมี

คณะวิศวกรรมศาสตร์ จุฬาลงกรณ์มหาวิทยาลัย

ปีการศึกษา 2550

ลิขสิทธิ์ของจุฬาลงกรณ์มหาวิทยาลัย

DETAILED INVESTIGATION ON TITANIUM (IV) OXIDE NANOFIBER
SYNTHESIZED BY COMBINED SOL-GEL AND ELECTROSPINNING
TECHNIQUES



Mr. Jaturon Supapol

สถาบันวิทยบริการ
จุฬาลงกรณ์มหาวิทยาลัย

A Thesis Submitted in Partial Fulfilment of the Requirements
for the Degree of Master of Engineering Program in Chemical Engineering

Department of Chemical Engineering

Faculty of Engineering

Chulalongkorn University

Academic Year 2007

Copyright of Chulalongkorn University

Thesis Title DETAILED INVESTIGATION ON TITANIUM (IV) OXIDE
 NANOFIBER SYNTHESIZED BY COMBINED SOL-GEL
 AND ELECTROSPINNING TECHNIQUES

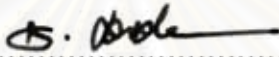
By Mr. Jaturon Supapol

Field of study Chemical Engineering


Thesis Advisor Assistant Professor Varong Pavarajarn, Ph.D

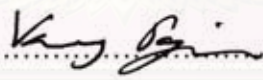
Thesis Co-advisor Associate Professor Pitt Supaphol, Ph.D

Accepted by the Faculty of Engineering, Chulalongkorn University in Partial
Fulfillment of the Requirements for the Master's Degree



.....Dean of the Faculty of Engineering
(Associate Professor Boonsom Lerthirunwong, Dr.Ing.)


THESIS COMMITTEE


.....Chairman
(Associate Professor Tawatchai Charinpanitkul, D.Eng.)


.....Thesis Advisor
(Assistant Professor Varong Pavarajarn, Ph.D.)


.....Thesis Co-advisor
(Associate Professor Pitt Supaphol, Ph.D.)


.....External Member
(Assistant Professor Okorn Mekasuwandumrong, Ph.D.)


.....Member
(Akawat Sirisuk, Ph.D.)

จาดุรงค์ ศุภผล : การศึกษาในรายละเอียดของการสังเคราะห์เส้นใยไททาเนียม (IV) ออกไซด์ขนาดนาโนด้วยเทคนิคโซลเจลผสมกับการปั่นเส้นใยด้วยไฟฟ้าสถิต (DETAILED INVESTIGATION ON TITANIUM (IV) OXIDE NANOFIBER SYNTHESIZED BY COMBINED SOL-GEL AND ELECTROSPINNING TECHNIQUES) อ.ที่ปรึกษา: ผศ.ดร. วรงค์ ปวราจารย์, อ.ที่ปรึกษาร่วม: รศ.ดร. พิชญ์ ศุภผล, 85 หน้า

เส้นใยขนาดนาโนของไททาเนียมสามารถเตรียมได้จากวิธีโซลเจลผนวกกับการปั่นเส้นใยด้วยไฟฟ้าสถิต โดยใช้สารละลายไททาเนียมเตตระไฮดรอกไซด์, พอลิไวนิลไพโรลิโดน และเอทานอล ในการปั่นเส้นใยคอมโพสิตระหว่างไททาเนียมและพอลิไวนิลไพโรลิโดนภายใต้ความต่างศักย์ 16 กิโลโวลต์ การเผาเส้นใยที่ 500 องศาเซลเซียส ทำให้เส้นใยไททาเนียมมีการเปลี่ยนแปลงโครงสร้างไปเป็นเฟสผสมที่ประกอบด้วยอนาเทสและรูไทล์ พร้อมกับการสลายตัวของพอลิเมอร์ออกจากเส้นใย การเปลี่ยนตัวรองรับในกระบวนการปั่นเส้นใยจากตัวรองรับในแบบราบเป็นตัวรองรับทรงกลมแบบหมุนได้ส่งผลให้เส้นใยเกิดการจัดเรียงตัวในทิศทางเดียวที่มีขนาดเส้นผ่านศูนย์กลางของเส้นใยก่อนเผา 220 นาโนเมตร และหลังเผา 120 นาโนเมตร ในงานวิจัยนี้ได้มีการศึกษาผลของสภาวะการบ่มเส้นใยไททาเนียมและการเติมกรดอะซิติกในสารละลายตั้งต้น ต่อลักษณะพื้นฐานและการเปลี่ยนแปลงเฟสของเส้นใยภายหลังการเผา ซึ่งผลจากการศึกษาพบว่า การบ่มเส้นใยไททาเนียมภายใต้ความชื้นสูงสามารถลดสัดส่วนรูไทล์ในเส้นใยหลังจากการเผาได้ หากแต่การบ่มเส้นใยภายใต้ความชื้นสูงนั้น ส่งผลให้เกิดการเปลี่ยนแปลงลักษณะพื้นฐานของเส้นใยไททาเนียม ความหนาของชั้นเส้นใยเป็นอีกตัวแปรหนึ่งที่ส่งผลต่อกระบวนการบ่มเส้นใย การเติมกรดลงในสารละลายสำหรับการปั่นเส้นใยนั้น สามารถลดอุณหภูมิการเกิดผลึก อนาเทสให้มีค่าต่ำลงได้ และพบว่าขนาดผลึกเฉลี่ยของเส้นใยไททาเนียมมีขนาดเล็กลงในสภาวะที่มีกรดอะซิติก รวมทั้งสามารถลดการกระจายตัวของเส้นใยที่เกิดขึ้น เมื่อเพิ่มปริมาณการเติมกรดอะซิติกมากขึ้น

ภาควิชา.....วิศวกรรมเคมี.....
สาขาวิชา.....วิศวกรรมเคมี.....
ปีการศึกษา..... 2550.....

ลายมือชื่อนิสิต.....จาดุรงค์ ศุภผล.....
ลายมือชื่ออาจารย์ที่ปรึกษา.....
ลายมือชื่ออาจารย์ที่ปรึกษาร่วม.....

4970253921: MAJOR CHEMICAL ENGINEERING

KEY WORD: TITANIA / ELECTROSPINNING / NANOFIBERS / AGING

JATURON SUPAPOL: DETAILED INVESTIGATION ON TITANIUM (IV) OXIDE NANOFIBER SYNTHESIZED BY COMBINED SOL-GEL AND ELECTROSPINNING TECHNIQUES. THESIS ADVISOR: ASSIST. PROF. VARONG PAVARAJARN, Ph.D, THESIS CO-ADVISOR: ASSOC. PROF. PITT SUPAPHOL, Ph.D, 85 pp.

Titania nanofibers were prepared from sol-gel method combining with the electrospinning technique. Titanium (IV) isopropoxide (TTIP), polyvinyl pyrrolidone (PVP) and ethanol were mixed together and electrospun into titania/PVP composite nanofibers under the potential of 16 kV. Calcination of the composite nanofibers at 500°C resulted in the removal of polymer from the fibers, as well as the phase transformation of titania from amorphous to mixed phase of anatase and rutile. Changing the electrospinning collector plate from a flat collector to a rotating collector led to the fabrication of the axially aligned titania nanofibers with average diameter of 220 nm for the as-spun fibers and 120 nm for the calcined fibers. Effects of aging conditions and acetic addition on morphology and phase transformation of titania nanofibers after calcination were also investigated. The aging of the as-spun titania nanofibers under high level of humidity results in the reduction of rutile in the fibers after calcination at 500°C. Nevertheless, the morphology of titania nanofibers is changed at high level of humidity. Thickness of fiber layer is also one of the parameters affecting the effectiveness of the aging process. The addition of acetic acid into the electrospinning solution enhanced the stability of the alkoxide solution. It was also found that the addition of acetic acid significantly lower the crystallization temperature of titania. The average crystallite size of the calcined fibers tends to decrease with the presence of acetic acid in the system. Moreover, the addition the acetic acid into the system causes the reduction in size distribution of the as-spun fibers.

Department Chemical Engineering

Field of study Chemical Engineering

Academic Year 2007

Student's signature *Jaturon Supapol*

Advisor's signature *Varong Pavrajarn*

Co-advisor's signature *Pitt Supaphol*

ACKNOWLEDGEMENTS

The author would like to express his greatest gratitude to his advisor, Assistant Professor Varong Pavarajarn, and his co-advisor, Associate Professor Pitt Supaphol for their help, invaluable suggestions and guidance throughout the entire of this work. Their precious teaching the way to be good in study and research have always been greatly appreciated. In addition, their friendliness motivated the author with strength and happiness to do this work.

The author wishes to express his thanks to Associate Professor Tawatchai Charinpanitkul, as the chairman of the committee, as well as Dr. Akawat Sirisuk and Assistant Professor Okorn Mekasuwandumrong, who have been his committee members. He also would like to give many thanks for kind suggestions and useful help to many friends in the Research Center on Catalysis and Catalytic Reaction Engineering who always provide the encouragement and co-operate along the thesis study. Moreover, he gratefully acknowledges Mektec Manufacturing Corporation (Thailand) for many supports such as SEM analysis.

Finally, the author would like to dedicate the achievement of this work to his dearest parents. Their unyielding support and unconditional love have always been in his mind.

สถาบันวิทยบริการ
จุฬาลงกรณ์มหาวิทยาลัย

CONTENTS

	Page
ABSTRACT (IN THAI)	iv
ABSTRACT (IN ENGLISH)	v
ACKNOWLEDGMENTS	vi
CONTENTS	vii
LIST OF TABLES	x
LIST OF FIGURES	xi
CHAPTER	
I INTRODUCTION	1
II THEORY AND LITERATURE SURVEY	5
2.1 Physical and Chemical Properties of Titanium (IV) Oxide.....	5
2.2 Sol-Gel Process.....	7
2.2.1 Titanium (IV) dioxide synthesis by sol-gel process....	11
2.2.2 Effects of sol-gel parameters on phase transformation of titania.....	13
2.2.3 Effects of acid addition on sol-gel reaction of titania.	13
2.3 Electrospinning Process.....	14
2.3.1 Background.....	14
2.3.2 Machanism of electrospinning process.....	17
2.3.3 Controlling the orientation of electrospun fibers.....	18
2.3.4 Effects of electrospinning parameters.....	19
III EXPERIMENTAL	21
3.1 Materials.....	21
3.2 Electrospinning Apparatus.....	22
3.3 Experimental Procedures.....	23
3.3.1 Preparation of spinning solution.....	23
3.3.2 Spinning of the TiO ₂ /PVP composite fibers.....	23
3.3.3 Aging of the as-spun fibers.....	24
3.3.4 Calcination of the TiO ₂ /PVP composite fibers.....	24

CHAPTER	Page
3.4 Sample Characterizations.....	25
3.4.1 Scanning electron microscopy (SEM).....	25
3.4.2 Transmission electron microscope (TEM).....	25
3.4.3 Viscometer.....	25
3.4.4 X-ray diffraction (XRD).....	25
3.4.5 Fourier transform infrared spectroscopy (FTIR).....	26
3.4.6 Thermogravimetric and differential thermal analysis (TG-DTA).....	26
IV RESULTS AND DISCUSSION.....	27
4.1 Fabrication of Axially Aligned Titania Nanofibers.....	27
4.1.1 Preliminary experiments.....	27
4.1.2 Properties of the synthesized titania nanofibers.....	29
4.1.3 Fabrication of axially aligned titania nanofibers.....	35
4.2 Effects of Aging Conditions on Properties of Titania Nanofibers.....	37
4.2.1 Effects of aging time on properties of aged fibers.....	37
4.2.2 Effects of humidity on aging.....	39
4.2.3 Effects of thickness of fiber layer on properties of aged fibers.....	47
4.3 Effects of Acetic Acid Addition on Properties of Titania Nanofibers.....	49
4.3.1 Effects of acetic acid on gelation time.....	49
4.3.2 Effects of acetic acid on morphology of titania nanofibers.....	51
4.3.3 Effects of amount of acetic acid on phase structure of titania nanofibers.....	54
4.3.4 Effects of acetic acid on crystallite size of titania nanofibers.....	59
4.3.5 Effects of calcination temperature on crystallite size of titania nanofibers.....	61

	Page
CHAPTER	
V CONCLUSIONS AND RECOMMENDATIONS.....	63
5.1 Conclusions.....	63
5.2 Recommendations for Future Work.....	64
REFERENCES.....	65
APPENDICES.....	74
APPENDIX A: CALCULATION OF THE CRYSTALLITE SIZE..	75
APPENDIX B: TGA ANALYSIS OF PVP.....	78
APPENDIX C: SEM IMAGES OF PVP NANOFIBERS AGING	
UNDER 100% RH.....	79
APPENDIX D: LIST OF PUBLICATION.....	80
VITA.....	85



สถาบันวิทยบริการ
จุฬาลงกรณ์มหาวิทยาลัย

LIST OF TABLES

TABLE		Page
2.1	Crystallographic properties of anatase, brookite, and rutile.....	7
4.1	Phase properties of titania nanofibers calcined at 500°C.....	31
4.2	Viscosity of the spinning solution.....	52
4.3	Phase structure and rutile fraction of titania nanofibers after calcination at 500°C.....	55
4.4	Crystallite size of titania nanofibers after calcination at 500°C for 3 hours prepared with various amount of acetic acid added into the spinning solution.....	61
4.5	Crystallite size of titania nanofibers prepared with no acetic addition and calcined at various temperatures.....	62
4.6	Crystallite size of titania nanofibers prepared with 4 ml of acetic acid and calcined at various temperatures.....	62



 สถาบันวิทยบริการ
 จุฬาลงกรณ์มหาวิทยาลัย

LIST OF FIGURES

FIGURE		Page
2.1	A diagram of anatase crystal structure.....	6
2.2	A diagram of rutile crystal structure.....	6
2.3	Schematic illustration of basic setup for electrospinning.....	18
3.1	Schematic of an electrospinning setup.....	22
4.1	SEM micrographs of titania nanofibers before and after calcination at 500°C for 3 hours in air.....	28
4.2	Frequency distribution for diameter of titania nanofibers spun on flat collector, before and after calcination at 500°C	29
4.3	X-ray diffraction pattern of the electrospun titania nanofibers after calcined at 500°C for 3 hours in air.....	30
4.4	TEM results of the titania nanofibers calcined at 500°C.....	32
4.5	Thermogravimetric curves of the as-spun TiO ₂ /PVP composite fibers analyzed in oxygen atmosphere.....	33
4.6	FT-IR spectra of the synthesized titania nanofibers before and after calcination at 500°C.....	35
4.7	SEM micrographs of calcined electrospun titania nanofibers fabricated on various types of collector.....	36
4.8	Frequency distribution for diameter of electrospun titania nanofibers fabricated on various types of collectors.....	36
4.9	Plot of aging time versus fraction of rutile in the titania nanofibers calcined at 500°C at 0.1 mm fiber thickness aging under ambient condition.....	38
4.10	Plot of extended aging time versus fraction of rutile in the synthesized titania nanofibers calcined at 500°C at 0.1 mm fiber thickness aging under ambient condition.....	38

FIGURE	Page
4.11 SEM micrographs of nanofibers aged for 7 days under various humidity levels and subsequently calcined at 500°C.....	40
4.12 Plot of aging time versus fraction of rutile in the synthesized titania nanofibers calcined at 500°C at 0.1 mm fiber thickness aging under various humidity levels.....	41
4.13 Plot of extended aging time versus fraction of rutile in the synthesized titania nanofibers calcined at 500°C at 0.1 mm fiber thickness aging under various humidity levels.....	42
4.14 Plot of aging time versus fraction of rutile in the synthesized titania nanofibers calcined at 500°C at 0.05 mm fiber thickness aging under various humidity levels.....	43
4.15 FT-IR spectra of as-spun titania fibers aged under different humidity levels.....	44
4.16 TGA curves of as-spun titania fibers aged under various humidity levels for 7 days.....	46
4.17 DTA curves of as-spun titania fibers aged under various humidity levels for 7 days.....	47
4.18 Plot of aging time versus fraction of rutile in the titania nanofibers aged under 100% RH.....	48
4.19 Plot between solution aging time and viscosity of the spinning solution prepared with and without acetic acid addition.....	50
4.20 SEM micrographs of as-spun TiO ₂ /PVP composite nanofibers fabricated from the spinning solution prepared with and without acetic acid addition.....	51
4.21 Frequency distribution for diameter of as-spun TiO ₂ nanofibers fabricated from the spinning solution prepared with and without acetic acid addition.....	52
4.22 SEM micrographs of calcined titania nanofibers fabricated from the spinning solution prepared with and without acetic acid addition.....	53

FIGURE	Page	
4.23	Frequency distribution for diameter of calcined titania nanofibers fabricated from the spinning solution prepared with and without acetic acid addition.....	53
4.24	X-ray diffraction patterns of titania nanofibers prepared with different amount of acetic acid added into the spinning solution and subsequently calcined at 500°C.....	54
4.25	X-ray diffraction patterns of titania nanofibers prepared with different amount of acetic acid added into the spinning solution and subsequently calcined at 250°C.....	56
4.26	X-ray diffraction patterns of titania nanofibers prepared with different amount of acetic acid added into the spinning solution and subsequently calcined at 400°C.....	57
4.27	X-ray diffraction patterns of titania nanofibers prepared with different amount of acetic acid added into the spinning solution and subsequently calcined at 750°C.....	58
4.28	FT-IR spectra of the as-spun titania nanofibers prepared with and without acetic acid addition.....	59
4.29	TEM micrographs of titania nanofibers prepared with different amount of acetic acid added into the spinning solution.....	60
A1	The 101 diffraction peak of titania for calculation of the crystallite size.....	76
A2	The plot indicating the value of line broadening due to the equipment.....	77
B1	TGA analysis of PVP under O ₂ atmosphere.....	78
B2	FT-IR spectra of PVP nanofibers.....	78
C1	SEM image of pure PVP nanofibers aging under 100% RH for 24 hours (1,000x magnification).....	79
C2	SEM image of pure PVP nanofibers aging under 100% RH for 24 hours (5,000x magnification).....	79

CHAPTER I

INTRODUCTION

Titanium (IV) oxide or titania (TiO_2) is one of the most common materials suitable for many applications. It has been known as an excellent catalyst in the field of photocatalysis. Titania is a wide bandgap semiconductor with many interesting properties, such as transparency to visible light, high refractive index and low absorption coefficient. Other than these properties, its eminent capability of photocatalytic decomposition of organic materials has come to utilization in the environmental applications, i.e. organic pollutant treatment (Kwon et al. 2004).

Generally, titania is a very important commercial material as a white pigment because of its maximum light scattering with virtually no absorption. It is also nontoxic, chemically inert, and considered as dielectric ceramic material due to its high dielectric constant. Although it is used primarily in the pigment industry for painting, varnish, paper, cosmetic, and plastic, titania is also used in catalyst, ceramic, coated fabric, and roofing granule. Since titania is also one of the most common photocatalyst, good thermal properties are often required for the use at high temperature, as well as large surface area to increase catalytic performance. The two most common and important phases of titania are anatase and rutile. Most commercially available titania powders are either one of those two phases or a mixture of the two.

Titania can be synthesized by various techniques, such as precipitation (Kim et al. 1999), chemical vapor deposition (Ding et al. 2000), hydrothermal method (Yang et al. 2001), and glycothermal method (Iwamoto et al. 2000). Another common technique that can result in titania with extremely high surface area is sol-gel method (Dagan and Tomkiewicz 1994; Jung and Park 2000; Cheng et al. 2003). The method basically consists of many steps, i.e. hydrolysis of alkoxide to form sol, gelation, gel-aging, drying and thermal stabilization. Each step can be manipulated to obtain product with specific characteristic, such as narrow pore size distribution and narrow particle size distribution (Montoya et al. 1992). However, titania obtained usually

contains certain amount of amorphous phase, of which the surface area decreases drastically during calcination (Fujishima et al. 1999; Payakgul 2002).

Anatase is an unstable polymorph of titania. Phase transformation from anatase to rutile, the less chemically active polymorph, generally takes place above 600°C (Banfield et al. 2000). However, the transformation temperature strongly depends upon how titania is synthesized (Jung and Park. 1999). Anatase titania which transforms to rutile at high temperature is considered having good thermal stability. In catalytic applications, large surface area and reasonably good thermal stability are often desired.

Although nanocrystalline titania particles have shown many beneficial features, handling of such small particles is difficult in some cases. In this case, nanofibers consisting of nanocrystalline titania can be advantageous. Nanofiber is an exciting new class of material used for several value-added applications such as medical, filtration, barrier, wipes, personal care, composite, garments, insulation, and energy storage. Special properties of nanofibers make them suitable for a wide range of applications from medical to consumer products and industrial to high-tech applications for aerospace, capacitors, transistors, drug delivery systems, battery separators, energy storage, fuel cells, and information technology. Hence, titania as nanofibers would exhibit many special properties mainly due to extremely high surface to weight ratio compared to conventional nonwovens fibers. Moreover, titania nanofibers would also have low density, large surface area, high pore volume, and uniform pore size. These special properties make the titania nanofibers appropriate for a wide range of applications, especially as photocatalyst or catalyst support.

Electrospinning technique is a relatively simple and versatile method for fabricating nanofibers. In a typical electrospinning process, a droplet of polymer solution held by its surface tension at the end of a capillary tube is subjected to an electric field. Charge is induced on the liquid surface by electric field. As the intensity of the electric field is increased, the hemispherical surface of the solution at the tip of the capillary tube elongates to form a conical shape known as the Taylor cone. When the electric field reaches a critical value at which the repulsive electric force overcomes the surface tension force, a charged jet of the solution is ejected from the

tip of the Taylor cone. Since this jet is charged, its trajectory can be controlled by the electric field. As the jet travels in air, the solvent evaporates, leaving a charged polymer fiber behind which lays itself randomly on a collecting metal screen. Thus, continuous fibers are laid to form a non-woven fabric (Srinivasan and Reneker 1995). In the continuous-feeding mode, the number of fibers can be formed within short period of time, as short as a few seconds. Those fibers are often collected on the surface of a conductor to form non-woven mats that have high surface areas and relatively small pore sizes.

For the past several decades, more than 20 different types of organic polymers have been successfully processed as ultrathin fibers using the electrospinning technique, with typical examples including various engineering plastics, biopolymer, and electronically conductive polymer (Srinivasan and Reneker 1995; Li and Xia 2004). At present, many oxide nanofibers have been fabricated, including titania nanofibers. Amorphous titania nanofibers have also been preliminarily produced by electrospinning technique from titanium(IV) isopropoxide (TTIP) mixed with acetic acid and high molecular weight polyvinylpyrrolidone using ethanol as solvent (Watthanaarun et al. 2005). The phase content analyzed from the product after calcination process tends to be affected by many factors. Since the optical and electrical properties of anatase and rutile are different, it is desirable to be able to control the phase content. While previous studies have shown that method of preparation (Chang et al. 2000), dopant concentration (He et al. 2002; Watthanaarun et al. 2005), atmosphere (Gamboa et al. 1992), pH (Cannon et al. 2005), and particle size (Gribb et al. 1997) can influence the anatase-rutile phase transformation, results have often been contradictory and the relative importance of these variables is not known. Although many research groups have explored the characteristics of titania nanofibers prepared by controlling the electrospinning parameters, none has examined the influence of acetic acid addition and aging condition on the phase transformation of titania nanofibers and their characteristics.

In this study, effects of many parameters in sol-gel and electrospinning process to fabricate titania nanofibers were investigated in detail to understand the correlation between electrospinning parameters and properties of the synthesized titania fibers, including morphology and phase stability of titania nanofibers.

Objectives of the research:

1. To synthesized titania nanofibers with axially array and characterized properties of synthesized fibers.

2. To study the effects of humidity, aging time and thickness of fiber layer on morphological appearance, crystal structure and phase transformation as well as physical and chemical properties of titania nanofibers synthesized by sol-gel and electrospinning method.

3. To study the effects of acetic acid addition on the morphology and crystallization temperature of titania nanofibers including crystallite size of titania particle.

The present study is arranged as follows:

Chapter I presents the introduction of this work.

Chapter II explains basic theory about titania such as general properties of titania, sol-gel process and electrospinning process. Furthermore, literature survey of the previous works related to this research is also presented in this chapter.

Chapter III shows materials, the experimental equipments, the preparation procedure of titania nanofibers by the electrospinning process and characterization equipments.

Chapter IV describes the results and discussion of the research.

In the last chapter, the overall conclusions of this research and recommendations for the future studies are shown.

CHAPTER II

THEORY AND LITERATURE SURVEY

Titanium (IV) oxide (TiO_2) is a ceramic material, commonly known as titania. Titania has been used in many fields of application such as catalyst, catalyst support, electronics, cosmetic pigment and filter coating (Fox and Dulay 1993). In recent years, main attention has been devoted to its photocatalytic activity and photoinduced superhydrophilicity. Titania is the most important form of titanium compound commercially available. Physical and chemical properties of titania as well as its various preparation procedures have been long studied.

2.1 Physical and Chemical Properties of Titanium (IV) Oxide

Titanium (IV) oxide is thermally stable (melting point of 1855°C) and has high resistance to chemical attack. When it is severely heated under vacuum, there is a chance of slight loss in oxygen atom that results in a change in composition to $\text{TiO}_{1.97}$. The product is dark blue but can be reverted to the original white color when it is heated in air (Fujishima et al. 1999)

Titania exists in three polymorphs: brookite, anatase, and rutile. All polymorphs possess the same chemical formula, TiO_2 , but each has a different crystal structure. In comparison to other crystalline phases of TiO_2 , the most photoactive phase of TiO_2 is anatase (Watson et al. 2004). The photogenerated holes and electrons from anatase TiO_2 are highly reactive.

Brookite has an orthorhombic crystal structure and spontaneously transforms to rutile around 650°C (Zhu et al. 2005). Its mechanical properties are very similar to those of rutile, but it is the least common of the three phases and it is rarely used commercially.

The predominant commercial phase of titania is anatase, although it is rarely found in ore form. It is metastable with respect to rutile under all conditions and reverts spontaneously to rutile at temperatures above 600°C (Banfield et al. 2000; Musić et al. 1997). Anatase has a tetragonal crystal structure, in which the Ti-O octahedra share four corners, as shown in Figure 2.1

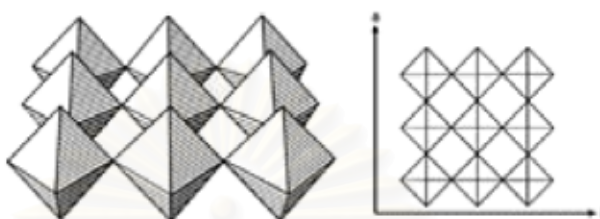


Figure 2.1 A diagram of anatase crystal structure

The stable form of titania is rutile, to which the other forms of titania transform at sufficiently high temperature. Rutile has a crystal structure similar to that of anatase, with an exception that the octahedra share four edges instead of four corners. This leads to the formation of chains, which are subsequently arranged in a four-fold symmetry, as shown in Figure 2.2



Figure 2.2 A diagram of rutile crystal structure

A comparison of Figure 2.1 and Figure 2.2 shows that the rutile structure is more densely packed than anatase as the data shown in Table 2.1

จุฬาลงกรณ์มหาวิทยาลัย

Table 2.1 Crystallographic properties of anatase, brookite, and rutile (Othmer 1999).

Properties	Anatase	Brookite	Rutile
Crystal Structure	Tetragonal	Orthorhombic	Tetragonal
Optical	Uniaxial, negative	Biaxial, positive	Uniaxial, negative
Density, g/cm ³	3.9	4.0	4.23
Hardness, Mohs scale	$5\frac{1}{2}$ - 6	$5\frac{1}{2}$ - 6	7 - $7\frac{1}{2}$
Unit cell	D _{4h} ¹⁹ .4TiO ₂	D _{2h} ¹⁵ .8TiO ₂	D _{4h} ¹² .3TiO ₂
Dimension, nm			
<i>a</i>	0.3758	0.9166	0.4584
<i>b</i>		0.5436	
<i>c</i>	0.9514	0.5135	2.953

Generally, if nanometer-sized TiO₂ is heated, crystal growth leads to an alteration of phase stabilities and, ultimately, to a conversion of both anatase and brookite to rutile. However, it has been proposed that the anatase-to-rutile transformation may depend not only on grain size, but also on other parameters such as impurity content, reaction atmosphere, and synthesis conditions.

Phase transformation from anatase to rutile is accompanied by the evolution of ca. 12.6 kJ/mol (3.01 kcal/mol). Nevertheless, the rate of transformation is greatly affected by temperature and the presence of other substances which may either catalyze or inhibit the transformation. The anatase-to-rutile transformation is not reversible since Gibb's free energy for the change is always negative (Othmer 1999).

2.2 Sol-Gel Process

The sol-gel process involves the formation of sol followed by gelation. Sol, which is suspension of solid particles with size ranging from 1 nm to 1 micron in liquid, can be obtained by hydrolysis and partial condensation of a precursor such as inorganic salt or metal alkoxide. Further condensation of sol particles into a three-dimensional network produces gel, which is a diphasic material with solids encapsulating solvent. Alternatively, gel can be produced by destabilizing the solution

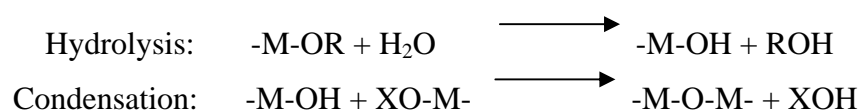
of preformed sols. In either case, the materials are referred as aquasol (or aquagel) if water is used as a solvent, and alcosol (or alcogel) if alcohol is used. The encapsulated liquid can be removed from gel by either evaporative drying or drying with supercritical extraction (supercritical drying in short).

The single most important characteristic of the sol-gel preparation of catalytic materials is its ease of control that translates into the following advantages:

- (i) ability to maintain high purity (because of purity of starting materials);
- (ii) ability to change physical characteristics such as pore size distribution and pore volume;
- (iii) ability to vary compositional homogeneity at molecular level;
- (iv) ability to prepare samples at low temperature;
- (v) ability to introduce several components in a single step;
- (vi) ability to produce samples in different physical forms.

The four key steps to convert a precursor to a particular product via sol-gel preparation are; formation of gel, aging of gel, removal of solvent, and heat treatment. The versatility of this preparative approach lies in the number of parameters that can be manipulated in each of these steps.

The precursor in sol-gel preparation can either be metal salt/alkoxide dissolved in appropriate solvent or stable colloidal suspension of preformed sols. Metal alkoxides have been most extensively used because they are commercially available in high purity and their solution chemistry has been well documented. At its simplest level, sol-gel chemistry with metal alkoxides can be described in terms of two classes of reaction:



where X can be either H or R (an alkyl group).

Such description oversimplifies the overall process because it does not correctly represent the molecular formula of intermediates as well as end products, nor does it depict the simultaneous occurrence of the two reactions. However, this oversimplification captures the key phenomenological idea that a three-dimensional gel network comes from the condensation of partially hydrolyzed species. Any parameters affecting either or both of these reactions are thus likely to have impact on properties of the product. In fact, the important variables are the reactive rates of hydrolysis and condensation.

Because hydrolysis and condensation are both nucleophilic displacement reactions, the reactivity of metal alkoxides depends on the positive charge of partially charged the metal atom and its coordination number. For example, TEOS, which has slight positive charge on silicon, is the least reactive species among the common alkoxides. In general, the longer and bulkier the alkoxide group attached to a particular metal atom, the less reactive that precursor is in hydrolysis and condensation. Changing the type of precursor and/or its concentration are thus effective means to control the reaction rates.

The amount of water used in sol-gel preparation and the rate by which it is added into the system also influence gel characteristics. The former is usually expressed in terms of the hydrolysis ratio h , defined as the moles of water per mole of metal alkoxide, $M(OR)_m$. There are three specific regions of interest:

- (i) $h < 1$: An infinite network seldom forms due to low functionality of the precursor towards condensation. Because there are few M-OH groups for cross-linking, gelation or precipitation can not occur when there is no local excess of water.
- (ii) $1 < h < m$: Polymeric gels can form.
- (iii) $h < m$: Cross-linked polymers, particulate gels, or precipitates can form when an excess of water is added to the alkoxides.

For given amount of water, another level of control comes from the rate of addition. Common approaches to slowly add water into the system are: using a

micropipette, absorbing moisture from a controlled humidity environment, and generating water in the solution from another chemical reaction.

Two other important sol-gel parameters are temperature and solvent. Both hot and cold plates, which can be used to increase and decrease the reaction rate, are commercially available. Varying the temperature is most effective when it can alter the relative rate of competing reactions. Solvent can change the nature of an alkoxide precursor through solvent exchange or affect the condensation reaction directly. It is also possible to prepare gel without solvent as long as another mean, such as ultrasound irradiation, is used to homogenize an otherwise immiscible alkoxide/water mixture.

Using preformed sols instead of metal alkoxides as precursors is an attractive alternative in sol-gel preparation because recent advances in inorganic colloidal dispersions allow some control over the characteristic of the starting sols. Colloidal suspension of sol particles is often stabilized (i.e. prevented from flocculation) by pH adjustment. Thus, pH of the solution, which can be changed by the addition of either acid or base, is the single most important parameter in obtaining gel from preformed sols. Other parameters that influence gel quality are size and concentration of the starting sol particles.

For any of the sol-gel parameters discussed so far, its effect on gel properties can often be observed by an experimental parameter known as gel time. Gel time is defined as the time that the solution undergoes rapid rise in viscosity which is corresponding to the transition from viscous fluid to elastic gel. At the gel point, the solid phase forms a continuous structure that reflects the formation and branching of particles under specific growth condition. This particular phase is important because it is the genesis of structural evolution that takes place in all subsequent processing steps (Ertl et al. 1999).

2.2.1 Titanium (IV) dioxide synthesis by sol-gel process

For titania synthesis via sol-gel technique, the process starts with the mixing of titanium alkoxide with alcohol. Acid aqueous solution is subsequently added to the mixture (Jung et al. 1999). This technique can be adapted by using ultrasonication to aid dispersion, which can result in titania with higher surface area and better thermal stability than titania prepared by using conventional stirring (Awati et al. 2003). The average crystal size of titania synthesized by this method has been reported to be in the range of 4 – 8 nm with BET surface area in the range of 91-120 m²/g, depending on calcination temperature. However, the limit of this method is that strong reactivity of alkoxide toward water often results in uncontrolled precipitation.

The effects of sol-gel solution parameters were reported by Montoya et al. (1992). They studied the effects of the sol-gel synthesis parameters on textural and structural characteristics of TiO₂. It was found that parameters such as type of solvent, synthesis temperature, acid addition and alcohol/alkoxide as well as water/alkoxide molar ratios influenced the texture, structure and morphology of the samples. Microcrystalline anatase was obtained after drying at 80°C in most of the samples. When TiO₂ was calcined at 500°C, its surface area significantly decreased. The calcination of microcrystalline anatase at 500°C also brought about the coalescence of the fine material, producing larger size particles. They found that amorphous titania had crystallized to anatase after calcination at 400°C.

Adding carboxylic acids can control hydrolysis reaction in sol-gel process. In 1987, Sivananda added acetic acid to the acidic alcoholic tetraethyl orthosilicate (TEOS) solution and reported that TEOS hydrolysis could be controlled and prolonged for hours by controlling the frequency and amount of acid addition. In this way, nuclear magnetic resonance (NMR) has been successfully used to monitor the structural changes associated with hydrolysis and ester formation. Nucleophilic substitution mechanisms were proposed for TEOS hydrolytic behavior under esterification conditions (Sivananda 1987).

Moriguchi et al. (1997) reported the preparation of TiO₂ thin film by a newly developed two-dimensional (2D) sol-gel process. When a chloroform solution of

monomer or tetramer of tetrabutoxytitanium (TBT) was spread on the surface of an aqueous subphase, the TBT was hydrolyzed and polycondensed at the air/water interface to give floating gels. These gels were gathered by 2D compression to yield a uniform gel film on the water surface. The addition of chelating agents such as acetic acid and acetylacetone to the aqueous subphase or spreading solution was effective in suppressing the 2D hydrolysis/polycondensation reactions and in increasing the stability of the floating gel film. Up to 20 layers of the floating gel film prepared on aqueous acetic acid could be quantitatively transferred onto a suitable substrate using Langmuir-Blodgett techniques. The addition of n-octadecyl acetoacetate in the spreading solution of monomeric Ti butoxide and ethoxide resulted in quantitative transference of the gel films onto substrates without a limitation on the number of depositions. The deposited TiO₂-based gel films could be converted into nanometered-thick TiO₂ films by calcination at 773 K for 30 min. In conclusion, oxide films prepared from gel films of less than a few tens of layers were composed of quantum-size TiO₂ particulates. The thickness and the density of the nanoparticulated TiO₂ films could be controlled by the number of layer of deposited gel film layers and the surface pressure of the gel film layer during deposition.

Sol-gel method can be modified in separate way. In 2003, Balasubramanian and coworkers prepared thick film of TiO₂ on glass and stainless steel substrates using an alkoxide sol-gel process modified by addition of Degussa P-25 powder. The prepared films were characterized by SEM, EDS, XRD and other methods. The TiO₂ films obtained from the powder modified sol were compared to films obtained from the alkoxide sol-gel process without modification. The films obtained from the modified sol-gel were about ten times thicker for a single dip coating/heat treatment cycle than the films obtained from the sol without powder addition. The prepared thick films were smooth and free of macrocracking, fracture or flaking. The grain size of these films was uniform and in the range 100–150 nm and the films were a mixture of anatase and rutile TiO₂. The films obtained from the powder modified sol on the stainless steel substrate were also much harder compared to the films obtained from sols without modification and displayed excellent adhesion to the substrate (Balasubramanian et al. 2003).

2.2.2 Effects of sol-gel parameters on phase transformation of titania

Many sol-gel parameters have much effected on the properties of synthesized titania. In 1995, Ding and coworkers synthesized titania powders from titanium tetrabutoxide (TTB) by controlling water concentration during hydrolysis. They reported that the grain size of powders prepared at low H₂O/TTB molar ratios was smaller than that of powders synthesized at high molar ratios. As a result, the anatase-to-rutile phase transformation temperature of powders synthesized at low H₂O/TTB molar ratios was lower than that of powders with high H₂O/TTB ratios (Ding et al. 1995). Sasamoto and his coworkers (1993) also prepared titania powders from TTIP by controlling the initial water concentration. However, they found that the water concentration had no effect on the anatase-to-rutile transformation temperature. In contrast, Kato (1995) reported that anatase-to-rutile transformation rate and specific surface area of titania powders increased with increasing H₂O/TTIP molar ratio.

2.2.3 Effects of acid addition on sol-gel reaction of titania

The role of acid added in sol-gel process was described many years ago. It is know that, in order to avoid the use of the harsh conditions and high temperatures required by the calcination process, a hypothetical mechanistic model was envisioned. In this hypothetical model, the hydrated titanium oxide molecules undergo a condensation polymerization (via loss of water) to form Ti-O-Ti linkages. In sol-gel reaction, many such polymerization sites occur simultaneously. These “nucleated” sites undergo multidirectional growth as the polymerization continues. In the hypothetical model, solution bound TiO₂ monomers exclusively add to the growing particle’s surface and no interparticle interactions occur because the Brownian motion of the developing particles does not allow for interparticle reactivity. Only when extremely high temperatures are applied can the activation energy required to overcome the Brownian motion be surpassed. In this hypothetical model, it is imagined that an auxiliary reagent might be added to the growing particles that could facilitate interparticle reactions. This auxiliary reagent would have to compete effectively with substrate sites on the TiO₂ to form irreversible linkages. If the auxiliary reagent can form two or more such linkages, it would function to hold “two or more” of the particles together and allow for the particles to coalesce. Carboxylic

acids are well known to form strong covalent linkages with TiO₂. It has been shown that the addition of small aromatic acids will alter the viscosity of the TiO₂ suspension drastically (Cannon et al. 2005). Therefore, acetic acid was chosen to test this hypothesis in this study.

2.3 Electrospinning Process

2.3.1 Background

Electrospinning is a straightforward method to produce polymer nanofibers. When the electrical force at the surface of a polymer solution or polymer melt overcomes the surface tension, a charged jet is ejected. The jet extends in a straight line for a certain distance, and then bends and follows a looping and spiraling path. The electrical forces elongate the jet thousands or even millions of times and the jet becomes very thin. Ultimately the solvent evaporates, or the melt solidifies, resulting in very long fibers, often in the form of a non-woven fabric.

The electrospinning process produces fibers with diameter in the range of one or two orders of magnitude smaller than those of conventional textile fibers. The small diameter provides large surface area-to-mass ratio, in the range from 10 m²/g (when the diameter is around 500 nm) to 1000 m²/g (when the fiber diameter is around 50 nm). The equipment required for electrospinning is simple and only a small amount of polymer sample is needed to produce nanofibers.

Polymer nanofibers are being used or finding uses in filtration, protective clothing, and biomedical applications including wound dressings and drug delivery systems. Other possible uses include solar sails, light sails, and mirrors for using in space. Nanofibers offer advantages for the application of pesticides to plants, as structural elements in artificial organs, as supports for enzymes or catalysts that can promote chemical reactions, and in reinforced composites. Ceramic or carbon nanofibers made from polymeric precursors extend nanofiber applications to uses involving high temperature and high modulus. The electrospinning process can incorporate particles such as pigments or carbon black particles into nanofibers. Flexible fibers are needed on a scale commensurate with micro or nano-electrical

mechanical and optical systems. The use of electrical forces may lead to new ways to fabricate micro or nano scale devices.

The literatures related to electrostatic spray contain many helpful insights into the electrospinning process. Lord Rayleigh (1882) studied the instabilities that occur in electrically charged liquid droplets. He showed, over 100 years ago, that when the electrostatic force overcame the surface tension, a liquid jet was created. Zeleny (1935) considered the role of surface instability in electrical discharges from droplets. He published a series of papers around 1910 on discharges from charged droplets falling in electric fields, and showed that, when the discharge began, the theoretical relations for surface instability were satisfied. In 1952, Vonnegut and Neubauer (1952) produced uniform stream of highly charged droplets with diameter of around 0.1 mm, by applying potential of 5 to 10 kilovolts to liquid flowing from capillary tubes. Their experiment proved that monodispersed aerosols with a particle radius of a micron or less could be formed from the pendent droplet at the end of the pipette. The diameter of the droplet was sensitive to the applied potential. Wachtel and coworkers (1962) prepared emulsion particles using an electrostatic method to make monodispersed emulsion of oil in water. The diameter of the emulsion particles was in the range from 0.5 to 1.6 microns. In the 1960's, Taylor studied the disintegration of water droplets in an electrical field. His theoretical papers demonstrated that a conical interface, with a semi-angle close to 49.3° , was the limiting stable shape (Taylor 1964; Taylor 1969).

Electrospinning of solutions of macromolecules can be traced back to 1934, when Formhals invented a process for making polymer fibers by using electrostatic force. Fibers were formed from a solution of cellulose acetate. The potential difference required for electrospinning depended on properties of the spinning solution such as molecular weight and viscosity. Formhals obtained a series of patents on his electrospinning inventions (Formhals 1934; Formhals 1937; Formhals 1939a; Formhals 1939b; Formhals 1940a; Formhals 1940b; Formhals 1944).

Gladding (1939) and Simons (1966) improved the electrospinning apparatus and produced more stable fibers. They used movable devices such as a continuous belt for collecting the fibers. Later, Bornat (1987) patented another electrospinning

apparatus that produced a removable sheath on a rotating mandrel. The basic principles were similar to previous patents. He determined that the tubular product obtained by electrospinning polyurethane materials in this way could be used for synthetic blood vessels and urinary ducts.

In 1971, electrospinning of acrylic fibers was described by Baumgarten (1971). Acrylic polymers were electrospun from dimethylformamide solution into fibers with diameters less than 1 micron. A stainless steel capillary tube was used to suspend droplet of polymer solution and the electrospun fibers were collected on a grounded metal screen. Baumgarten observed relationships between fiber diameter, jet length, solution viscosity, feed rate of the solution and the composition of the surrounding gas.

In 1981, Manley and Larrondo (1981a; 1981b; 1981c) reported that continuous fibers of polyethylene and polypropylene could be electrospun from the melt, without mechanical forces. A drop of molten polymer was formed at the end of a capillary. A molten polymer jet was formed when high electric field was established at the surface of the polymer. The jet became thinner and then solidified into a continuous fiber. The polymer molecules in the fiber were oriented by an amount similar to that found in conventional as-spun textile fibers before being drawn. The fiber diameter depended on the electric field, the operating temperature and the viscosity of the sample. The electrospun fibers were characterized by X-ray diffraction and mechanical testing. As either the applied electric field or the take-up velocity was increased, the diffraction rings became arcs, showing that the molecules were elongated along the fiber axis.

Many researchers have made further contributions to understanding the electrospinning process and characterizing the electrospun nanofibers in recent years. Doshi and Reneker (1995) prepared electrospun nanofibers from water soluble poly(ethylene oxide), with diameters of 0.05 to 5 microns. They described the electrospinning process, the processing conditions, fiber morphology and some possible uses of electrospun fibers. Srinivasan and Reneker (1995) electrospun liquid crystal polyaramid and poly (aniline), each from solution in sulfuric acid. They monitored electron diffraction patterns of the polyaramid nanofibers, both as-spun and

after annealing at 400°C. Reneker and Chun (1996) used transmission electron microscopy, scanning electron microscopy and atomic force microscopy to characterize electrospun fibers of poly (ethylene terephthalate). Fang and Reneker (1997) electrospun DNA into nanofibers, some of which were beaded. Polybenzimidazole nanofibers were electrospun by Kim and Reneker (1999), who also studied the reinforcing effects of these nanofibers in an epoxy matrix and in a rubber matrix. Fong et al described the electrospinning of beaded nanofibers (Fong et al. 1999). They also studied the morphology of phase separation in electrospun nanofibers of a styrene-butadiene-styrene tri-block copolymer (Fong and Reneker 1999). Elastomeric nanofibers were made from this thermo-elastic copolymer. The smallest fibers of this tri-block copolymer had diameters around 3 nm. Chun and coworker (1999) also prepared carbon nanofibers, from polymers. The resulting carbon nanofibers had diameter in the range from 50 to 500 nm. The morphology ranged from highly oriented, crystalline, nanofibers to very porous ones with high values of surface area per unit mass.

Electrospinning is a remarkably simple method for generating nanofibers of polymers. When combined with conventional sol-gel processing, it provides a versatile technique for producing ceramic nanofibers with either a solid, porous, or hollow structure (Li et al. 2006).

2.3.2 Mechanism of electrospinning process

Electrospinning technique is a unique process that uses an electrical field to create an electrically charged jet of polymer solution or melt, which dries or solidifies to leave a polymer fiber. The properties of fiber obtained from this process depend on two types of parameter. The first sets of parameters are system parameters including molecular weight, molecular weight distribution, architecture of the polymer (e.g. branched or linear chain), and solution properties (viscosity, conductivity and surface tension). The second ones are processing parameters including electrical field strength, flow rate, solution concentration, distance between the capillary and the collector, and ambient parameters (temperature, humidity and air velocity in the chamber) (Doshi and Reneker 1995).

Like an electrospray, electrospinning is a technique based on electrostatic interactions. Once the liquid is ejected from the orifice by electrical force, the electrified jet experiences rapid bending and whipping process in which the jet is continuously stretched and elongated by electrostatic repulsive forces, leading to the formation of a long, thin, and uniform thread as shown in Figure 2.3. Unlike the conventional spinning processes, the drawing and thinning of fibers in electrospinning is accomplished through electrostatic repulsions of charges on the liquid jet itself, making it a contactless stretching process. As the solvent rapidly evaporates during the spinning process, the diameter of the thread is constantly reduced, leading to the formation of an ultrathin fiber. In the end, the charged fibers are deposited on the grounded collector placed under the spinneret as a result of electrostatic attraction. Depending on the rheological properties of the solution and other spinning parameters, the diameter of the resulting fiber can be varied from tens of nanometers to a few micrometers (Li and Xia 2004)

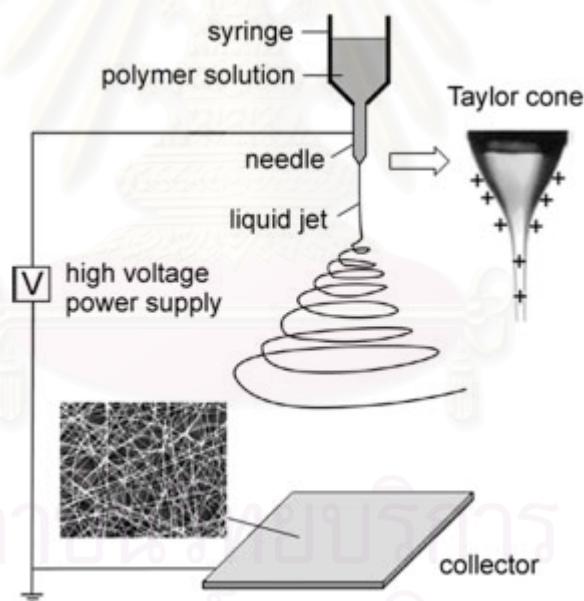


Figure 2.3 Schematic illustration of basic setup for electrospinning.

2.3.3 Controlling the orientation of electrospun fibers

The challenge to control the spatial orientation of electrospun fibers has been met with some success. Both mechanical and electrostatic means have been explored to improve the alignment of electrospun fibers. Li and Xia (2004) have shown that the

as-spun fibers could be aligned more or less parallel to each other when a drum rotating at high speed was used at the collector.

Under appropriate conditions, the alkoxide precursor from sol-gel method could be rapidly hydrolyzed by the moisture in air to generate an amorphous oxide as the liquid jets which were accelerated toward the collector. If the percentage of the alkoxide precursor was sufficiently high, it was possible to obtain continuous nanofibers made of various polycrystalline metal oxides as uniaxially aligned arrays (Li and Xia 2004).

2.3.4 Effects of electrospinning parameters

In 2003, Li and Xia (2003) studied fabrication of titania nanofibers by using electrospinning method with controllable diameters and porous structures. When ethanol solution containing both poly(vinyl pyrrolidone) (PVP, $M_w \sim 1,300,00$) and titanium tetraisopropoxide was injected through a needle under strong electrical field, composite nanofibers made of PVP and amorphous TiO_2 were formed as a result of electrostatic jetting. These nanofibers could be subsequently converted into fibers of anatase titania without changing their morphology via calcination in air at $500^\circ C$. The average diameter of these ceramic nanofibers could be controlled in the range from 20 to 200 nm. It was found that, after calcined at $500^\circ C$, the nanofibers remained in continuous structure with their average diameter reduced. This size reduction could be accounted by the loss of PVP from the nanofibers and the crystallization of titania. They also reported the followings: the nanofibers increased in diameter as the PVP concentration was increased; thinner nanofibers were obtained when the strength of the electric field was increased; faster feeding rate of PVP solution often resulted in thicker fibers; the use of titanium tetraisopropoxide at lower concentration led to the formation of thinner ceramic nanofibers. Furthermore, it was suggested that the electrospinning procedure could be extended to provide a generic route to nanofibers made of other oxides such as SnO_2 , SiO_2 , Al_2O_3 , and ZrO_2 .

In 2004, Viswanathamurthi and coworkers (2004) prepared nano to sub-micron fibers of ruthenium doped titanium dioxide/poly(vinylacetate) hybrid by electrospinning method. Pure ceramic metal oxide fibers were obtained by high

temperature calcination of the organic-inorganic hybrid fibers. It was observed that diameter of as-synthesized titania fibers was slightly increased by the addition of ruthenium. However there was no change in the diameter of ruthenium-doped fibers with the increase in ruthenium content. The surface of the fibers obtained was smooth and uniform. The fibers calcined at 600°C contained only anatase phase of titanium dioxide and metallic ruthenium, while the fibers calcined at 800°C showed the presence of rutile in addition to those two phases. When the ruthenium content was increased, the fibers were no longer straight and some of fibers are broken. Moreover, the fiber surface showed shrinkage and roughness. It was seen that the surface of high ruthenium content fibers appeared smooth and porous. The porosity increased with the increase in ruthenium content. The fiber calcined at 1000°C showed only rutile and metallic ruthenium. At this stage no change in fiber morphology with respect to ruthenium content was observed. They found that the porous and polycrystalline structure of the electrospun fibers provided a surface area to volume ratio roughly 1-2 orders of magnitude higher than that has been known for continuous thin films.

Wattanaarun and his coworkers (2005) studied the effects of preparation conditions and secondary metal dopant on fabricating TiO₂/PVP composite nanofibers by combined sol-gel with electrospinning technique. The spinning solution was prepared by titanium (IV) tetraisopropoxide (TTIP) in ethanol mixed with acetic acid and polyvinyl pyrrolidone (PVP) in ethanol. The diameter range of the obtained fibers was about 120-350 nm, while the diameter range of ceramic fibers after calcination was about 100-230 nm. The effects of spinning conditions were determined. Increasing PVP concentration led to an increase in the fiber diameters, while increasing electrostatic field strength led to a decrease in the fiber diameters. Moreover, the choice of the calcination temperature has a strong influence on the crystalline phase formation of as-spun titania fibers, with the transformation from anatase to rutile occurring more readily with increasing calcination temperature. Addition of silicon as the second metal dopant helped increasing the thermal stability of the resulting titania fibers.

CHAPTER III

EXPERIMENTAL

This chapter describes the experimental procedures for titania nanofiber preparation. It is divided into four parts: materials used, electrospinning apparatus, experimental procedures and sample characterizations.

3.1 Materials

The starting materials are titanium tetraisopropoxide (TTIP), poly (vinyl pyrrolidone) (PVP), ethyl alcohol, acetic acid, potassium nitrate and sodium chloride.

Titanium tetraisopropoxide (TTIP), 97%, was purchased from Sigma-Aldrich Chemical Company and used as received. It was kept in dry environment prior to use to prevent moisture adsorption.

Poly (vinyl pyrrolidone) (PVP), $M_w \approx 1,300,000$, was purchased from Sigma-Aldrich Chemical Company and used as received.

Ethyl alcohol, 98%, was purchased from Sigma-Aldrich Chemical Company and used as received.

Acetic acid, glacial, was purchased from Fluka Chemical Company and used as received.

Potassium nitrate and sodium chloride, both with 99.9% of purity were purchased from Fluka Chemical Company and used as received.

3.2 Electrospinning Apparatus

Schematic of the electrospinning apparatus used in this work is shown in Figure 3.1. The components of the apparatus and their functions are described as follows.

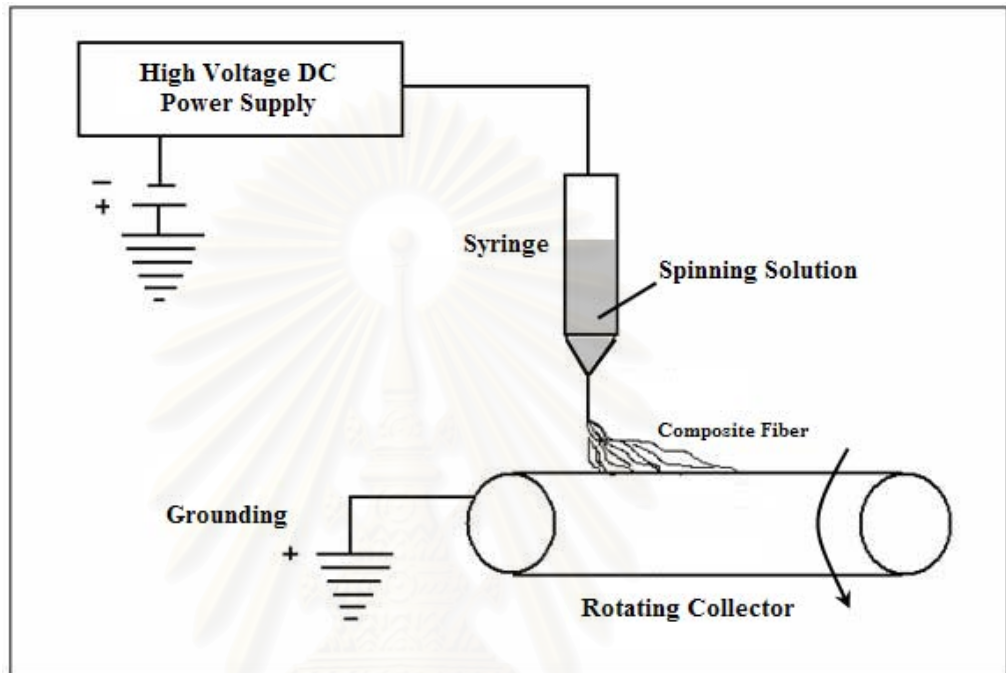


Figure 3.1 Schematic of an electrospinning setup.

The system is consisting of:

- A high-voltage power supply (ES30PN, Gamma High Voltage Research Inc., Ormond Beach, Florida) is used to generate either positive or negative DC voltage upto 30 kV, with very low electrical current of 166 microamperes.
- A 5 ml syringe is used as a container for electrospinning solution. The syringe is made of a plastic and set in vertical orientation.
- A stainless steel needle (guage No.20 and the outside diameter of 0.90 mm) is used as a nozzle or electrode to conduct the electrical energy from the power supply to the solution. The tip of the needle is cut into a flat shape and the length of the needle is 1 cm.
- Aluminum foil is used as a ground collector which is attached to a collecting drum with 25 mm of diameter rotating at 2,400 rpm.

3.3 Experimental Procedures

3.3.1 Preparation of spinning solution

In a typical procedure, 1.5 g of titanium tetraisopropoxide (TTIP) was mixed with 3 ml of acetic acid (for the study of acetic acid addition, the amount of acetic acid was varied between 0 – 4 ml.) and 3 ml of ethanol. The solution was constantly stirred for 10 min before being added into 7.5 ml of polyvinylpyrrolidone (PVP, $M_w \approx 1,300,000$) solution in ethanol. The concentration of the PVP solution was 10 wt% and the resulting mixture was further stirred for 1 hour. The as-prepared solution was referred as the spinning solution.

3.3.2 Spinning of the TiO_2 /PVP composite fibers

The spinning solution was immediately loaded into a plastic syringe. A blunt-ended 20-gauge stainless steel needle was used as the nozzle. The emitting electrode from a Gamma High Voltage Research ES30PN power supply capable of generating DC voltages up to 30 kV was attached to the needle. The grounding electrode from the same power supply was attached to a collecting drum with 25 mm of diameter rotating at 2,400 rpm, and covered with a piece of aluminum foil which was used as the collector plate and was placed approximately 7 cm horizontally from the tip of the needle. The syringe was also placed 45° align from vertical axis. Upon the application of high voltage at 16 kV across the needle and the collective plate, a fluid jet was ejected from the nozzle. As the jet accelerated towards the collector, the solvent evaporated, leaving only ultrathin fibers on the collector. For experiments on aging conditions, the obtained fibers deposited on the collector plate were periodically collected according to the thickness of fiber layer, in the range from 0.05 - 0.3 mm. For acid addition experiments, the fibers were collected at 0.3 mm-thick of fiber layer.

3.3.3 Aging of the as-spun fibers

For part of the study where the effects of aging conditions were investigated, the as-spun titania fibers with different thickness of fiber layer, were aged under different levels of humidity at constant temperature approximately 27 °C. The relative humidity was controlled to be 100%, 90% and 75% by placing an open container containing water, saturated solution of KNO₃ and saturated solution of NaCl into aging chamber, respectively (Astrup et al. 1994; Vertucci et al. 1993). The aging process was taken place for predetermined period of time. The aged fibers were then characterized by fourier transform infrared spectroscopy, scanning electron microscopy and thermogravimetric and differential thermal analysis.

3.3.4 Calcination of the TiO₂/PVP composite fibers

The electrospun TiO₂/PVP composite fibers were subjected to heat treatment at 500°C for 3 hours and heating rate of 10°C/min by using a box furnace to remove residual PVP. It should be note that, for some parts of the study, the calcination temperature was varied from 250 to 750°C. The obtained titania fibers were finally characterized by X-ray diffraction, fourier transform infrared spectroscopy, scanning electron microscopy and transmission electron microscopy.

3.4 Sample Characterizations

3.4.1 Scanning electron microscopy (SEM)

The surface morphology and size of the resulting electrospun TiO₂/PVP composite fibers and TiO₂ ceramic fibers were observed by a JSM 6400 Scanning Electron Microscopy (SEM), which operated at 15 kV, at the Scientific and Technological Research Equipment Center (STREC), Chulalongkorn University. Samples were coated by thin film of gold prior to the analysis.

3.4.2 Transmission electron microscope (TEM)

The morphology of an individual grain in the sample was observed on a JEOL JEM-2100 Analytical Transmission Electron Microscope, operated at 80-200 keV at National Metal and Materials Technology Center, Thailand. The crystallographic information was also obtained from the selected area electron diffraction (SAED) analysis performed in the same instrument.

3.4.3 Viscometer

The viscosity of electrospinning solution was identified on a Brookfield Model DV III Rheometer at the Petroleum and Petrochemical College, Thailand. The samples were prepared at room temperature and the percentage of torque employed was over 90 % throughout the measurement.

3.4.4 X-ray diffraction (XRD)

The crystalline phase of TiO₂ nanofibers were identified by a Siemens D5000 X-ray diffractometer using Ni-filtered CuK α radiation. The measurements were carried out in the 2 θ range of 20-80 degree at the scan step of 0.04 degree.

3.4.5 Fourier transform infrared spectroscopy (FTIR)

Functional groups of as-prepared fibers as well as calcined fibers were identified by a Nicolet Impact 400 Fourier transform infrared spectrophotometer (FT-IR) using smart diffuse reflectance method. Infrared spectra were recorded between wavenumber of 400 and 4000 cm^{-1}

3.4.6 Thermogravimetric and differential thermal analysis (TG-DTA)

As-spun titania fibers were subjected to thermogravimetric and differential thermal analysis (Diamond Thermogravimetric and Differential Thermal Analyzer, TG-DTA, Perkin-Elmer) to determine the temperature of possible decomposition and phase change. The analysis was performed at temperature in the range of 25 - 1000°C using heating rate of 10°C/min in 100 ml/min flow of oxygen.



CHAPTER IV

RESULTS AND DISCUSSION

In this chapter, titania nanofibers synthesized by combined electrospinning and sol-gel method are investigated in detail. Effects of aging condition and acetic acid addition are also reported in this chapter. This chapter is divided into 3 sections as follows:

Section 4.1 presents results from preliminary experiments, preparation of axially aligned titania nanofibers and properties of the synthesized fibers.

Section 4.2 describes effects of aging conditions on properties of titania nanofibers. Physical and morphological properties, as well as phase transformation of aged fibers, are also reported in this section.

Section 4.3 describes effects of acetic acid in the spinning solution on morphology and crystallization temperature of the synthesized titania nanofibers including crystallite size of titania particle.

4.1 Fabrication of Axially Aligned Titania Nanofibers

4.1.1 Preliminary experiments

In the preliminary experiments, TiO₂/PVP composite fibers were prepared from combined sol-gel and electrospinning process according to the procedures reported by Wattanaarun and coworkers (Wattanaarun et al. 2005). The spinning solution was consisted of TTIP as titania source, poly(vinyl)pyrrolidone (PVP) as spinning aid, and ethanol as solvent. Small amount of acetic acid was added into the solution to improve stability of the solution. In this study, the PVP concentration was fixed at 10 wt.% The applied voltage and tip-to-collector distance (TCD) used for electrospinning process were 16 kV and 7 cm, respectively. By applying high

electrical potential across the syringe needle and the collector plate, ultrafine fibers with smooth surface were spun and deposited on the collector plate. To complete the formation of titania nanofibers, electrospun composite TiO_2/PVP fibers were calcined at 500°C for 3 hours in order to eliminate the organic components and to activate the crystallization of TiO_2 . Figure 4.1 shows morphology of the as-spun fibers comparing to the calcined fibers.

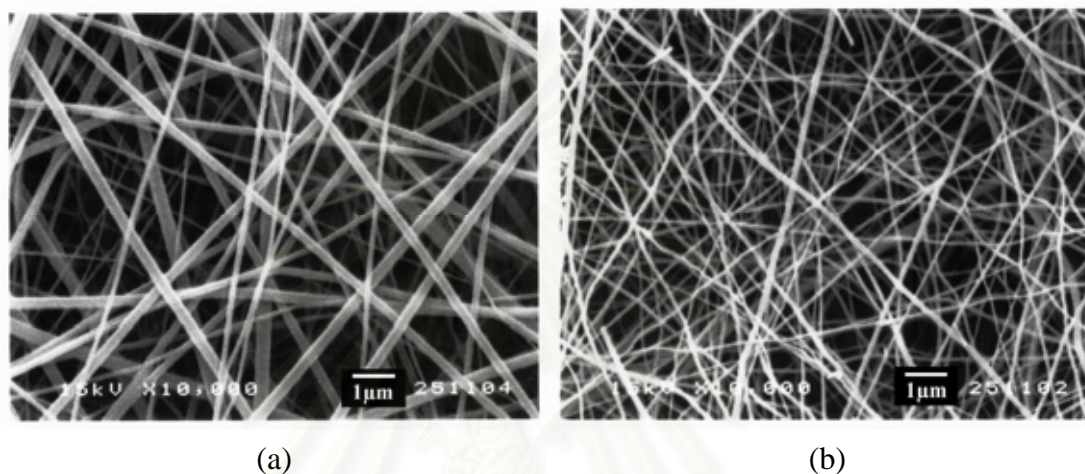


Figure 4.1 SEM micrographs of TiO_2/PVP composite nanofibers before (a) and after (b) calcination at 500°C for 3 hours in air. Noted that the PVP concentration and electric field employed were 10% wt. and 16 kV/7cm, respectively, and the electrospinning was done using flat collector.

From Figure 4.1(a), it can be seen that the as-spun composite TiO_2/PVP fibers are uniform and smooth without the presence of beads. In addition, after calcination at 500°C for 3 hours, the fibers appear to be more distorted and the surface appears to be rough. However, no breakage of fibers is found. It is clearly seen that, after the calcination process, there is shrinkage in fiber diameter. The diameter is reduced by almost half due to the decomposition of PVP. According to the frequency distribution of fiber diameters shown in Figure 4.2, this spinning condition gives fibers with narrow size distribution, before and after calcination. It should be note that fiber diameters were determined by randomly selected 100 fibers from a SEM image and measured the size by image processing program (SemAfore 5.0).The diameter of the as-spun composite fibers is in the range of 200-400 nm, while that for calcined fibers

is 80-210 nm. The average diameter of the as-spun composite TiO₂/PVP fibers and calcined titania fibers is about 230 and 130 nm, respectively.

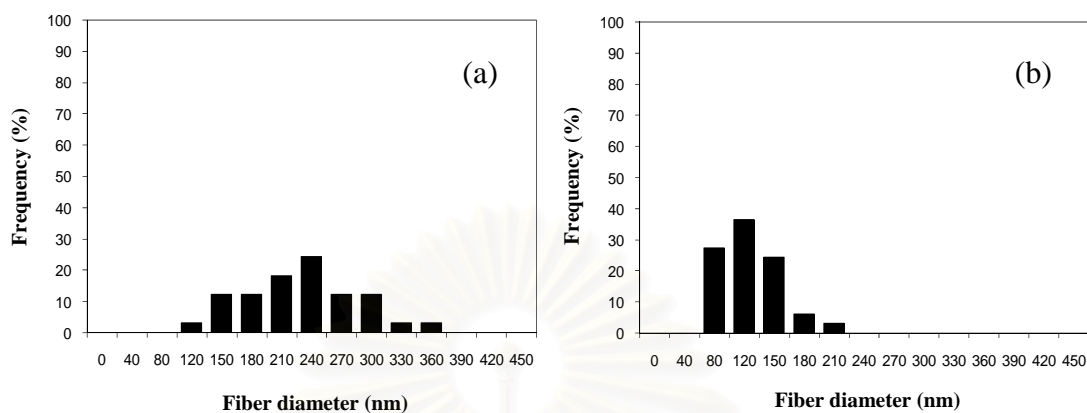


Figure 4.2 Frequency distribution for diameter of titania nanofibers spun on flat collector, before (a) and after (b) calcination at 500°C for 3 hours.

4.1.2 Properties of the synthesized titania nanofibers

After the TiO₂/PVP composite nanofibers were electrospun on flat collector with the electrospinning conditions as mentioned above, the fibers were collected and calcined at 500°C in air for 3 hours. The crystal structure and crystallite size of the calcined titania nanofibers were characterized by X-ray diffraction. Diffraction peaks corresponding to anatase and rutile phases are labeled separately in the 2θ range of 20-80° as shown in Figure 4.3.

สถาบันวิทยบริการ
จุฬาลงกรณ์มหาวิทยาลัย

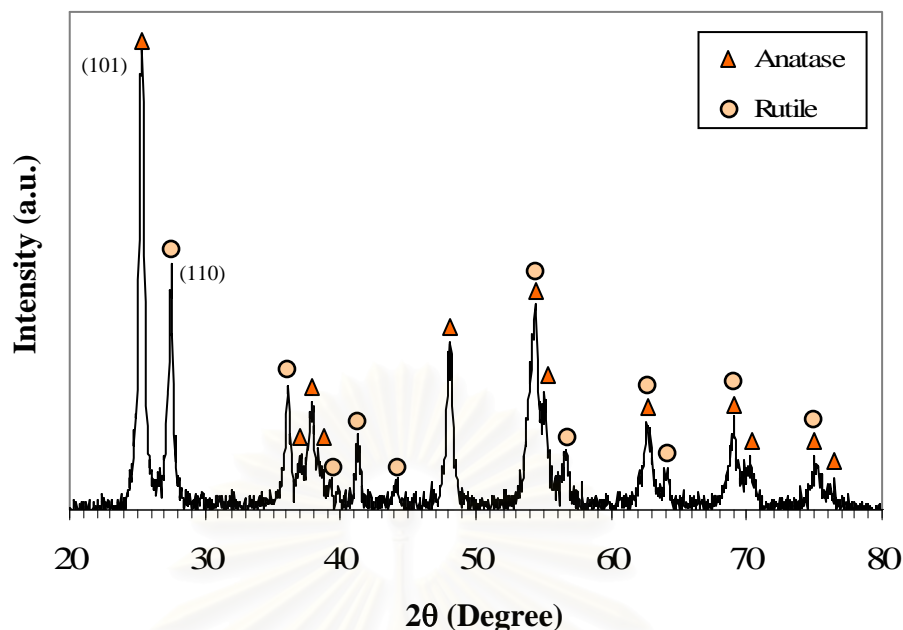


Figure 4.3 X-ray diffraction pattern of the electrospun titania nanofibers after calcined at 500°C for 3 hours in air.

According to Figure 4.3, after calcination at 500°C, the crystallization of titania occurs. There is a change in phase transformation from amorphous to the mixed phase of anatase and rutile as labeled in X-ray diffraction pattern. Although the transformation of anatase to rutile can take place over a wide range of temperature (i.e. 400-1100°C), it usually occurs at temperature higher than 700°C (Jung and Park 1999; Robson et al. 2005; Wu et al. 2007; Grzmil et al. 2007; Wetchakun and Phanichphant 2008). The appearance of rutile after calcination at 500°C in this result can be described by the existence of PVP in the spinning solution. The presence of PVP in sol-gel derived media is capable of restraining this phase transformation temperature at 500°C, according to the previous research (Zheng et al. 2001). However, there are still other parameters which affect the phase transformation and crystallization temperature of titania. Those parameters were investigated and will be reported in the next section.

The crystallite size of the product can be determined from the broadening of the X-ray diffraction pattern, using the Scherrer equation. The calculation results are shown in Table 4.1.

Table 4.1 Phase properties of titania nanofibers calcined at 500°C for 3 hours.

Phase structure	Rutile fraction (%)	Crystallite size of anatase ^a (nm)	Crystallite size of rutile ^a (nm)	Particle size of anatase ^b (nm)
Anatase/Rutile	35	19	20	18

^a obtained from XRD pattern broadening, using the Scherrer equation.

^b obtained from TEM observation.

As shown in Table 4.1, titania nanofibers synthesized at 500°C contain mixed phase structure of anatase and rutile. Fraction of rutile in the product was calculated according to the following equation (Fu et al. 1996)

$$\% \text{Rutile} = \frac{1}{((A/R) \times 0.884) + 1} \times 100$$

where *A* and *R* are the peak areas of the major peaks in XRD pattern for anatase and rutile phases, respectively.

For the crystallite size calculated from the Scherrer equation, the values for anatase and rutile phases shown in Table 4.1 are nearly equal. These values are also consistent with the observation by TEM, as shown in Figure 4.4. Therefore, not only that anatase and rutile phases obtained by the calcination at 500°C have roughly the same crystallite sizes, they are also single crystals.

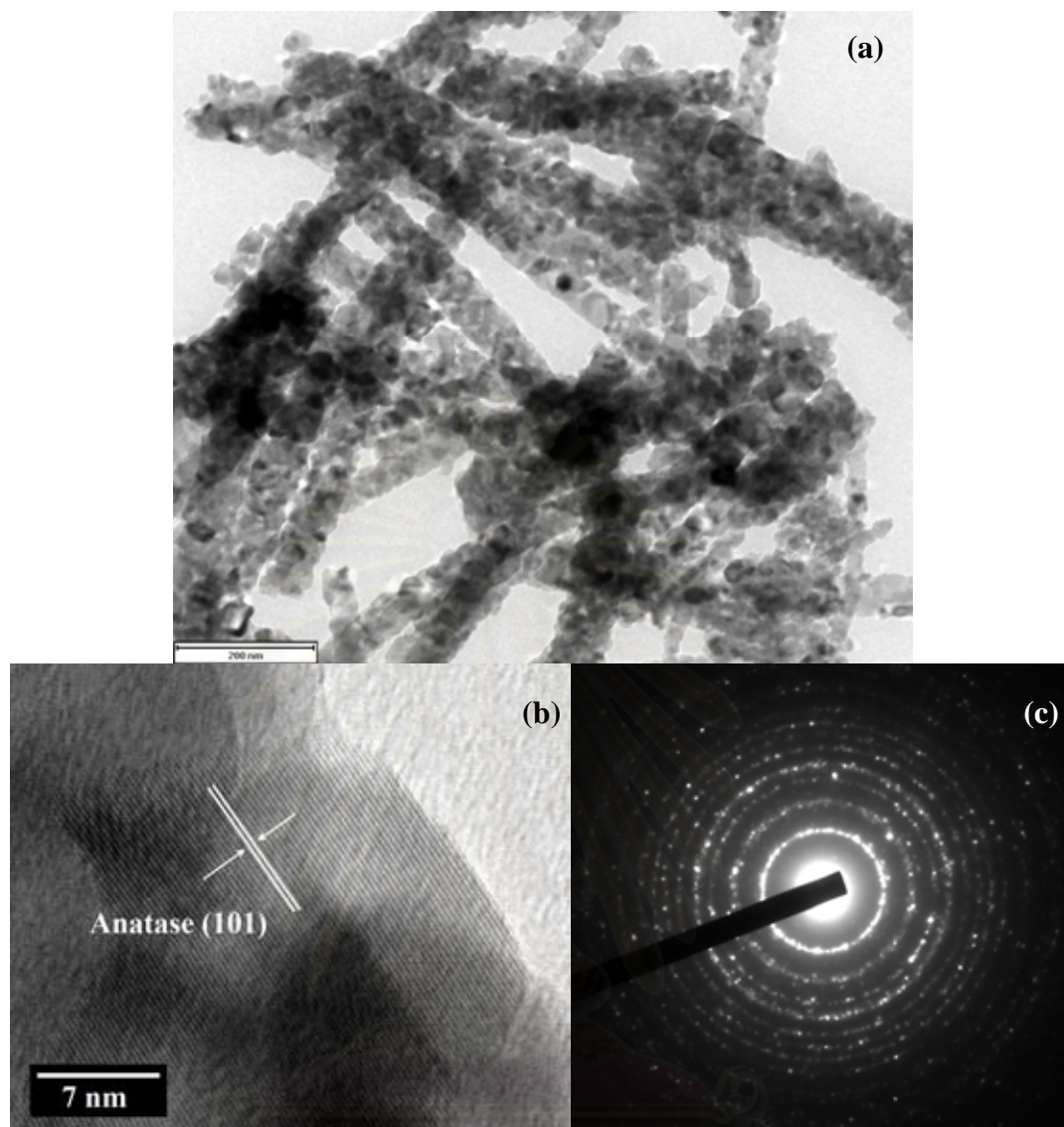


Figure 4.4 TEM results of the titania nanofibers calcined at 500°C: (a) TEM micrograph, (b) HR-TEM micrograph, and (c) SAED pattern.

Figure 4.4 illustrates the TEM images of the titania nanofibers. It is found that the fiber is consisting of numerous nanocrystallites. Each fiber contains small grains of less than 5 nm in diameter. Titania is uniformly dispersed in the PVP matrix as reported by Li and Xia (2004). When the PVP is decomposed by calcination, the remaining titania crystallizes and agglomerates together. Selected area electron diffraction (SAED) in Figure 4.4(c) reveals the polycrystalline nature of the fiber, which agrees with the previous XRD results. Nevertheless, the high-resolution TEM image (HRTEM) shown in Figure 4.4(b) provides further details regarding nanostructure of the titania nanofibers. The nanocrystallites observed in Figure 4.4(a)

are indeed single crystals. The lattice spacing of about 0.35 nm labeled in the figure can be assigned to the d spacing of (1 0 1) crystal planes (Yuan et al. 2002).

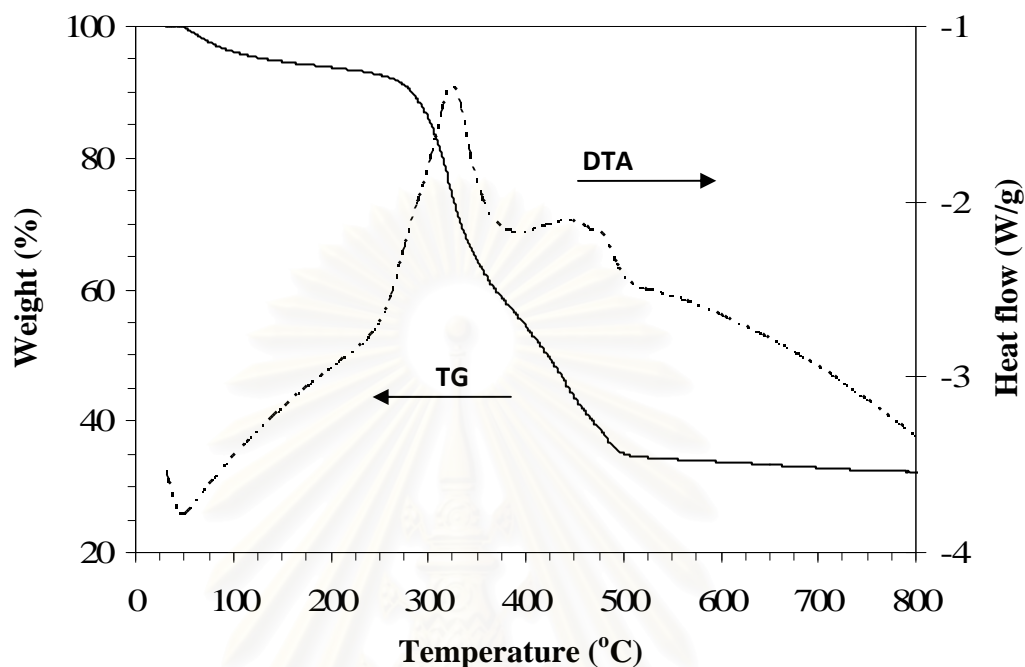


Figure 4.5 Thermogravimetric curves of the as-spun TiO_2/PVP composite fibers analyzed in oxygen atmosphere, using heating rate of $10^\circ\text{C}/\text{min}$.

Thermogravimetric analysis (TGA) of the as-spun TiO_2/PVP composite nanofibers was carried out in order to investigate the sample weight loss and thermal behavior during the calcination process. Under oxygen atmosphere and the TGA temperature profile set at a heating rate of $10^\circ\text{C min}^{-1}$, it is found that the thermal decomposition of PVP is completed at 500°C as shown in Figure 4.5. This result also agrees with the TGA result of pure PVP sample (Appendix B). From TG and DTA curves, it is obviously seen that the loss of PVP and the formation of titania occur at temperature between 300 and 500°C . The broad DTA peak at 334°C suggests the decomposition of main chain of PVP. The exothermic energy peak at 427°C corresponds to the crystallization from amorphous to anatase (Hong et al. 2003). It is also suggested that an exothermic broad peak at 462°C is corresponding to phase transformation from anatase to rutile, due to the fact that rutile is already presented in the sample calcined at 500°C (see Figure 4.3). Therefore, titania nanofibers calcined at this temperature range would apparently contain mixed phase of anatase and rutile.

According to the TG curve, there is a remaining of sample mass about 38 wt.% after 500°C where the decomposition of PVP is already completed. This value is corresponding to TiO₂ in nanofibers. No further mass loss is observed afterward, which indicates that the obtained fibers are pure titania. It should be noted that the initial weight loss of 7.5 wt% before 150°C is mainly attributed to moisture, ethanol and acetic acid initially resided in the as-spun fibers.

The formation of titania fibers is further investigated by FT-IR spectra, as shown in Figure 4.6. These spectra were recorded in the wavenumber range of 400 - 4000 cm⁻¹. For the as-spun titania nanofibers before calcination, the strong bands at 1,000 and 1,280 cm⁻¹ due to residual organic polymer are clearly observed, as well as the strong bands at 1,670 and 1,500 cm⁻¹ which are corresponding to the C-O stretching vibration and the secondary amide bond of PVP, respectively (Tang et al. 2007). Comparison between the FT-IR spectra of the as-spun composite fibers and that of the calcined titania fibers reveals that these IR absorption bands disappear after the calcination process. This result confirms the disappearance of PVP, which has been observed by TG analysis. Moreover, intensity of the wide band at wavenumber between 3,200 and 3,500 cm⁻¹, which is assigned to the O-H stretching vibration of hydroxyl groups from water (H₂O) and titanium hydroxyl groups (Ti-OH) (Song et al. 2000) decreases with increasing calcination temperature. After calcination at 500°C, weak peak observed at 1,450 cm⁻¹, which is associated to the bending of C-H bonds in TTIP (Song et al. 2000) also disappears due to the activation of titania crystallization.

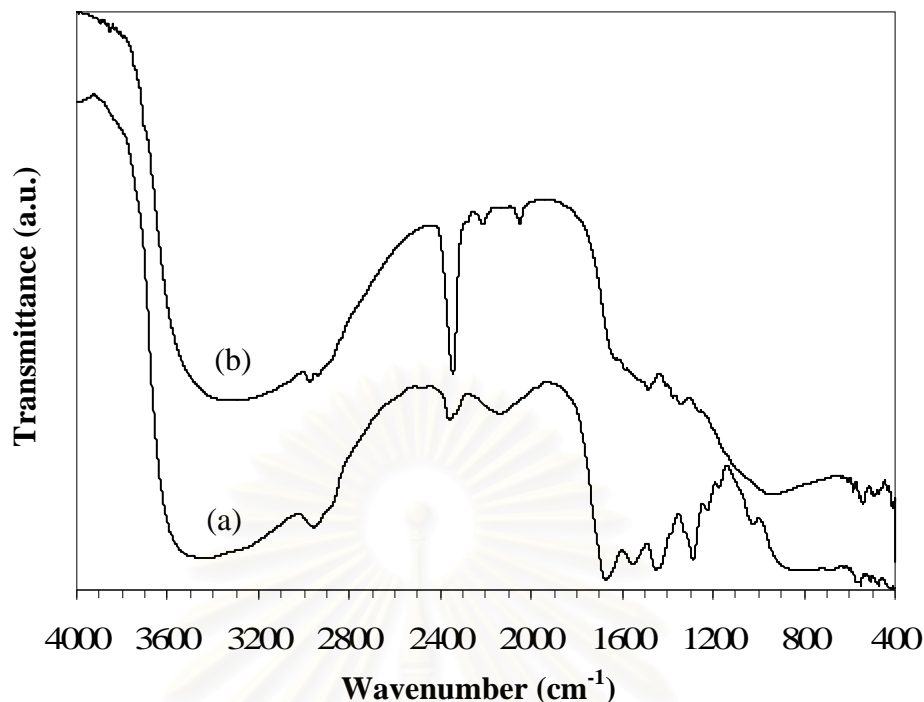


Figure 4.6 FT-IR spectra of the synthesized titania nanofibers: (a) as-spun fibers (b) calcined fibers at 500°C for 3 hours..

4.1.3 Fabrication of axially aligned titania nanofibers

The electrospinning process can be adapted by varying the collector grounding design to improve the axial alignment of fibers (Li and Xia 2004). Generally, electrospun fibers are often deposited on the surface of the collector as randomly oriented fibers. At present, there are two ways reported in literatures to collect electrospun nanofibers as uniaxially arrays. The simple method is to use a rotating drum as the collector. Therefore, in this study, axially aligned titania nanofibers were fabricated by using rotating grounding drum as the collector instead of the stationary flat collector. By using the rotating collector, the other electrospinning parameters are maintained as those mentioned earlier. It is found that the physical and chemical properties of the axially aligned fibers are the same as randomly aligned fibers described in Section 4.1.2. Nevertheless, alignments of the obtained fibers are different, as shown in Figure 4.7. The rotating drum is a means for improving the air flow and attracting the electrospun fibers along the winding direction, resulting in the alignment of fibers on the collector.

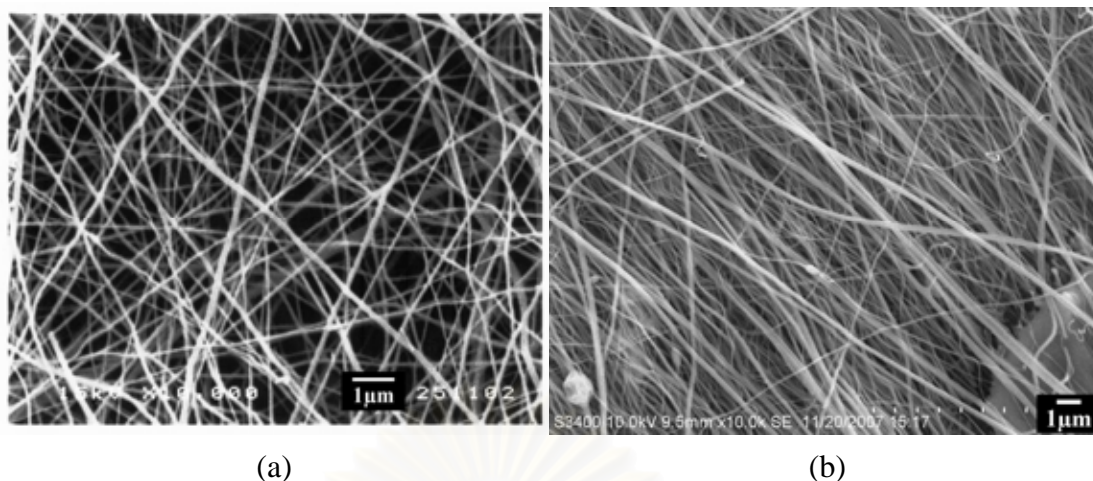


Figure 4.7 SEM micrographs of calcined electrospun titania nanofibers fabricated on: (a) flat collector (b) rotating drum.

From the frequency distribution of size of titania fibers shown in Figure 4.8, it is observed that the distribution patterns of fibers collected by the rotating drum is very similar to that observed in fibers collected with flat collector. Moreover, the calculated average diameters for titania fibers collected by flat and rotating collectors are relatively close together, i.e. 130 vs. 120 nm. Therefore, it can be concluded that there is no change in fiber diameter from the change in type of the grounded because the rotating drum affects only the orientation of fibers in the electrospinning process (Li and Xia 2004).

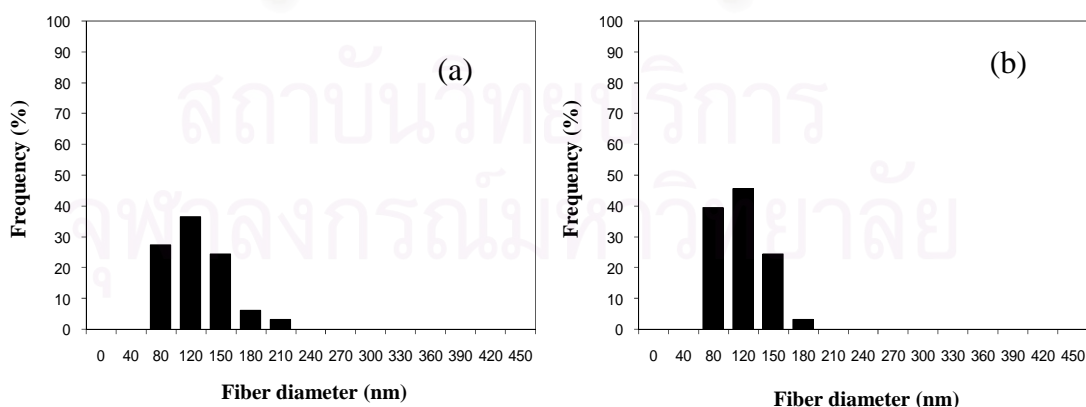


Figure 4.8 Frequency distribution for diameter of electrospun titania nanofibers fabricated on: (a) flat collector (b) rotating drum, after calcined at 500°C for 3 hours.

4.2 Effects of Aging Conditions on Properties of Titania Nanofibers

In this section, the effects of aging conditions were investigated to find the influences of aging time, thickness of fiber layer and humidity of the aging atmosphere on morphology, physical properties and phase transformation of the synthesized titania nanofibers.

After the TiO₂/PVP composite nanofibers were prepared by electrospinning method using parameters described earlier, these as-spun fibers were collected and separated according to the desired thickness of fiber layer, which was measured by a digital thickness meter. The thickness used in this study was 0.05, 0.1 and 0.3 mm, respectively. After that, the fibers were aged under various conditions, with different aging times before subsequently calcined to get titania nanofibers.

4.2.1 Effects of aging time on properties of aged fibers

The aging time is one of the factors that influence the formation of titania (Venkatachalam et al. 2007). In order to study the effect of factor, the as-spun TiO₂/PVP composited nanofibers were consequently aged at different periods of times under the ambient condition at 27°C and 55% relative humidity. After that, the aged fibers were calcined at 500°C for 3 hours. Then, the fraction of rutile in the samples can be calculated from X-ray diffraction analysis results using the equation discussed in Section 4.1.2. Figure 4.9 shows the plot of aging time, within a short time period, versus rutile fraction in the synthesized titania fibers. For the unaged sample, the rutile fraction in the calcined sample is higher than the aged sample. The fraction of rutile in the fibers can be significantly discussed by the aging period of 0 to 24 hours. For the aging time longer than 24 hours, it seems that there is no significant change in the rutile fraction in the calcined fibers. It is suggested that, the hydrolysis reaction of titania precursor in the fibers spontaneously occurs when the fibers are exposed to moisture, resulting in fast hydrolysis rate at the beginning of aging period. Though there is no previous report on the relation of hydrolysis rate and the crystallization of rutile, it can be concluded from the results in this work that the completion of hydrolysis can reduce the rutile fraction in the sample. This hypothesis can be proved further by prolonging the aging time, as shown in Figure 4.10.

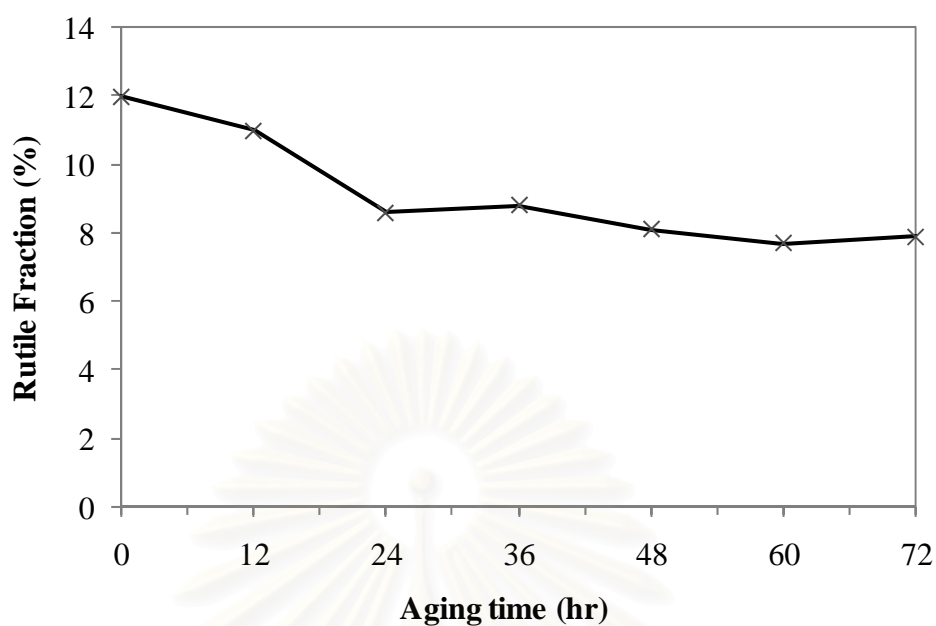


Figure 4.9 Plot of aging time versus fraction of rutile in the synthesized titania nanofibers calcined at 500°C. The aging was conducted on 0.1 mm-thick layer of fibers under ambient condition (55% RH), before calcination.

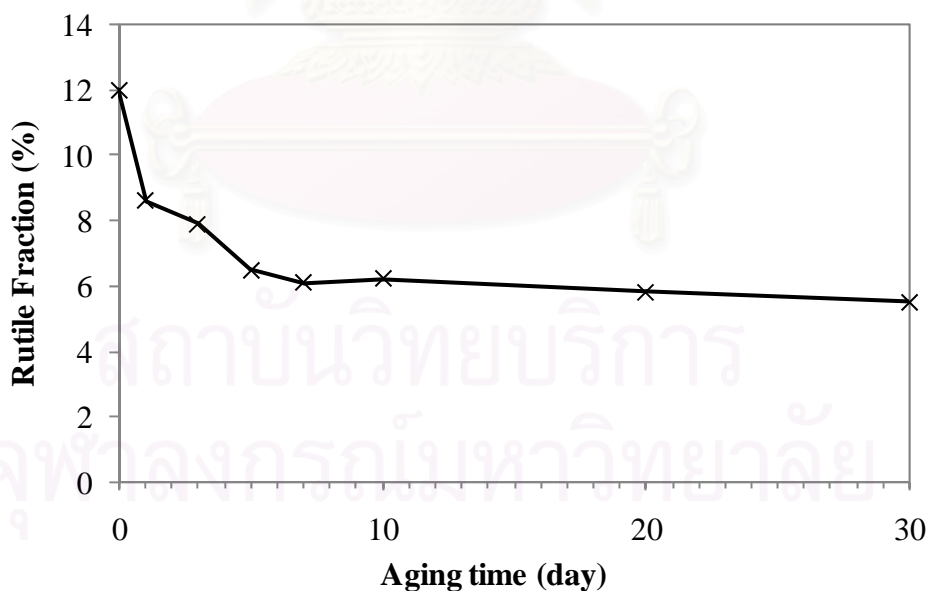


Figure 4.10 Plot of extended aging time versus fraction of rutile in the synthesized titania nanofibers calcined at 500°C. The aging was conducted on 0.1 mm-thick layer of fibers under ambient condition (55% RH), before calcination.

According to the Figure 4.10, when the aging time is prolonged, the fraction of rutile in the sample after calcination at 500°C is not significantly changed. The minimum rutile fraction found in the sample is about 6% after aging for 7 days. It can be concluded that the hydrolysis reaction of titania precursor is nearly completed at this point. The rutile fraction is not further reduced afterward. Though the mechanism of aging is unidentified, it is suggested that the different properties of the amorphous phase is affected by the aging time, resulting in the different amount of rutile fraction of calcined titania fibers.

4.2.2 *Effects of humidity on aging*

For the experiments, humidity of the aging atmosphere was controlled to various levels by placing saturated aqueous of different compound within the aging chamber. In this study, pure water, saturated solution of potassium nitrate and saturated solution of sodium chloride were used to control the relative humidity of the aging system to be 100%, 90% and 75% at 26°C, respectively. The SEM micrographs of titania nanofibers aged for 7 days at different levels of humidity are shown in Figure 4.11. It should be note that the thickness of fiber layer was controlled to 0.1 mm and the fibers were calcined at 500°C for 3 hours after aging.

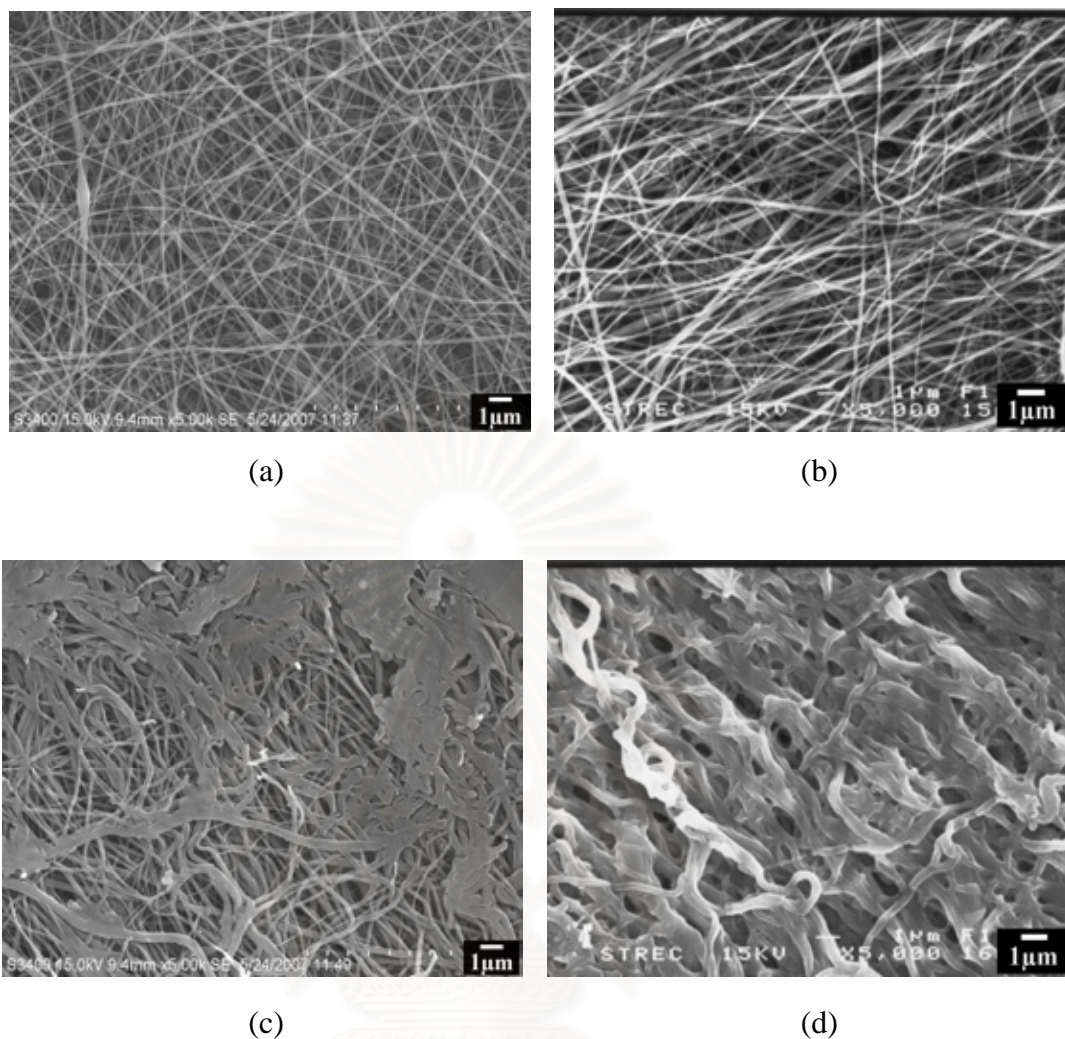


Figure 4.11 SEM micrographs of nanofibers aged for 7 days under various aging conditions on 0.1 mm-thick layer of fibers and subsequently calcined at 500°C: (a) ambient condition (55% RH) (b) 75% RH (c) 90% RH and (d) 100% RH.

Humidity level has many effects on the morphology of the synthesized titania after calcination at 500°C, as seen in Figure 4.11. For the fibers aged in ambient condition (Figure 4.11(a)), their morphology after calcination is the same as morphology of unaged fibers reported in Section 4.1, which is smooth and not distorted. For an equal aging time of 7 days, morphology of fibers aged under 75% relative humidity is not significantly different from the fibers aged under ambient condition. However, if the relative humidity reaches 90%, it will affect morphology of the fibers due to the solubility of PVP into water, as seen in Figure 4.11(c) and Figure 4.11(d). Under 90% of relative humidity, some fibers are found to be fused together,

and fibers are heavily distorted. For the maximum relative humidity of 100%, almost all fibers appear to be fused together as a porous sheet because of the expansion of PVP affected by moisture. Nevertheless, PVP fibers after aging under 100% humidity are completely fused because of highly permeability of moisture into PVP (as shown in Appendix C).

From the results mentioned in Section 4.1, titania nanofibers calcined at 500°C are mixed phase of anatase and rutile. It is found from the Section 4.2.1 that, aging of the as-spun TiO₂/PVP composite fibers before calcination results in reduction of rutile. In this section, the fraction of rutile in the sample aged under different level of humidity was calculated from X-ray diffraction pattern in the same manner as presented in Section 4.1.2, and plotted against the aging time. The results are shown in Figure 4.12.

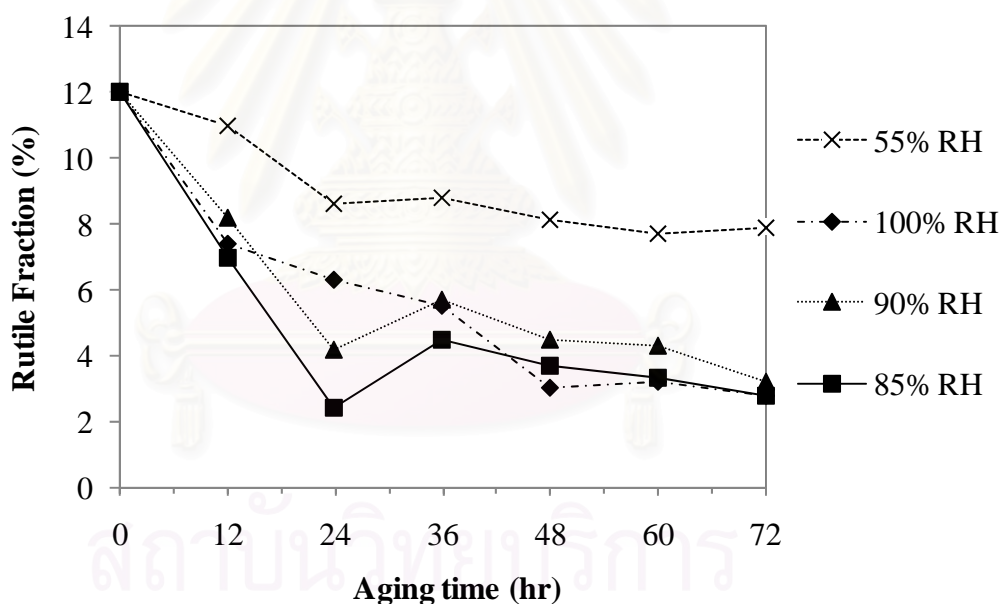


Figure 4.12 Plot of aging time versus fraction of rutile in the synthesized titania nanofibers calcined at 500°C. Before calcination, the 0.1 mm-thick layer of fibers were aged under different level of relative humidity (RH).

Figure 4.12 shows the plot between aging time in the first 72 hours versus rutile fraction of the sample subsequently calcined at 500°C. It was found that,

regardless of the humidity level, fraction of rutile is decreased rapidly by the first 24 hours of aging due to the effect of aging time discussed earlier in the Section 4.2.1. For the next 48 hours of aging, the rutile fraction of the sample aged under high level of humidity continues to decrease gradually, unlike the sample age under ambient condition. It is suggested that the crystallization mechanism of fiber aged under high humidity level is rather different than that of the fiber aged under normal condition. This is not caused by the effect of aging time, but it is the result from the effect of humidity. For the prolonged period of aging time, the results are shown in Figure 4.13.

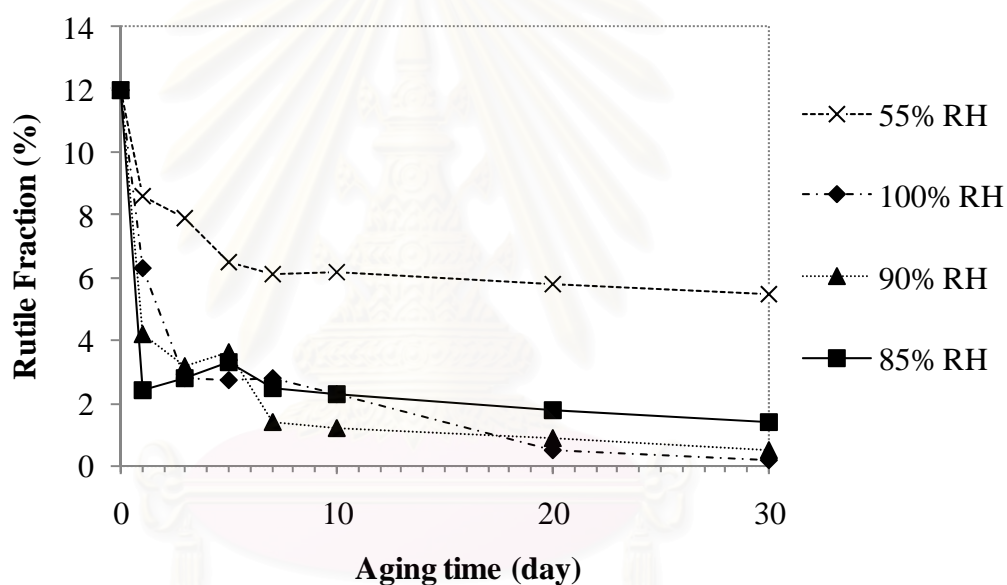


Figure 4.13 Plot of extended aging time versus fraction of rutile in the synthesized titania nanofibers calcined at 500°C. Before calcination, the 0.1 mm-thick layer of fibers were aged under different level of relative humidity (RH).

Figure 4.13 illustrates the rutile fraction of titania nanofibers calcined at 500°C after long period of fiber aging. The result shows that, after aging in high level of humidity for 3 days, the fraction of rutile in the subsequently calcined fibers can be reduced to around 3%, which is obviously different from the value obtained from aging under ambient condition. However, among the treatment at high humidity level,

the effect is not significantly different. For the fibers aging after 7 days, fraction of rutile still tardily decreases until the rutile fraction value is almost 0% after 30 days. On the other hand, rutile fraction of sample aged under ambient condition is not significantly changed after 7 days and remains at about 6%. Therefore, it confirms the previous observation that the mechanism of aging under high humidity should be different from the aging under ambient condition, although the true mechanism can not be identified in this work due to the lack of information from previous research.

The same trend for the effect of humidity is also observed, when the thickness of fiber layer is decreased to 0.05 mm. High humidity level still has dominating effect in reducing the fraction of rutile in the calcined fibers in the same manner as those observed in Figure 4.13, although the initial rutile fraction is significantly different due to the effect of fiber layer thickness which will be reported in detail in the next section.

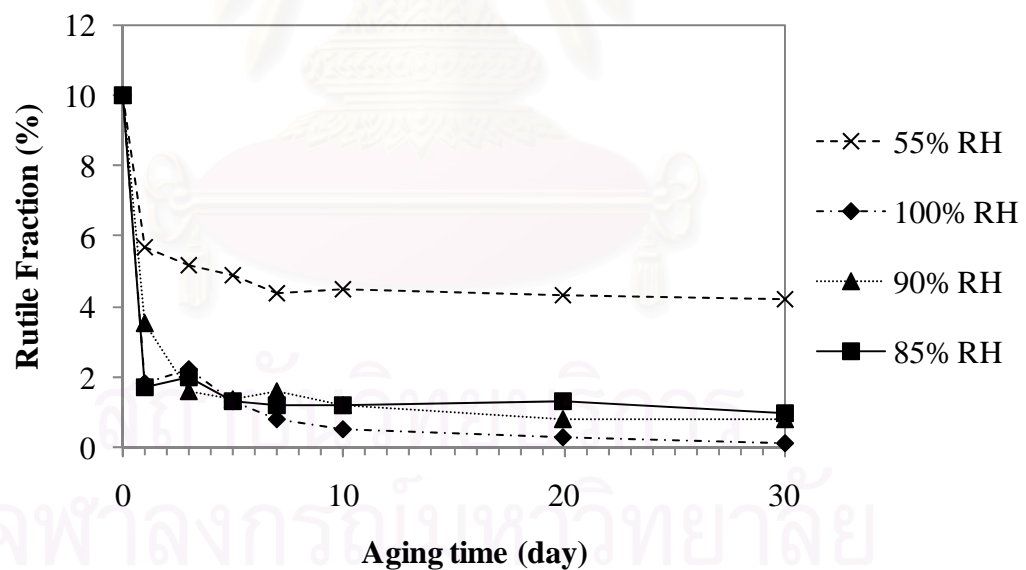


Figure 4.14 Plot of aging time versus fraction of rutile of synthesized titania nanofibers calcined at 500°C. Before calcination, the 0.05 mm-thick layer of fibers were aged under different level of relative humidity (RH).

Figure 4.15 shows FT-IR spectra of as-spun titania fibers aged after 7 days under different conditions. After aging in high level of humidity (90% and 100% RH), there is a change in PVP structure within the fibers as observed on FT-IR spectra. The absorption band corresponding to C-N vibration bonds of PVP observed at $1,274\text{ cm}^{-1}$ (Tang et al. 2007) in the sample aged under 55 and 75% RH becomes sharper when aging under 90 and 100% RH. Moreover, a broad absorption band at $1,380\text{ cm}^{-1}$ corresponding to residual organic group also becomes sharper when the sample is aged under high humid level (Zheng et al. 2000). All of these evidences show that there is a change in chemical structure of PVP as the fibers are aged at high level of humidity. This change may relate to the change in the fiber structure at high humid level as seen from SEM results in Figure 4.11(c) and 4.11(d). Since there has been a report that PVP existence can reduce phase transformation temperature of TiO_2/PVP composite (Zheng et al. 2001), the change in PVP structure observed in this work may affects the crystallization temperature of rutile as well.

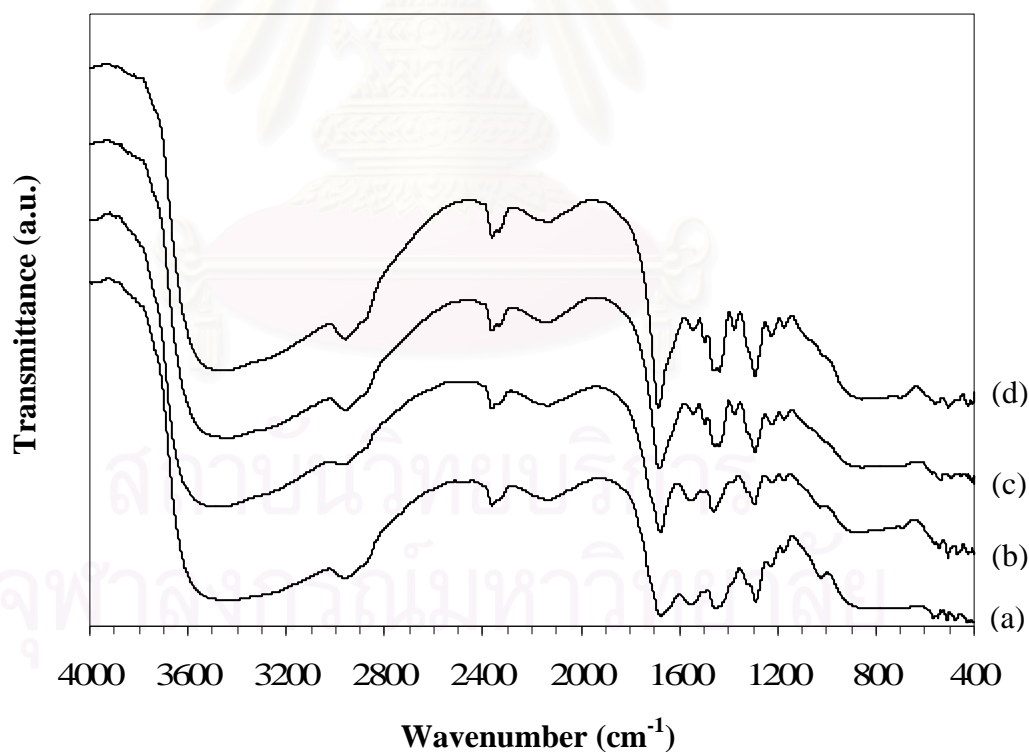


Figure 4.15 FT-IR spectra of as-spun titania fibers aged under 55% RH (a), 75% RH (b), 90% RH (c), and 100% RH (d) for 7 days. The aging was conducted on 0.1 mm-thick layer of fibers.

Thermal stability of the aged titania fibers was measured using a thermal gravimetric analysis (TGA). According to the results from TG analysis of the as-spun fibers as shown in Figure 4.16, the patterns of weight loss for fibers aged under various conditions are quite similar to each other. Three main zones of weight loss are identified. The first zone from 50 to 150°C corresponds to the removal of physically adsorbed water, acetic acid and alcohol resided in the sample. The second zone from 250 to 350°C corresponds to the decomposition of PVP and the formation of Ti-O network in the TiO₂/PVP composited fibers. The third zone from 370 to 450°C is caused by the decomposition of other residual organic groups such as 2-pyrrolidone and alcoxy group (Zheng et al. 2000) as well as the formation of anatase structure. For fibers aged under high humidity, the weight loss at low temperature is higher than the fibers aged under low humidity, because of the different quantity of moisture absorbed inside the fibers and the change in fibers structure from polymer merging. Nevertheless, it is obvious that PVP can be totally removed from the fibers aged under all of these conditions, by calcination at 500°C. It is also observed that, at the temperature above 500°C, the remaining weight of fibers aged under ambient condition (55% RH) is different from those fibers aged under high humidity level. This result is consistent with the results for rutile fraction in the sample aged for 7 days and subsequently calcined at 500°C, as seen in Figure 4.13, i.e. the rutile fractions of all sample treated with high humidity level are relatively close together and significantly different than that of sample aged under ambient condition.

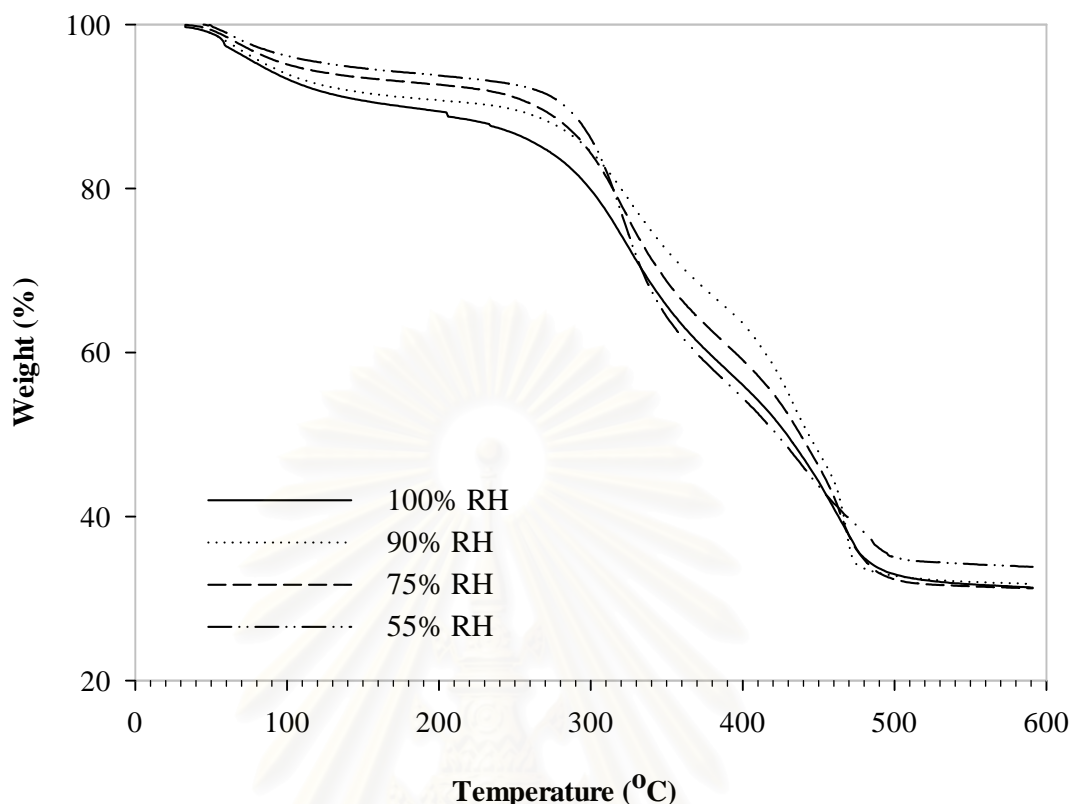


Figure 4.16 TGA curves of as-spun titania fibers aged under various humidity levels for 7 days. Noted that the TG analyses were conducted in oxygen atmosphere, using heating rate of $10^{\circ}\text{C}/\text{min}$, and the thickness layer of fiber was 0.1 mm.

The change in energy associated with the phase transformation of titania can be identified from DTA curves as shown in Figure 4.17. According to the XRD results discussed earlier, the phase structure of titania nanofibers becomes mixed phase of anatase and rutile after calcination at 500°C . This is consistent with the results from DTA. The exothermic peaks are observed at 328°C , 450°C and 477°C for the fibers aged under all of these 4 levels of humidity. These peaks can be ascribed to the elimination of PVP, the change in phase structure from amorphous to anatase and the change in phase structure from anatase to rutile, respectively. Although there is no difference in position of DTA peaks observed among those 4 samples, the energy level associated with each sample is different. It is seen that the behavior of the fibers aged under ambient condition (55% RH) is obviously different from the others aged

under high humidity level. This result is consistent with the TGA results in Figure 4.16 and the results of rutile fraction as mentioned earlier. It is probably related to the existence of PVP (Zheng et al, 2001) and also the change in PVP chemical structure based on the IR spectrum analysis observed in Figure 4.17.

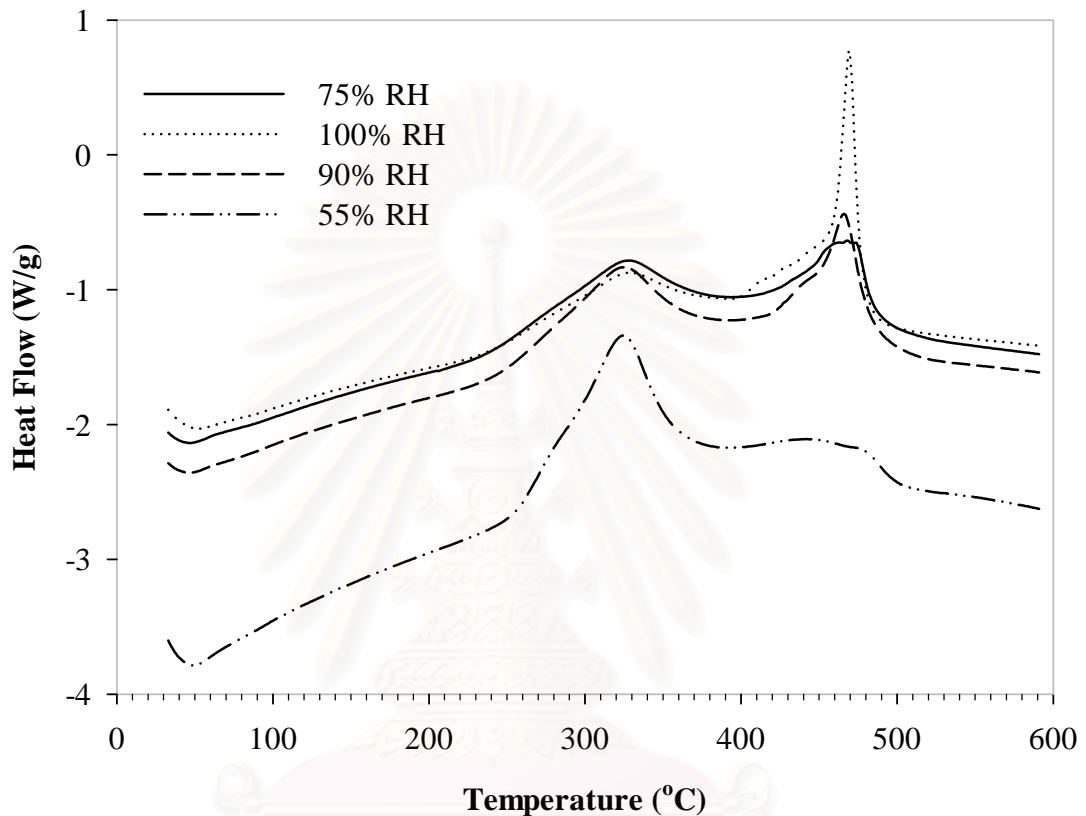


Figure 4.17 DTA curves of as-spun titania fibers aged under various humidity levels for 7 days. Noted that the TG analyses were conducted in oxygen atmosphere, using heating rate of $10^{\circ}\text{C}/\text{min}$, and the thickness layer of fiber was 0.1 mm.

4.2.3 Effects of thickness of fiber layer on properties of aged fibers

From the results partially discussed in Section 4.2.2, thickness of fiber layer is another parameter that affects the aging process, which subsequently influences rutile fraction of synthesized titania nanofibers. Its effect can be clearly seen in the plot of fraction of rutile against aging time at various thickness of fiber layer, as shown in Figure 4.18.

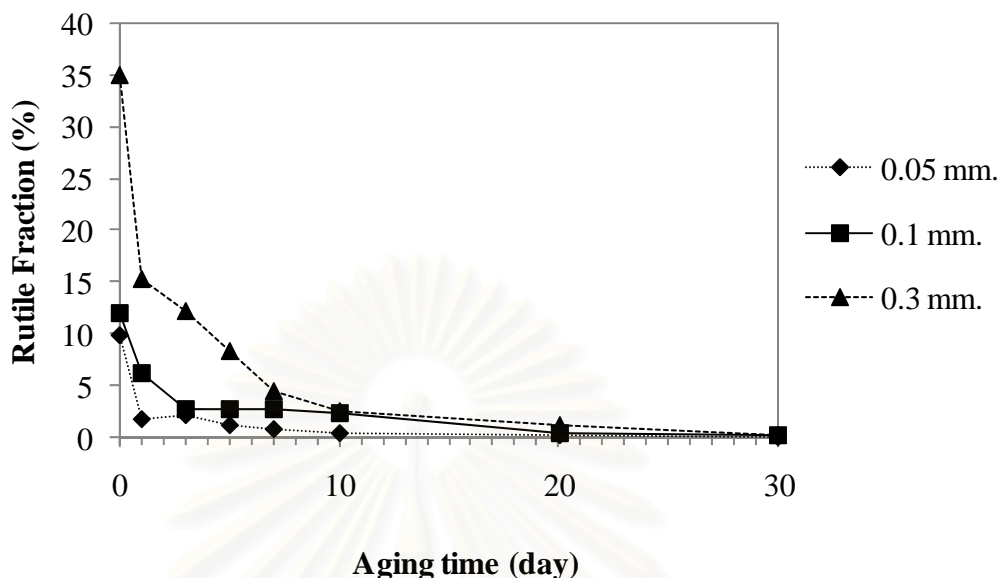


Figure 4.18 Plot of aging time versus fraction of rutile in the titania nanofibers aged under 100% RH condition, using various thickness of fiber layer. The fibers were subsequently calcined at 500°C.

From Figure 4.18, it is found that the rutile fraction in thick layer (i.e. 0.3 mm) of calcined titania fibers is obviously much higher than those in thin layer (e.g. 0.1 and 0.05 mm) when no aging was applied, i.e. aging time of 0 day. Nevertheless, the fraction of rutile is decreased as the aging time is prolonged. Thin layer of fibers at 0.05 and 0.1 mm tend to have rutile fraction below 5% after aging for 3 days. For thick layer of electrospun fibers, longer aging time is required to reduce rutile fraction to low level. However, after aging under 100% RH for 7 days, the fraction of rutile gradually decreased for all fiber thicknesses until the value reaches almost zero after 30 days of aging. However, aging fibers for all thicknesses under this condition results in the change of fibers structure as seen in Figure 4.11(d). Though there is no previous research for the true mechanism regarding factors affecting rutile formation, it is suggested that the as-spun fibers with various layer thicknesses have different properties from each others due to the difference in moisture diffused into fiber layer and the remaining acid in the fiber layer which subsequently affect the hydrolysis and condensation of titania.

4.3 Effects of Acetic Acid Addition on Properties of Titania Nanofibers

There are many parameters that affects the properties of titania. One important factor affecting the properties of titania nanofibers is the addition of carboxylic acid into the spinning solution. In this work, acetic acid was chosen and added into the spinning solution in different amount. Many properties were investigated such as gelation time of the spinning solution, crystallite sizes, and phase transition temperature of titania fibers.

4.3.1 Effects of acetic acid on gelation time

In the preparation of the spinning solution, the solution prepared without acetic acid addition became white and cloudy solution, while the solution prepared with acetic acid addition became clear and yellow solution. These evidences indicate the difference of solution properties. This hypothesis can be further proved by studying the gelation time of the as-prepared solution. The gelation time can be determined by the rapidly change in viscosity of the solution. Plots between solution aging time and viscosity for the solution with and without acetic acid addition are shown in Figure 4.19. It shows that the addition of acetic acid also influences the gelation time of the solution prepared from sol-gel method. Therefore, it is confirmed that the presence of acetic acid causes a change of the solution properties.

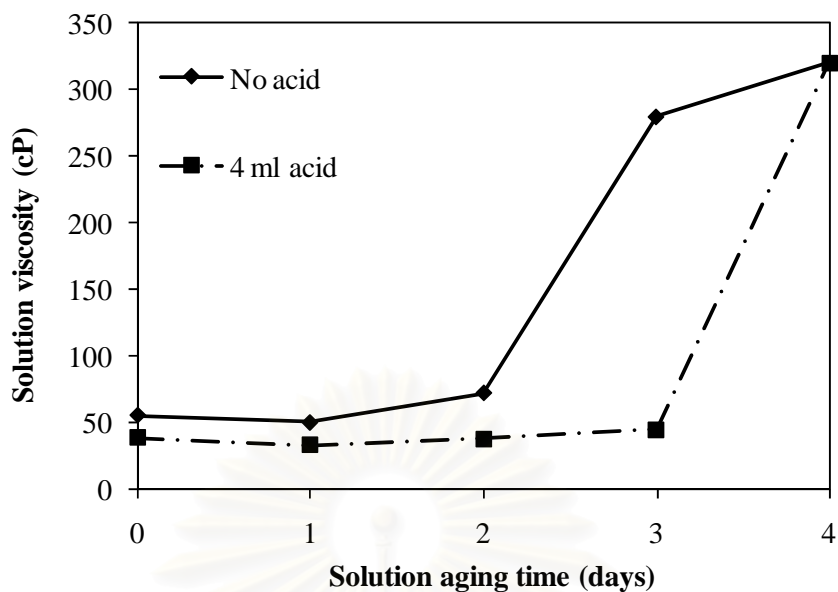


Figure 4.19 Plot between solution aging time and viscosity of the spinning solution prepared by sol-gel method with and without the addition of acetic acid.

According to Figure 4.19, there is a difference in the initial viscosity of the solution with and without acid addition due to acetic acid itself. For the solution prepared with no acetic acid, sol transforms into gel after 2 days. On the other hand, after the addition of 4 ml of acetic acid, the solution can be stable for 3 days. This result is consistent with the previous research on the stability of TEOS by controlling the amount of acetic acid addition (Sivananda and Jada 1987). Moreover, the previous research from Gopal and his coworkers (1997) has shown that both hydrolysis and condensation reactions occur well at low pH. The presence of acid causes proton absorption on the surface of the nuclei, making them positively charged. The resulting electrostatic repulsion causes larger particles to break down into smaller particle until an equilibrium size is reached. At this stage, the particles are sufficiently small such that little light scattering occurs, and the suspension becomes an optically transparent sol. The addition of acid is not only promotes hydrolysis, it also causes a marked decrease in the rate of condensation (Livage et al. 1988). Without the presence of acid, the condensation rate could not be controlled, resulting in an increase of the solution viscosity faster than sol with the addition of acetic acid. Therefore, it is clearly indicated that the presence of acetic acid can improve the stability of sol.

4.3.2 Effects of acetic acid on morphology of titania nanofibers

Adding acetic acid in certain amount can affect morphology of electrospun titania nanofibers. Figure 4.20 shows SEM micrographs of as-spun TiO_2/PVP composite nanofibers with and without acetic acid addition. In both cases, the fibers were electrospun after the spinning solution was aged for 3 hours to make sure that the solution viscosity is suitable for the electrospinning process, using a rotating collector. It is obviously seen that the fibers fabricated from the spinning solution without acetic acid addition appear to consist of many beads. When the proper amount of acetic acid is added (i.e. 3 ml) to the spinning solution, the obtained as-spun fibers appear to be uniform in both size and surface texture. Size distributions of fiber diameter for both cases are shown in Figure 4.21.

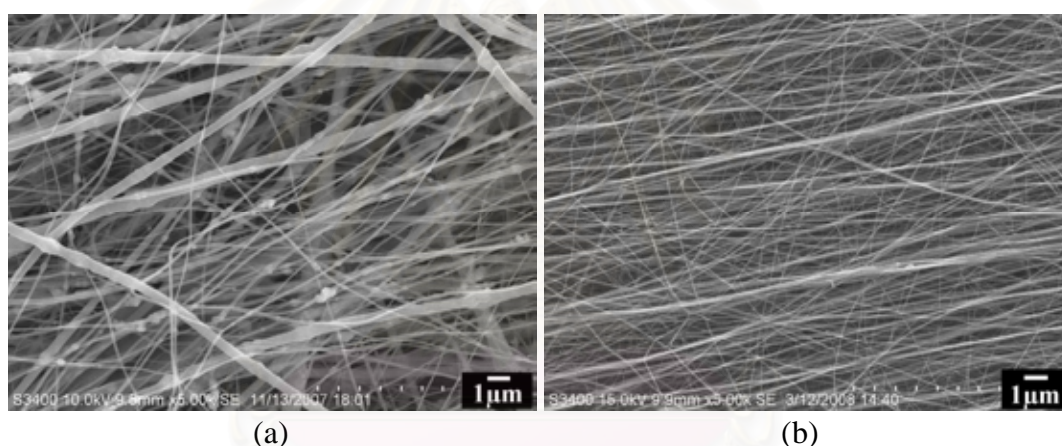


Figure 4.20 SEM micrographs of as-spun TiO_2/PVP composite nanofibers fabricated from the spinning solution prepared with no acetic acid addition (a) and with 3 ml of acetic acid (b). Noted that the PVP concentration and electric field employed were 10 wt.% and 16 kV/7cm, respectively.

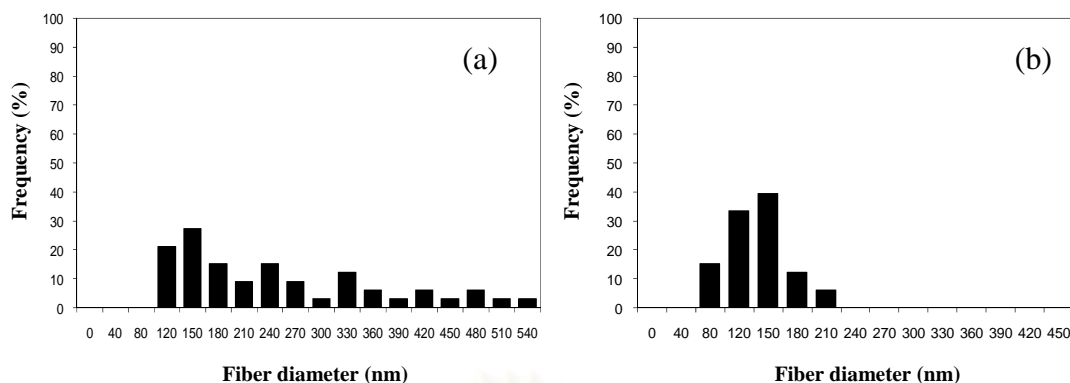


Figure 4.21 Frequency distribution for diameter of as-spun TiO_2/PVP composite nanofibers fabricated from the spinning solution prepared with no acetic acid addition (a) and with 3 ml of acetic acid addition (b).

According to the Figure 4.21, the as-spun fibers without acetic acid addition have much broader distribution in diameter than the fibers with acetic acid addition. This is mainly the result from the difference in viscosity of the spinning solution, as shown in Table 4.2, which also agrees with the results from previous research (Fong et al. 1999). Moreover, the addition of acetic acid can improve the stability of the spinning solution as described in Section 4.3.1. For the fibers calcined at 500°C , the morphology of the fibers is shown in Figure 4.22.

Table 4.2 Viscosity of the spinning solution.

Amount of acetic acid added (ml)	pH of the solution	Viscosity (cP)
0	6.7	55
3	3.5	38.5

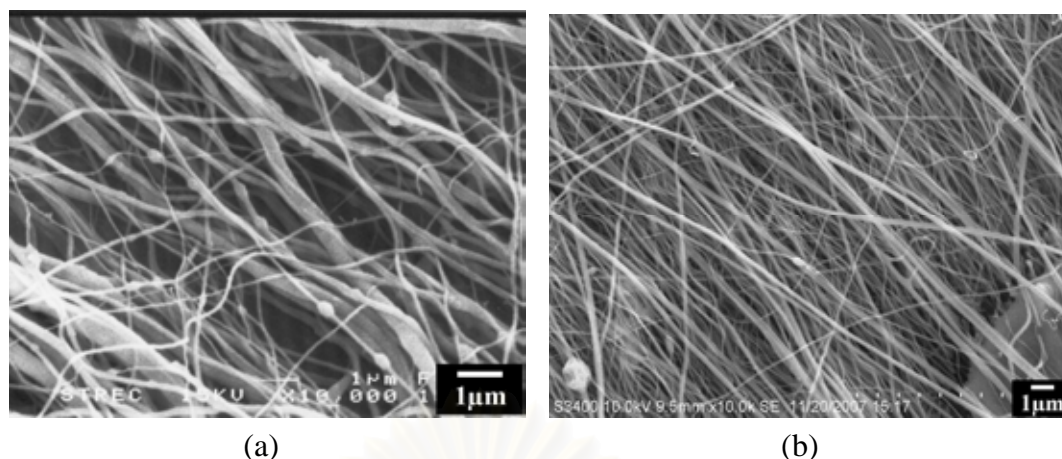


Figure 4.22 SEM micrographs of titania nanofibers fabricated from the spinning solution prepared with no acetic addition (a) and with 3 ml of acetic acid addition (b), and subsequently calcined at 500°C for 3 hours. Noted that the PVP concentration and electric field employed were 10% wt. and 16 kV/ 7cm, respectively.

Figure 4.22 shows SEM micrographs of titania nanofibers calcined at 500°C. The results appear to be the same trend as the as-spun fibers described earlier. For size distribution for diameter of the calcined fibers shown in Figure 4.23, it is seen that the fibers prepared with acetic acid addition have narrow size distribution. This is the consequent result from different size distribution of the as-spun fibers. It should be noted that the average size of the calcined fibers is smaller than that of the as-spun fibers due to the removal of PVP as described in the previous section.

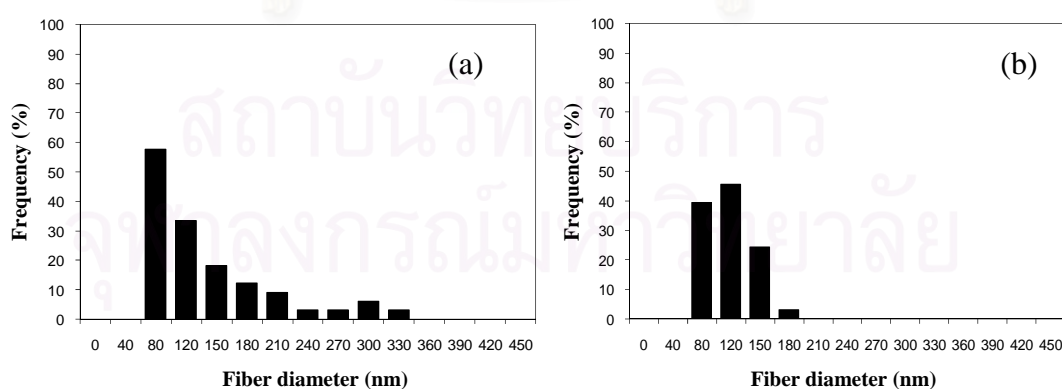


Figure 4.23 Frequency distribution for diameter of titania nanofibers fabricated from the spinning solution prepared with no acetic addition (a) and with 3 ml of acetic acid (b), and subsequently calcined at 500°C for 3 hours.

4.3.3 Effects of amount of acetic acid on phase structure of titania nanofibers

The influences of acetic acid affect not only the morphology of the as-spun titania fibers, but the phase structure of fibers after calcination as well. Figure 4.24 shows X-ray diffraction patterns for the fibers prepared by using various amounts of acetic acid added into the spinning solution and calcined at 500°C for 3 hours. It is obviously seen that the titania nanofibers calcined at this temperature contains mixed phase of anatase and rutile, which corresponds to the result presented in Section 4.1.2. The higher the amount of acetic acid added into the spinning solution, the higher the fraction of rutile in the calcined products, as clearly seen in Table 4.3. It should be noted that the fraction of rutile was calculated from the equation reported in the Section 4.1.2.

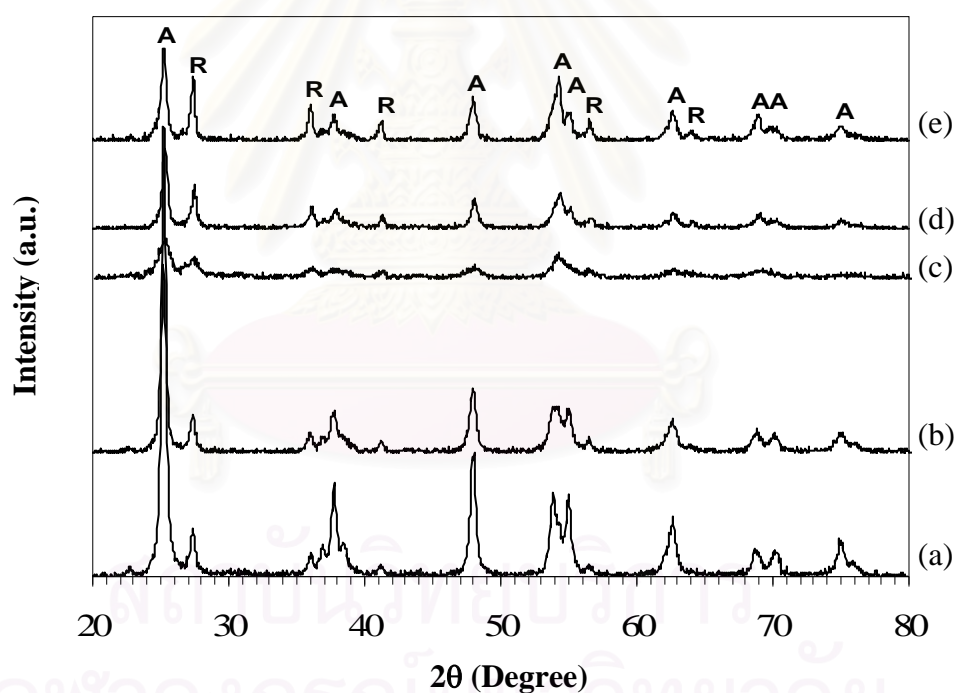


Figure 4.24 X-ray diffraction patterns of titania nanofibers prepared with different amount of acetic acid added into the spinning solution: (a) no acetic acid added, (b) 1 ml, (c) 2 ml, (d) 3 ml, and (e) 4 ml of acetic acid added. The as-spun fibers were calcined at 500°C for 3 hours and the thickness layer of fiber was controlled at 0.3 mm.

Table 4.3 Phase structure and rutile fraction of titania nanofibers after calcination at 500°C for 3 hours.

Amount of acetic acid added (ml)	pH of the solution	Phase structure	Fraction of rutile* (%)
-	6.7	Anatase/Rutile	14
1	4.6	Anatase/Rutile	18
2	3.8	Anatase/Rutile	33
3	3.5	Anatase/Rutile	35
4	3.3	Anatase/Rutile	41

*The thickness layer of fiber was controlled at 0.3 mm throughout the experiments.

To describe the influence of acetic acid addition on the formation of anatase and rutile, it is found that the results presented in Figure 4.24 and Table 4.3 support the model proposed by Gopal and coworkers (1997). The acid concentration affects the phase transformation of titania. The phase formation is governed by the rate of aggregation of the octahedral complexes. In the presence of acid, the aggregation processes are inhibited due to repulsion from adsorbed H^+ ions. The higher the acid concentration, the larger the repulsion, results in the slower aggregation. Rutile can be formed from the heat treatment of aggregates in this state. At higher pH, the repulsive forces are less pronounced, promoting faster aggregation and therefore the formation of anatase. However, for low calcination temperature (i.e. 250°C), the fibers are still amorphous although high amount of acetic acid (e.g. 4 ml) is added to the spinning solution (see Figure 4.25). It shows that, at this low temperature, the energy is not high enough to overcome the activation energy for the crystallization of titania.

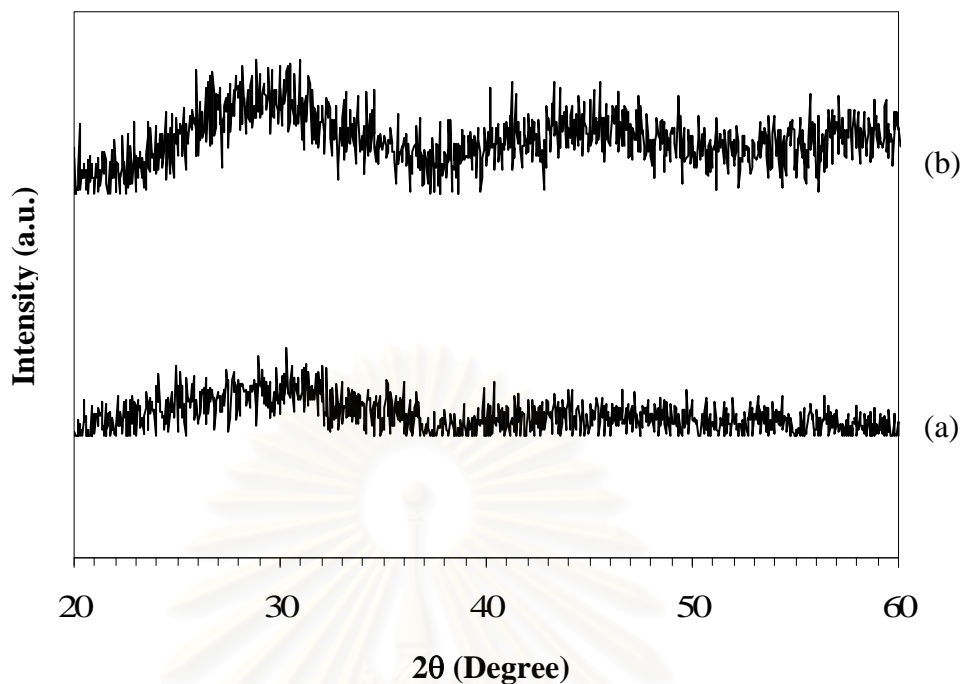


Figure 4.25 X-ray diffraction patterns of titania nanofibers prepared with different amount of acetic acid added into the spinning solution: (a) no acetic acid added, and (b) 4 ml of acetic acid added. The as-spun fibers were calcined at 250°C for 3 hours and the thickness layer of fiber was controlled at 0.3 mm.

For the calcination at the temperature of 400°C, effect of the acetic acid addition on the crystallization of titania can also be observed. According to the XRD analysis results shown in Figure 4.26, titania fibers prepared with no acetic acid appears to be pure anatase. After adding higher amount of acid into the spinning solution, the intensity of peak at 27.4° corresponding to rutile phase in the calcined fibers increases. The highest fraction of rutile about 12% is found when 4 ml of acetic acid is added to the spinning solution. It is also obvious that the sample calcined at this temperature still contains anatase as the most prominent phase.

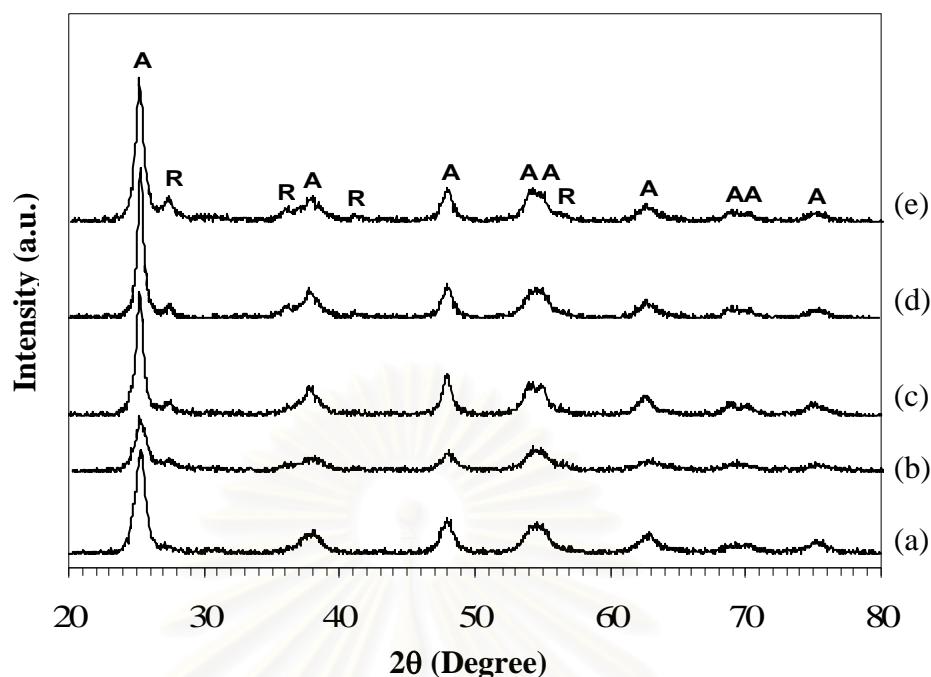


Figure 4.26 X-ray diffraction patterns of titania nanofibers prepared with different amount of acetic acid added into the spinning solution: (a) no acetic acid added, (b) 1 ml, (c) 2 ml, (d) 3 ml, and (e) 4 ml of acetic acid added. The as-spun fibers were calcined at 400°C for 3 hours and the thickness layer of fiber was controlled at 0.3 mm.

When the calcination temperature is increased above 500°C (i.e. 750°C), anatase is still found (with 89% of rutile fraction) in the fibers prepared with no acetic acid addition, as seen from the X-ray diffraction pattern in Figure 4.27. However, the peak at 25.4° corresponding to anatase gradually disappears with higher amount of acid added. Pure rutile is found in the calcined fibers prepared with maximum amount of acetic acid addition (i.e. 4 ml). It is suggested that the presence of acetic acid suppress the formation of anatase at high temperature.

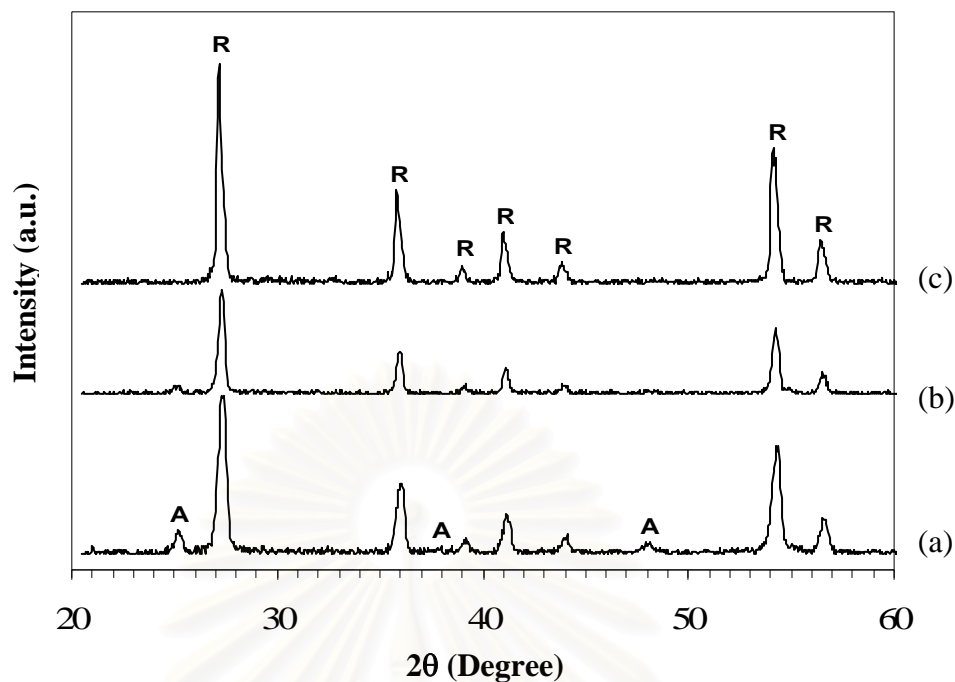


Figure 4.27 X-ray diffraction patterns of titania nanofibers prepared with different amount of acetic acid added into the spinning solution: (a) no acetic acid added, (b) 3 ml, and (c) 4 ml of acetic acid added. The as-spun fibers were calcined at 750°C for 3 hours and the thickness layer of fiber was controlled at 0.3 mm.

The presence of acetic acid in titania nanofibers is confirmed by FT-IR spectra. Figure 4.28 shows FT-IR spectra of the as-spun TiO₂/PVP composite nanofibers. Nevertheless, the broad peak at 1,550 cm⁻¹ corresponding to -COO- vibration mode of carboxyl group (Kim et al. 2005) confirms the presence of acetic acid only in the fibers prepared with acid addition. The strong peak at 1,676 cm⁻¹ corresponding to the stretching mode of water and hydroxyl group, as well as the -CH₂ bonding of PVP observed at 1,430 and 1,290 cm⁻¹ (Tang et al. 2007) are observed in fibers fabricated with and without acetic acid addition.

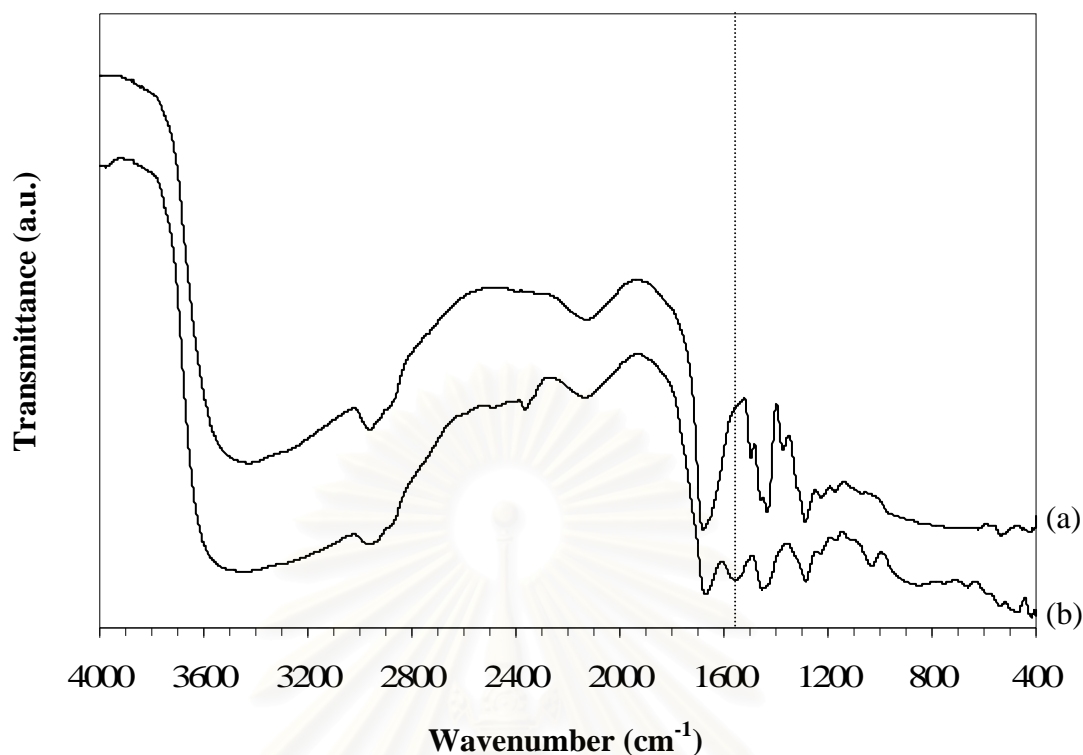


Figure 4.28 FT-IR spectra of the as-spun titania nanofibers prepared without acetic acid addition (a) and with 3 ml of acetic acid addition (b).

4.3.4 Effects of acetic acid on crystallite size of titania nanofibers

The addition of acetic acid also affects the crystallite size of titania nanofibers after calcination. As negligible lattice strain is expected in the anatase, the Scherrer equation provides a good approximation of the average crystallite size from the peak broadening observed in the diffraction peak profiles. In this study, the peak located near 2-theta of about 25° was used as basis for the calculation. It should be noted that this estimated crystallite size is volume averaged in the direction perpendicular to the plane of diffraction, and therefore provides no information about the nanocrystallite size distribution.

Transmission electron micrographs of the calcined titania fibers prepared with and without acetic acid are presented in Figure 4.29. The particles embedded within the fibers prepared with no acid addition have larger diameter and agglomerate more heavily than those in the fibers with the presence of acid. Table 4.4 shows the average crystallite size of the fibers calculated from broadening X-ray diffraction peak. The

crystallite size of anatase within the fibers prepared with no acid addition is larger than that of the fibers with the presence of acid. It is suggested that, if the pH value of the solution is low enough, the nucleation of rutile may occur without the formation of anatase as intermediate phase. The SAED patterns show that both fibers prepared with and without acid addition are polycrystalline.

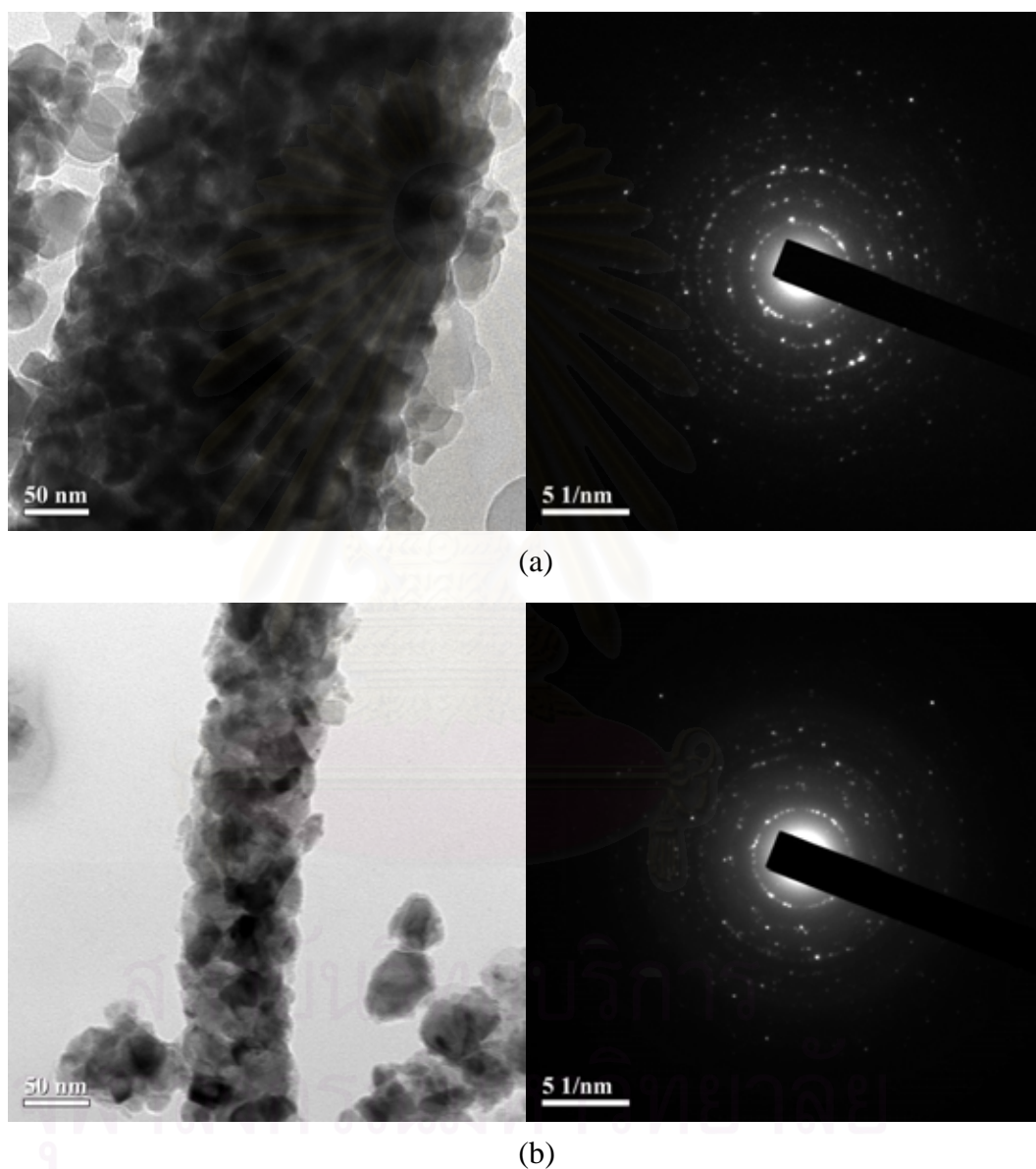


Figure 4.29 TEM micrographs of titania nanofibers prepared with different amount of acetic acid added into the spinning solution: (a) no acetic acid added, and (b) 4 ml of acetic acid added. The as-spun fibers were calcined at 500°C for 3 hours.

Table 4.4 Crystallite size of titania nanofibers after calcination at 500°C for 3 hours prepared with various amount of acetic acid added into the spinning solution.

Amount of acetic acid added (ml)	Phase structure	Crystallite size of anatase^a (nm)	Particle size^b (nm)
No acetic acid	Anatase/Rutile	24	28
4	Anatase/Rutile	20	21

^a calculated from XRD line broadening.

^b measured from TEM micrographs.

4.3.5 Effects of calcination temperature on crystallite size of titania nanofibers

The crystallite size of particle is affected by calcination temperature. The crystallinity increases with an increase of the calcination temperature can be determined from XRD analysis because higher ordering in the structure of titania nanofibers makes X-ray peak to be sharper and more narrow. Table 4.5 and 4.6 show the calculated crystallite size of titania nanofibers after calcined at various temperatures. For the fibers prepared with or without the addition of acetic acid and calcined at 250°C, the fibers are still amorphous as described from the XRD diffraction result in Figure 4.25. After calcination at high temperature, the crystallite size of titania fibers increases. The results are the same for both fibers prepared with and without acetic acid. It is suggested that the growth of crystallite size is due to the phase transformation of anatase to rutile. After the energy is closed to the activation energy for phase transformation, rutile nuclei are formed within the anatase and grow in size (Mohammadi et al. 2007). Therefore, crystallites should grow to the critical nuclei size before phase transformation occurs.

Table 4.5 Crystallite size of titania nanofibers prepared with no acetic addition and calcined at various temperatures.

Calcination temperature (°C)	Phase Structure	Crystallite size of anatase ^a (nm)	Particle size ^b (nm)
250	Amorphous	-	-
400	Anatase	11	13
500	Anatase/Rutile	24	28
750	Anatase/Rutile	44	72

^a calculated from XRD line broadening.

^b measured from TEM micrographs.

Table 4.6 Crystallite size of titania nanofibers prepared with 4 ml of acetic acid and calcined at various temperatures.

Calcination temperature (°C)	Phase Structure	Crystallite size of anatase ^a (nm)	Particle size ^b (nm)
250	Amorphous	-	-
400	Anatase/Rutile	13	14
500	Anatase/Rutile	20	21
750	Rutile	-	62

^a calculated from XRD line broadening.

^b measured from TEM micrographs.

CHAPTER V

CONCLUSIONS AND RECOMMENDATIONS

5.1 Conclusions

In this work, effects of many parameters in sol-gel and electrospinning processes to fabricate titania nanofibers were investigated. The conclusions of the present research are the following:

1. TiO₂/PVP composite titania nanofibers can be successfully prepared from combination of sol-gel and electrospinning techniques. After calcination at 500°C, crystallization takes place and results in the mixed phase of anatase and rutile within titania nanofibers.

2. Changing the electrospinning collector plate from a flat collector to a rotating collector led to the fabrication of the axially aligned titania nanofibers with average diameter of 120 nm after calcination.

3. Aging of the as-spun titania nanofibers under high level of humidity results in the reduction of rutile in the fibers after calcination at 500°C. Nevertheless, the morphology of the titania nanofibers is changed at high level of humidity. Thickness of fiber layer is also one of the parameters affecting the effectiveness of the aging process.

4. Addition of acetic acid into the spinning solution can improve stability of the solution and reduce gelation time. Without the presence of acetic acid, it can affect morphology of the fibers such that a broad size distribution and rough fiber surfaces are obtained.

5. Increased amount of acetic acid in the spinning solution led to the increased in rutile fraction in the calcined titania nanofibers.

6. The presence of acetic acid in the spinning solution affects both crystallite size of anatase and the degree of agglomeration of titania crystals within the fibers.

5.2 Recommendations for the Future Studies

From the previous conclusions, the following recommendations for the future studies are proposed.

1. The mechanism of aging conditions on phase transformation of titania nanofibers should be investigated in detail.

2. Although it is found that addition of acetic acid have many effects on phase transformation of fibers, other parameters such as TTIP and PVP concentration should be investigated as well.

3. The photocatalytic activity of axially aligned titania nanofibers with different amount of rutile fraction should be investigated.

4. The influence of the secondary metal dopant on phase transformation of titania nanofibers should be investigated.

5. The applications of titania nanofibers should be investigated.

REFERENCES

- Astrup E., Kristin, S. (1994). Saturated Salt Solutions for Humidity Control of Showcases Conditions for a Successful System. ICOM Committee for Cons., 8th Triennial Mtg
- Awati, P., S., Awate S., V., Shah, P., P., and Ramaswamy, V. (2003) Photocatalytic decomposition of methylene blue using nanocrystalline anatase titania prepared by ultrasonic technique. Catalysis Communications **4**(8): 393-400.
- Balasubramanian, G., Dionysio, D., D., Suidan, M., T., Subramanian, V., and Baudin, I. (2003). Titania powder modified sol-gel process for photocatalytic applications. Journal of Materials Sciences **38**: 823-831.
- Banfield, J., F., and Zhang, H. (2000). Phase transformation of nanocrystalline anatase-to-rutile via combined interface and surface nucleation Journal of Materials Research **15**(2): 437-448.
- Baumgarten, P., K. (1971). Electrostatic spinning of acrylic microfibers. Journal of Colloid and Interface Science **36**: 71.
- Bornat, A. (1987). U.S. Patent, 4,689,186.
- Cannon, S., A., Morelli, A., Pressler, W., Warner, C., J., and Guarrera, D. (2005). The low temperature processing of titanium dioxide films by the addition of trimesic acid. Journal of Sol-Gel Science and Technology **36**(2): 157-162
- Cheng, P., Zheng, M., Jin, Y., Huang, Q., and Gu, M. (2003). Preparation and characterization of silica-doped titania photocatalyst through sol-gel method. Materials Letters **57**: 2989-2994.
- Chun, I., Reneker, D., H., Fong, H., Fang, X., Deitzel, J., Tan, N., B., and Kearns, K. (1999). Carbon nanofibers from polyacrylonitrile and mesophase pitch. Journal of Advanced Materials **31**(1): 36-41.

- Dagan, G., and Tomkiewicz, M. (1994). Preparation and characterization of TiO₂ aerogel for use as photocatalysis. Journal of Non-Crystalline Solids **175**(2-3): 294-302.
- Ding, Z., Hu, X., Lu, G., Q., Yue, P.-L. and Greenfield, P., F. (2000). Novel silica gel supported TiO₂ photocatalyst synthesized by CVD method. Langmuir **16**: 6216-6222.
- Fox, M., A., and Dulay, M., T. (1993). Heterogeneous photocatalysis Chemical Reviews **93**: 341.
- Fujishima, A., Hashimoto, K., and Watanabe, T. (1999). TiO₂ fundamentals and applications BKC, Inc.
- Ding, X., Z., Qi, Z., Z., and He, Y., Z. (1995). Effect of hydrolysis water on the preparation of nano-crystalline titania powders via a sol-gel process. Journal of Materials Science Letters **14**(1): 21-22
- Doshi, J., and Reneker, D., H. (1995). Electrospinning process and applications of electrospun fibers. Journal of Electrostatics **35**(2-3): 151-160.
- Ertl, G., Knozinger, H. and Weitkamp, J. (1999). Preparation of solid catalysts Wiley VCH.
- Fang, X., and Reneker, D., H. (1997). DNA fibers by electrospinning. Journal of Macromolecular Science and Physics **B36**: 169-173.
- Fong, H., Chun, I., and Reneker, D., H. (1999). Beaded nanofibers formed during electrospinning. Polymer **40**: 4585-4592.
- Fong, H., and Reneker, D., H. (1999). Elastomeric nanofibers of styrene-butadiene-styrene triblock copolymer. Journal of Polymer Science Part B: Polymer Physics **37**(24): 3488-3493.
- Formhals, A. (1934). U.S. Patent, 1,975,504.

Formhals, A. (1937). U.S. Patent, 2,077,373.

Formhals, A. (1939a). U.S. Patent, 2,158,416.

Formhals, A. (1939b). U.S. Patent, 2,160,962.

Formhals, A. (1940a). U.S. Patent, 2,187,306.

Formhals, A. (1940b). U.S. Patent, 2,323,025.

Formhals, A. (1944). U.S. Patent, 2,349,950.

Fu, X.Z., Clark, L.A., Yang, Q. and Anderson, M.A. (1996) Enhanced photocatalytic performance of titania-based binary metal oxides: $\text{TiO}_2/\text{SiO}_2$ and $\text{TiO}_2/\text{ZrO}_2$. Environmental Science & Technology **30**: 647-653.

Gamboa, Julio, A., and Daniel, M., Pasquevich. (1992). Effect of chlorine atmosphere on the anatase-rutile transformation. Journal of the American Ceramic Society **75**(11): 2934-2938.

Gladding, E., K. (1939). U.S. Patent, 2,168,027.

Gopal, M., Chan, W.J.M., and DeJonghe, L.C. (1997). Room temperature synthesis of crystalline metal oxides. Journal of Materials Science **32**: 6001-6008.

Gouma, P., Kalyanasundaram, K., and Bishop, A. (2006). Electrospun single-crystal MoO_3 nanowires for biochemistry sensing probes. Journal of Materials Research **21**(11): 2904-2910.

Gribb, Amy, A., and Banfield, J., F. (1997). Particles size effects on transformation kinetics and phase stability in nanocrystalline TiO_2 . American Mineralogist **82**: 717-728.

- Grzmil, B., Rabe, M., Kic, B., and Lubkowski, K. (2007). Influence of phosphate, potassium, lithium, and aluminium on the anatase-rutile phase transformation. Industrial & Engineering Chemistry Research **46**: 1018-1024.
- He, C., Yu, Y., Hu, X., and Larbot, M. (2002). Influence of silver doping on the photocatalytic activity of titania films. Applied Surface Science **200**: 239-247.
- Hong, S., S., Lee, M., S., Park, S., S., and Lee, G., D. (2003). Synthesis of nanosized TiO₂/SiO₂ particles in the microemulsion and their photocatalytic activity on the decomposition of p-nitrophenol. Catalysis Today **87**: 99-105.
- Huang, Z., Zhang, Y., Z., Kotaki, M., and Ramakrishna, S. (2003). A review on polymer nanofibers by electrospinning and their applications in nanocomposites. Composites Science and Technology **63**: 2223-2253.
- Iwamoto, S., Tanakulrungsank, W., Inoue, M., Kagawa, K., and Praserttham, P. (2000). Synthesis of large-surface area silica-modified titania ultrafine particles by the glycothermal method. Journal of Materials Science Letter **19**: 1439-1443.
- Jung, K., Y., and Park, S., B. (1999). Anatase-phase titania: preparation by embedding silica and photocatalytic activity for the decomposition of trichloroethylene. Journal of Photochemistry and Photobiology A: Chemistry **127**: 117-122.
- Jung, K., Y., and Park, S., B. (2000). Enhanced photoactivity of silica-embedded titania particles prepared by sol-gel process for the decomposition of trichloroethylene. Applied Catalysis B: Environmental **25**: 249-256.
- Kato, K., Tsuzuki, A., Torii, Y., Taoda, H., and Kato, T. (1995). TiO₂ coating photocatalysts with nanostructure and preferred orientation showing excellent activity for decomposition of aqueous acetic acid. Journal of Materials Science **30**(3): 837-841

- Kim, J., and Reneker, D., H. (1999). Mechanical properties of composites using ultrafine electrospun fibers. Polymer Composites **20**(1): 124-131.
- Kim, S., J., Park, S., D., and Jeong, Y., H. (1999). Homogeneous Precipitation of TiO₂ Ultrafine Powders from Aqueous TiOCl₂ Solution. Journal of the American Ceramic Society **82**(4): 927-932.
- Kwon, C. H., Shin, H., Kim, J. H., Choi, W. S. and Yoon, K. H. (2004). Degradation of methylene blue via photocatalysis of titanium dioxide. Materials Chemistry and Physics **86**: 78-82.
- Larrondo, L. and Manley, R. S. J. (1981a). Electrostatic fiber spinning from polymer melts. I. and Experimental observations on fiber formation and properties. Journal of Polymer Science: Polymer Physics Edition **19**: 909.
- Larrondo, L. and Manley, R. S. J. (1981b). Electrostatic fiber spinning from polymer melts. II. Examination of the flow field in an electrically driven jet. Journal Polymer Science: Polymer Physics Edition **19**: 921.
- Larrondo, L. and Manley, R. S. J. (1981c). Electrostatic fiber spinning from polymer melts. III. Electrostatic deformation of pendant drop of polymer melt. Journal Polymer Science: Polymer Physics Edition **19**: 933.
- Li, D., and Xia, Y. (2003). Fabrication of Titania Nanofibers by Electrospinning. Nano Letters **3**(4): 555-560.
- Li, D., and Xia, Y. (2004). Electrospinning of nanofibers: reinventing the wheel? Advanced Materials **16**(14): 1151-1170.
- Li, D., McCann, T., J., and Xia, Y. (2006). Electrospinning: a simple and versatile technique for producing ceramic nanofibers and nanotubes. Journal of the American Ceramic Society **89**(6) 1861-1869.

- Montoya, I., A., Viveros, T., Dominguez, J., M., Canales, L., A., and Schifer, I. (1992). On the effect of the sol-gel synthesis parameters on textural and structural characteristics of TiO₂. Catalysis Letter **15**: 207-217.
- Moriguchi, I., Maeda, H., Teraoka, Y., and Kagawa, S. (1997). Preparation of a TiO₂ nanoparticulate film using a two-dimensional sol-gel process. Journal of Materials Chemistry, **9**: 1050–1057.
- Music, S., Gotic, M., Ivanda, M., Popovic, S., Turkovic, A., Trojko, R., and Sekulic, A. (1997). Chemical and microstructural properties of TiO₂ synthesized by sol-gel procedure. Materials Science and Engineering B, **47**: 33-40.
- Othmer, K. (1999). Encyclopedia of Chemical Technology, Wiley interscience.
- Payakgul, W. (2002). Crystallization and precipitation mechanism of titanium dioxide under the solvothermal condition and the effect of second element on titanium dioxide. Chemical Engineering. Bangkok, Chulalongkorn University.
- Reneker, D., H., and Chun, I. (1996). Nanometre diameter fibres of polymer, produced by electrospinning. Nanotechnology **7**: 216-223.
- Rayleigh, F.R., S. (1882). Philosophical Magazine. **44**: 184.
- Sasamoto, T., Enomoto, S., Shimoda, Z., and Saeki, Y. (1993) Effect of hydrolysis conditions on thermal transformation of alkoxide-derived titanium dioxide. Journal of the Ceramic Society of Japan **101**(2): 230-232
- Simons, H., L. (1966). U.S. Patent, 3,280,229.
- Sivananda, S., J. (1987). Study of tetraethyl orthosilicate hydrolysis by in situ generation of water. Journal of the American Ceramic Society **70**(11): 298-300

- Song, K., C., and Pratsinis, S., E. (2000). Synthesis of bimodally porous titania powders by hydrolysis of titanium tetraisopropoxide. Journal of Materials Research **15**: 2322-2329.
- Srinivasan, G., and D., H., Reneker (1995). Structure and morphology of small diameter electrospun aramid fibers. Polymer International **36**(2): 195-201.
- Taylor, G., I. (1964). Disintegration of water drops in an electric field. Proceedings of the Royal Society of London A280: 383.
- Taylor, G., I. (1969). Electrically driven jets. Proceedings of the Royal Society of London A313: 453.
- Vertucci, C., W., Roos, E., E. (1993). Theoretical basis of protocols for seed storage II. The influence of temperature on optimal moisture levels. Seed Science Research, **3**: 201–213.
- Viswanathamurthi, P., Bhattarai, N., Kim, C., K., Kim, H., Y., and Lee, D., R. (2004). Ruthenium doped TiO₂ fibers by electrospinning. Inorganic Chemistry Communications **7**: 679-682.
- Vonnegut, B., and Neubauer, R., L. (1952). Production of monodisperse liquid particles by electrical atomization. Journal of Colloid Science **7**(6): 616-622.
- Watthananarun, J., Pavarajarn, V., and Supaphol, P. (2005). Titanium (IV) oxide nanofibers by combined sol–gel and electrospinning techniques: preliminary report on effects of preparation conditions and secondary metal dopant. Science and Technology of Advanced Materials **6**(3-4): 240-245.
- Watchel, R., E., and LaMer, V., K. (1962). The preparation and size distribution of some monodisperse emulsions. Journal of Colloid Science **17**(6): 531-564.

- Watson, S., Beydoun, D., Scott, J., and Amal, R. (2004). Preparation of nanosized crystalline TiO₂ particles at low temperature for photocatalysis. Journal of Nanoparticle Research **6**(2): 193-207.
- Wetchakun, N., and Phanichphant, S. (2008). Effect of temperature on the degree of anatase-rutile transformation in titanium dioxide nanoparticles synthesized by the modified sol-gel method. Current Applied Physics **8**: 343-346.
- Wu, J.H., Hao, S.C., Lin, J.M., Huang, M.L., Huang, Y.F., Lan, Z. and Li, P.J. (2008). Crystal morphology of anatase titania nanocrystals used in dye-sensitized solar cells. Crystal Growth & Design **8**: 247-252.
- Yang, J., Mei, S., and Ferreira, J.M., F. (2001). Hydrothermal synthesis of nanosized titania powders: influence of tetraalkyl ammonium hydroxides on particle characteristics. Journal of the American Ceramic Society **84**(8): 1696-1702.
- Yuan, Z., Y., Colomer, J., F., and Su, B., L. (2002). Titanium oxide nanoribbons. Chemical Physics Letters **363**: 362-366.
- Zeleny, J. (1935). The role of surface instability in electrical discharges from drops of alcohol and water in air at atmospheric pressure. Journal of the Franklin Institute **219**(6): 659-675.
- Zheng, M.P., Gu, M.Y., Jin, Y.P., and Jin, G.L. (2000). Preparation, structure and properties of TiO₂-PVP hybrid films. Materials Science and Engineering B-Solid State Materials for Advanced Technology **77**: 55-59.
- Zheng, M.P., Gu, M.Y., Jin, Y.P., Wang, H.H., Zu, P.F., Tao, T., and He, J.B. (2001). Effects of PVP on structure of TiO₂ prepared by the sol-gel process. Materials Science and Engineering B-Solid State Materials for Advanced Technology **87**: 197-201.

Zhu, K., R., Zhang, M.S., Hong, J., M., and Yin, Z. (2005). Size effect on phase transition sequence of TiO₂ nanocrystal. Materials Science and Engineering A. **403**: 87–93.



สถาบันวิทยบริการ
จุฬาลงกรณ์มหาวิทยาลัย



APPENDICES

สถาบันวิทยบริการ
จุฬาลงกรณ์มหาวิทยาลัย

APPENDIX A

CALCULATION OF THE CRYSTALLITE SIZE

Calculation of the crystallite size by Debye-Scherrer equation

The crystallite size was calculated from the width at half-height of the diffraction peak of XRD pattern using the Debye-Scherrer equation.

From Scherrer equation:

$$D = \frac{K\lambda}{\beta \cos \theta} \quad (\text{A.1})$$

where D = Crystallite size, Å
 K = Crystallite-shape factor = 0.9
 λ = X-ray wavelength, 1.5418 Å for CuK α
 θ = Observed peak angle, degree
 β = X-ray diffraction broadening, radian

The X-ray diffraction broadening (β) is the pure width of a powder diffraction, free of all broadening due to the experimental equipment. Standard α -alumina is used to observe the instrumental broadening since its crystallite size is larger than 2000 Å. The X-ray diffraction broadening (β) can be obtained by using Warren's formula.

From Warren's formula:

$$\beta^2 = B_M^2 - B_S^2 \quad (\text{A.2})$$

$$\beta = \sqrt{B_M^2 - B_S^2}$$

Where B_M = The measured peak width in radians at half peak height.

B_S = The corresponding width of a standard material.

Example: Calculation of the crystallite size of titania

$$\begin{aligned} \text{The half-height width of 101 diffraction peak} &= 0.93125^\circ \\ &= 0.01625 \text{ radian} \end{aligned}$$

$$\text{The corresponding half-height width of peak of } \alpha\text{-alumina} = 0.004 \text{ radian}$$

$$\begin{aligned} \text{The pure width} &= \sqrt{B_M^2 - B_S^2} \\ &= \sqrt{0.01625^2 - 0.004^2} \\ &= 0.01577 \text{ radian} \end{aligned}$$

$$\beta = 0.01577 \text{ radian}$$

$$2\theta = 25.56^\circ$$

$$\theta = 12.78^\circ$$

$$\lambda = 1.5418 \text{ \AA}$$

$$\begin{aligned} \text{The crystallite size} &= \frac{0.9 \times 1.5418}{0.01577 \cos 12.78} = 90.15 \text{ \AA} \\ &= 9 \text{ nm} \end{aligned}$$

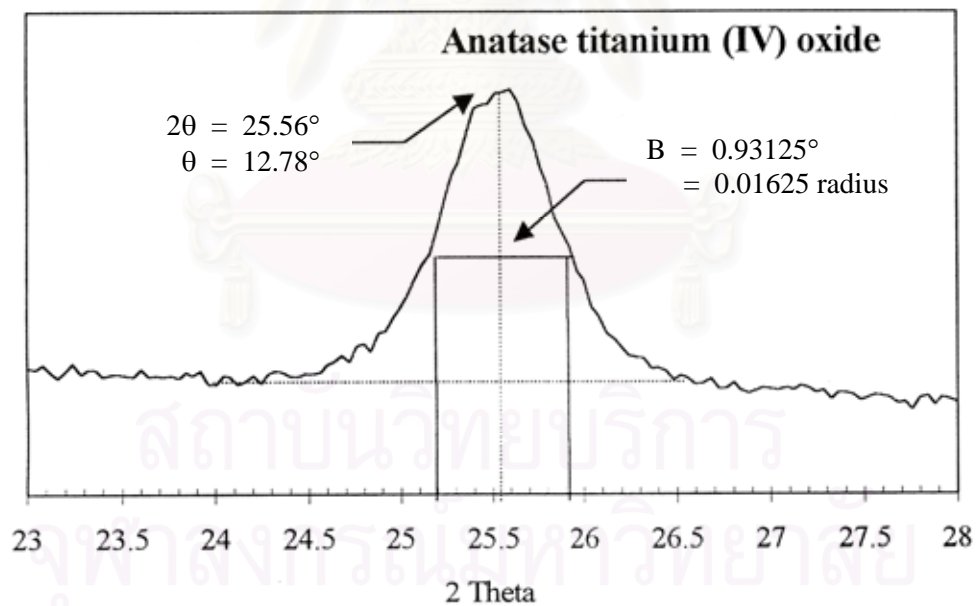


Figure A.1 The 101 diffraction peak of titania for calculation of the crystallite size

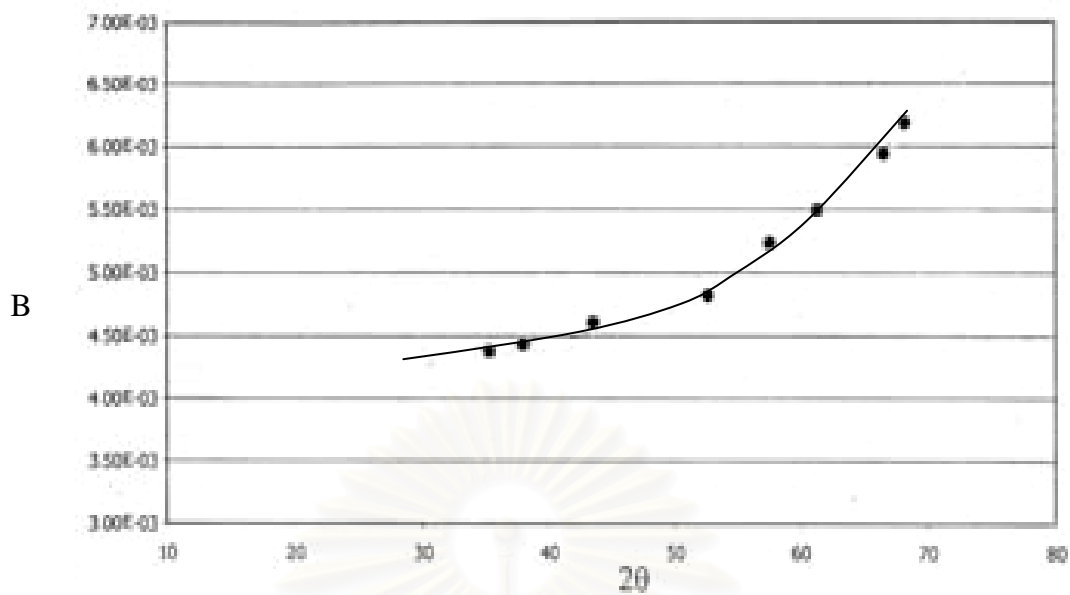


Figure A.2 The plot indicating the value of line broadening due to the equipment. The data were obtained by using α -alumina as standard.

สถาบันวิทยบริการ
จุฬาลงกรณ์มหาวิทยาลัย

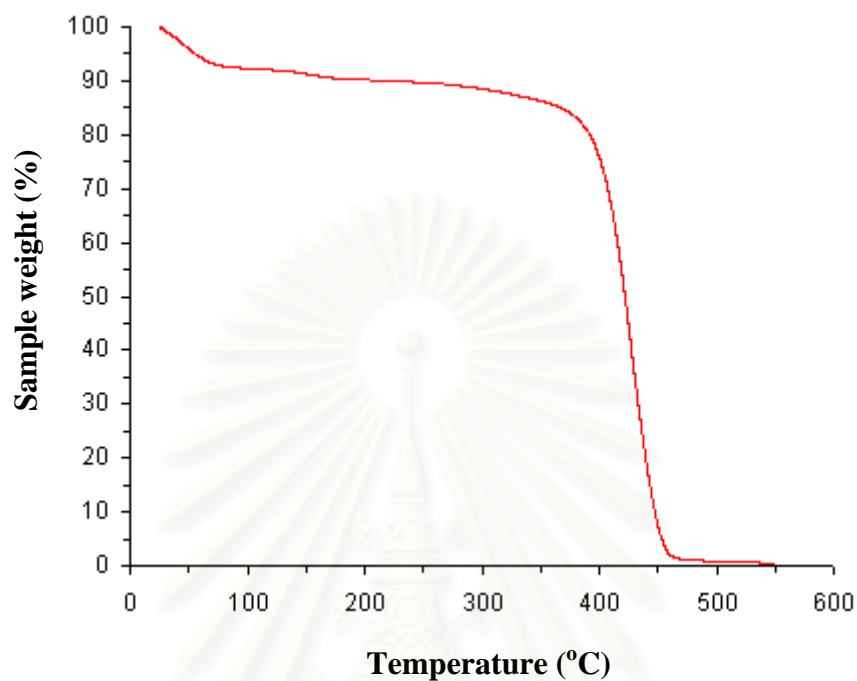
APPENDIX B**CHEMICAL PROPERTIES OF PVP NANOFIBERS**

Figure B.1 TGA analysis of PVP under O₂ atmosphere using heating rate at 10°C/min

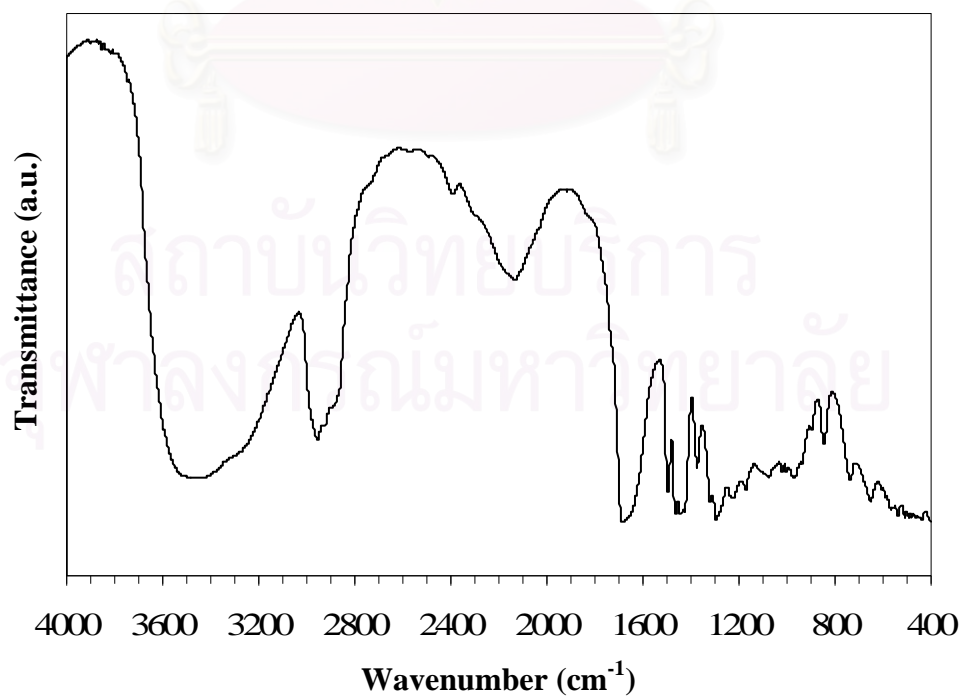


Figure B.2 FT-IR spectra of PVP nanofibers

APPENDIX C

SEM IMAGES OF PVP NANOFIBERS AGING UNDER 100% RH

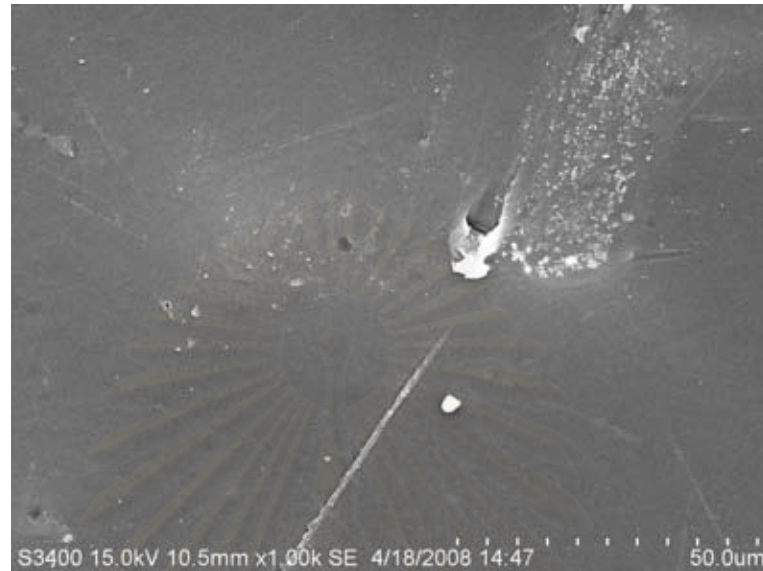


Figure C.1 SEM image of pure PVP nanofibers aging under 100% RH for 24 hours (1,000x magnification). It should be noted that the fiber thickness layer was controlled at 0.1 mm.

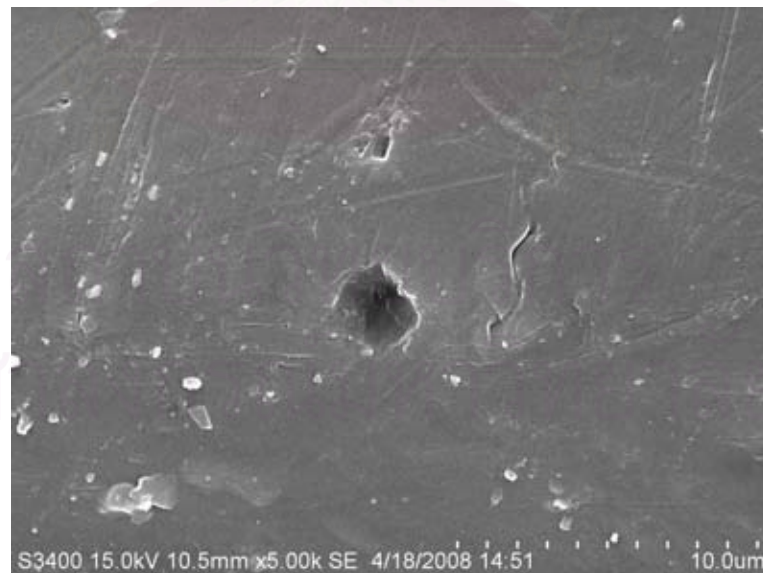


Figure C.2 SEM image of pure PVP nanofibers aging under 100% RH for 24 hours (5,000x magnification). It should be noted that the fiber thickness layer was controlled at 0.1 mm.

APPENDIX D

LIST OF PUBLICATION

1. Jaturon Supapol, Pitt Supaphol, and Varong Pavarajarn. Effects of aging conditions on the morphology and phase transformation behavior of electrospun titania nanofibers. The 17th Thailand Chemical Engineering and Applied Chemistry Conference, Chiang Mai, Thailand, October 29-30, 2007.



สถาบันวิทยบริการ
จุฬาลงกรณ์มหาวิทยาลัย

ผลของสภาวะการบ่มต่อลักษณะสัณฐานและพฤติกรรมการเปลี่ยนเฟสของ เส้นใยไททานเนียมขนาดนาโนที่สังเคราะห์โดยวิธีอิเล็กโตรสปินนิง

จาตุรนต์ ศุภผล¹, พิชญ์ ศุภผล^{2*} และ วรงค์ ปวรจารย์^{1**}

- 1) ภาควิชาวิศวกรรมเคมี คณะวิศวกรรมศาสตร์ จุฬาลงกรณ์มหาวิทยาลัย
- 2) ภาควิชาวิทยาศาสตร์พอลิเมอร์ วิทยาลัยปิโตรเลียมและปิโตรเคมี จุฬาลงกรณ์มหาวิทยาลัย

บทคัดย่อ

งานวิจัยนี้ศึกษาถึงผลของสภาวะการบ่มเส้นใยไททานเนียมที่มีขนาดอนุภาคอยู่ในระดับนาโนเมตรจากการสังเคราะห์ด้วยเทคนิคโซลเจลผสมผสานกับการปั่นเส้นใยด้วยไฟฟ้าสถิต โดยใช้สารละลายไททานเนียมเตตระไฮดรอกไซด์เป็นสารตั้งต้น สารผสมทั้งหมดจะถูกปั่นเป็นเส้นใยคอมโพสิทระหว่างไททานเนียมกับพอลิเมอร์ที่มีขนาดเส้นผ่านศูนย์กลางของเส้นใยในระดับนาโนเมตรด้วยวิธีอิเล็กโตรสปินนิง จากนั้นทำการบ่มเส้นใยที่สภาวะเวลาและความชื้นต่างๆ กัน และนำไปเผาที่อุณหภูมิ 500°C เป็นเวลา 3 ชม. จะได้เส้นใยไททานเนียมที่มีรูปผลึกปะปนระหว่างอนาเทสและรูไทล์ เส้นใยไททานเนียมที่สังเคราะห์ได้จะถูกนำไปวิเคราะห์ด้วยเทคนิค SEM, XRD และ TG-DTA ซึ่งผลจากการศึกษาพบว่า เส้นใยคอมโพสิทของไททานเนียมและพอลิเมอร์ที่ทำการบ่มด้วยสภาวะความชื้นสูง จะให้สัดส่วนของรูไทล์ค่อนข้างน้อย และพบว่าสัดส่วนของรูไทล์จะลดลงเมื่อทำการเพิ่มระยะเวลาการบ่ม นอกจากนี้การลดความหนาของชั้นเส้นใยจากกระบวนการอิเล็กโตรสปินนิงก็จะให้เส้นใยไททานเนียมที่มีสัดส่วนของรูไทล์ค่อนข้างน้อย โดยผลจากการศึกษานี้คาดว่าสามารถนำไปพัฒนาในการสังเคราะห์เส้นใยไททานเนียมที่สามารถควบคุมองค์ประกอบของเฟสเมื่ออุณหภูมิคงที่ได้ โดยเฉพาะเฟสอนาเทสซึ่งเหมาะกับการทำปฏิกิริยาแบบแสงร่วมได้เป็นอย่างดี

คำสำคัญ: ไททานเนียม, โซลเจล, คาร์บอนนาโนเช็น, อิเล็กโตรสปินนิง

1. บทนำ

ไททานเนียมไดออกไซด์ หรือ ไททานเนียม เป็นสารที่มีสมบัติที่ดีในการเป็นตัวเร่งปฏิกิริยา โดยเฉพาะอย่างยิ่ง ในปฏิกิริยาที่ใช้แสง (Photocatalytic reaction) ซึ่งการสังเคราะห์ตัวเร่งปฏิกิริยาเพื่อนำมาใช้ในงานในปัจจุบันนั้น จะต้องคำนึงถึงสมบัติทั้งในเชิงกายภาพ และเชิงเคมีของตัวเร่งปฏิกิริยาดังกล่าว โดยปัจจัยที่ทำให้ตัวเร่งปฏิกิริยามีความว่องไวมากขึ้นได้แก่ การมีขนาดผลึกในระดับนาโนเมตร เพื่อเพิ่มพื้นที่ผิวและเพิ่มสมบัติพิเศษบางอย่างให้กับตัวเร่งปฏิกิริยา ด้วยเหตุนี้การสังเคราะห์ไททานเนียมที่เป็นเส้นใยนาโนจึงได้ถูกพัฒนาขึ้น

การสังเคราะห์เส้นใยไททานเนียมขนาดนาโนสามารถทำได้จากหลายวิธี แต่วิธีที่นิยมและทำได้ง่ายที่สุดคือการอาศัยเทคนิคโซลเจล (Sol-gel process) ผสมผสานกับการปั่นเส้นใยด้วยไฟฟ้าสถิต (Electrospinning process) เพื่อสังเคราะห์เส้นใยคอมโพสิทระหว่างพอลิเมอร์กับวัสดุอนินทรีย์ (Inorganic material) จากนั้นจึงผ่านกระบวนการให้ความร้อนที่อุณหภูมิสูง เพื่อเปลี่ยนเส้นใยคอมโพสิทนี้ให้กลายเป็นเส้นใยเซรามิกของสารอนินทรีย์ (Ceramic nanofibers) เพียงอย่างเดียว [1-2] ซึ่งในปัจจุบันได้มีการนำวิธีดังกล่าวมาพัฒนาเพื่อสังเคราะห์เส้นใยไททานเนียมขนาดนาโนและสามารถประยุกต์ใช้กับงานได้จริง [3]

ในงานวิจัยนี้ได้ศึกษาผลของสภาวะในการบ่มเส้นใยที่มีผลต่อโครงสร้างของเส้นใยไททานเนียมขนาดนาโน รูปสัณฐานของผลึกที่เกิดขึ้น และพฤติกรรมการเปลี่ยนเฟสของไททานเนียมที่สังเคราะห์ได้ โดยทำการวิเคราะห์สมบัติเชิงกายภาพ และสัดส่วนรูปผลึกของเส้นใยนาโนที่สังเคราะห์ภายใต้สภาวะการบ่มที่แตกต่างกัน ซึ่งผลของการศึกษาใน

งานวิจัยนี้จะทำให้สามารถเลือกสังเคราะห์ไททานเนียมในเฟสที่ต้องการได้ดียิ่งขึ้น ทำให้สามารถประยุกต์ใช้เป็นตัวเร่งปฏิกิริยาในปฏิกิริยาที่ใช้แสง รวมไปถึงการผลิตเป็นเซลล์แสงอาทิตย์ที่มีประสิทธิภาพสูงในอนาคตได้

2. อุปกรณ์และวิธีการทดลอง

2.1 การเตรียมของเหลวสำหรับการบินเป็นเส้นใยด้วยเทคโนโซลเจล

การเตรียมของเหลวที่ใช้ในการปั่นให้เป็นเส้นใยนั้น เริ่มจากการผสมพอลิไวนิลไพโรลิโดน (PVP) ในเอทานอลในสัดส่วน 10% โดยน้ำหนัก แล้วจึงผสมเข้ากับสารละลายที่ประกอบด้วยไททานเนียมเตตระไฮดรอกไซด์ (TTIP) ในปริมาณ 1.5 กรัม กับกรดอะซิติกในเอทานอลในปริมาณ 3 และ 3 มิลลิกรัมตามลำดับ จากนั้นจึงทำการปั่นจนสารผสมทั้งสองเข้าด้วยกันเป็นเวลา 1 ชั่วโมง จะได้สารละลายเหลืองใสที่มีความหนืดพอสมควร

2.2 ขั้นตอนการสังเคราะห์เส้นใยนาโนโดยวิธี อิเล็กโตรสปินนิง

นำสารละลายที่ได้จากการเตรียมด้วยเทคนิคโซลเจล มาทำการปั่นลงในหลอดฉีดขนาด 5 มิลลิเมตรที่ต่อเข้ากับปลายเข็มโลหะ จากนั้นจึงทำการต่อหัวบวกรเข้ากับปลายเข็ม และใช้อะลูมิเนียมฟอยล์ที่ต่อเข้ากับมอเตอร์ความเร็วสูงเป็นแผ่นรองรับ โดยกำหนดให้ระยะห่างระหว่างหัวบวกรและแผ่นรองรับมีค่าประมาณ 7 เซนติเมตร จากนั้นทำการเพิ่มความต่างศักย์ไฟฟ้าระหว่างหัวบวกรกับแผ่นรองรับจนมีค่าเท่ากับ 16 กิโลโวลต์ จะได้เส้นใยออกมาจากปลายเข็มตกลงสู่แผ่นรองรับ จากนั้น

** corresponding author; fchvpv@eng.chula.ac.th

จะทำการคัดเลือกเส้นใยตามความหนาของชั้นเส้นใย และนำเส้นใยที่ได้ไปเผาไล่พอลิเมอร์ออกที่อุณหภูมิ 500 องศาเซลเซียส เป็นเวลา 3 ชม.

2.3 การศึกษาผลสภาวะการบ่มของเส้นใยโพลีเอทิลีนที่เตรียมได้จากวิธีโซลเจลและอิเล็กโตรสปินนิ่ง

เส้นใยโพลีเอทิลีนที่ได้จะถูกบ่มในสภาวะความชื้นต่างๆ ในห้องที่ควบคุมอุณหภูมิคงที่ประมาณ 27 °C โดยใช้ น้ำ, สารละลายอิมิตัวของโพแทสเซียมไนเตรต และสารละลายอิมิตัวของโซเดียมคลอไรด์ ในการควบคุมให้ความชื้นสัมพัทธ์ของระบบอยู่ที่ 100%, 90% และ 85% ตามลำดับ [4-5] จากนั้นทำการบ่มเส้นใยเป็นเวลาต่างๆ กัน แล้วนำเส้นใยที่ได้มาวิเคราะห์โดยใช้เทคนิคการกระเจิงรังสีเอ็กซ์ (X-ray diffraction, XRD) กล้องจุลทรรศน์อิเล็กตรอนแบบส่องกราด (Scanning electron microscopy, SEM) และการวิเคราะห์สมบัติทางความร้อน (Differential thermal and thermogravimetric analysis, DTA/TG) เพื่อค้นหาสาเหตุของเฟสที่เกิดขึ้นหลังการเผาเส้นใย, วิเคราะห์ลักษณะทางกายภาพของเส้นใย และหาค่าการเปลี่ยนแปลงเชิงพลังงานและน้ำหนักของเส้นใย

3.ผลการทดลองและวิจารณ์ผล

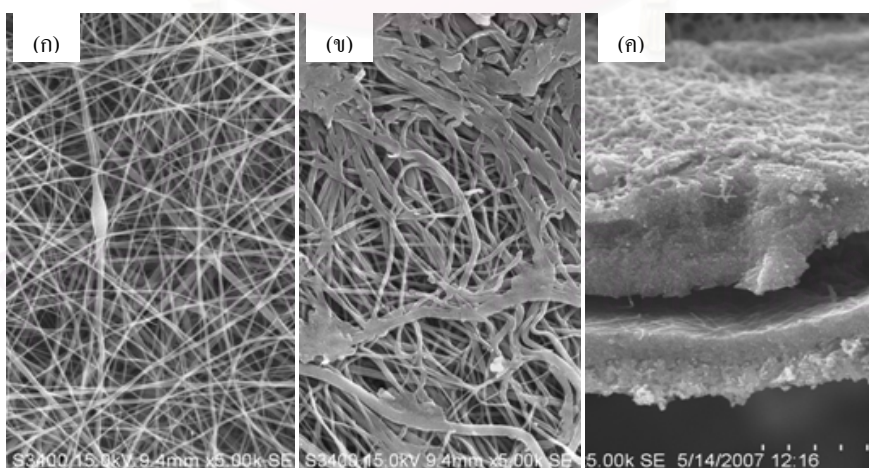
3.1 การวิเคราะห์สมบัติเชิงกายภาพของเส้นใยโพลีเอทิลีนด้วยเทคนิค SEM

เมื่อนำเส้นใยโพลีเอทิลีนที่มีรูปผลึกเป็นอสัณฐานมาทำการเผาที่อุณหภูมิ 500 องศาเซลเซียสเป็นเวลา 3 ชม. ผลจากการวิเคราะห์ด้วย SEM พบว่าเส้นใยที่ได้จะมีขนาดเล็กลดลงจาก 220-250 นาโนเมตร ไปเป็น 120-150 นาโนเมตร ดังแสดงในรูป (1ก) ซึ่งหากนำเส้นใยที่ได้จากการปั่นเส้นใยไปทำการบ่มในสภาวะความชื้นในน้ำก่อนการเผา จะพบว่าเส้นใยบางส่วนมีการรวมตัวกันทำให้ไม่อยู่ในสภาพของเส้นใยนาโนอีก

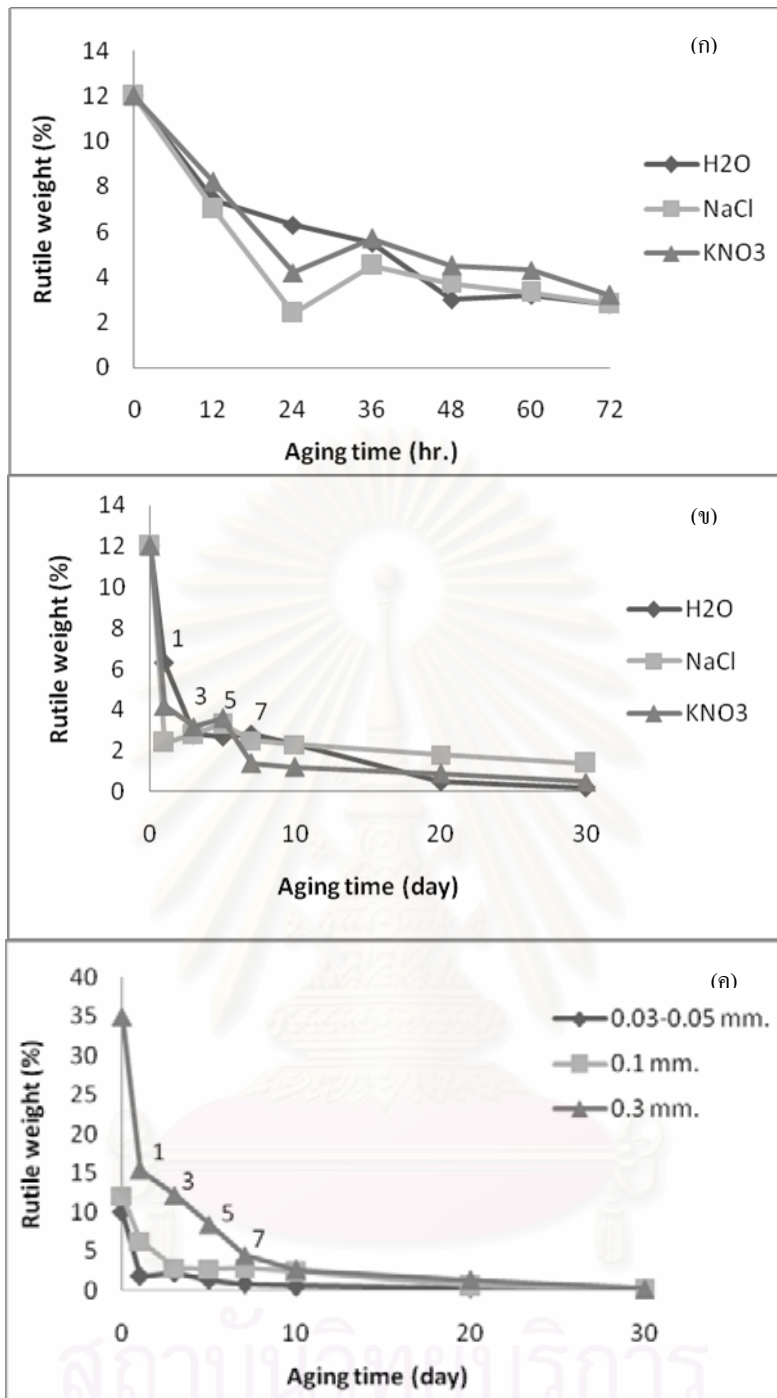
ต่อไปดังแสดงในรูป (1ข) และยังพบว่าการบ่มเส้นใยนั้นจะส่งผลต่อด้านนอกของชั้นเส้นใยเพียงเท่านั้น โดยจะเห็นว่าในบริเวณส่วนกลางของชั้นเส้นใยยังคงมีสภาพเป็นเส้นใยที่ยังไม่รวมตัวกันอยู่ ดังแสดงในรูป (1ค)

3.2 การวิเคราะห์หลักกษณะและสัดส่วนของรูปผลึกของเส้นใยโพลีเอทิลีนด้วยเทคนิค XRD

หลังจากนำเส้นใยที่ได้จากการปั่นเส้นใยไปทำการบ่มในสภาวะการบ่มต่างๆ ด้วยเวลาต่างๆ พบว่าเส้นใยโพลีเอทิลีนภายหลังจากการบ่มนั้นยังคงอยู่ในลักษณะเป็นผลึกอสัณฐาน (Amorphous) แต่เมื่อนำไปเผาที่อุณหภูมิ 500 องศาเซลเซียสเป็นเวลา 3 ชม. พบว่าเส้นใยจะอยู่ในรูปผลึกที่ปะปนกันระหว่างเฟสรูโพลีเอทิลีนและอนาเทส ซึ่งเมื่อวิเคราะห์หาสัดส่วนของเฟสรูโพลีเอทิลีนที่เกิดขึ้นด้วยเทคนิค XRD จะพบว่า การบ่มเส้นใยโพลีเอทิลีนในสภาวะที่แตกต่างกันจะส่งผลอย่างมากต่อสัดส่วนของเฟสรูโพลีเอทิลีนที่เกิดขึ้น โดยการบ่มเป็นระยะเวลา 3 วัน ในสภาวะความชื้นที่ต่างกัน จะให้สัดส่วนของเฟสรูโพลีเอทิลีนในผลึกกั้นที่หลังการเผาที่ใกล้เคียงกันดังรูป (2ก) และเมื่อเพิ่มเวลาการบ่มให้นานออกไปถึง 1 เดือนดังรูป (2ข) พบว่าสัดส่วนของเฟสรูโพลีเอทิลีนในผลึกกั้นที่นั้นลดลงเพียงเล็กน้อย โดยที่การบ่มในสภาวะความชื้นของอากาศที่ควบคุมด้วยน้ำ (ความชื้น 100%) กับในกรณีที่ควบคุมด้วยสารละลายอิมิตัวของโพแทสเซียมไนเตรต (ความชื้น 90%) จะให้ผลึกกั้นที่หลังการเผาที่เกือบเป็นอนาเทสบริสุทธิ์ (มีรูโพลีเอทิลีนเพียง 0.5%) โดยสำหรับชั้นเส้นใยที่ความหนาแตกต่างกันนั้น พบว่าจะให้ปริมาณผลึกรูโพลีเอทิลีนที่ไม่เท่ากัน โดยความหนาของชั้นเส้นใยที่มาก จะส่งผลให้เกิดรูโพลีเอทิลีนในปริมาณที่เพิ่มมากขึ้น อย่างไรก็ตามเมื่อทำการบ่มเส้นใยที่ความหนาแตกต่างกันเป็นเวลา 10 วัน ในสารละลายอิมิตัวทั้ง 3 ชนิดดังรูป (2ค) พบว่าจะให้ปริมาณรูโพลีเอทิลีนที่ใกล้เคียงกันคือต่ำกว่าร้อยละ 5



รูป 1 ภาพถ่ายจากเครื่อง SEM ของเส้นใยโพลีเอทิลีนหลังจากการเผาที่อุณหภูมิ 500 องศาเซลเซียส เป็นเวลา 3 ชม. (ก) เส้นใยที่ไม่ทำการบ่ม (ข) เส้นใยที่ทำการบ่มด้วยน้ำเป็นเวลา 7 วัน (ค) ภาพตัดของชั้นเส้นใยที่ทำการบ่มด้วยน้ำเป็นเวลา 7 วัน



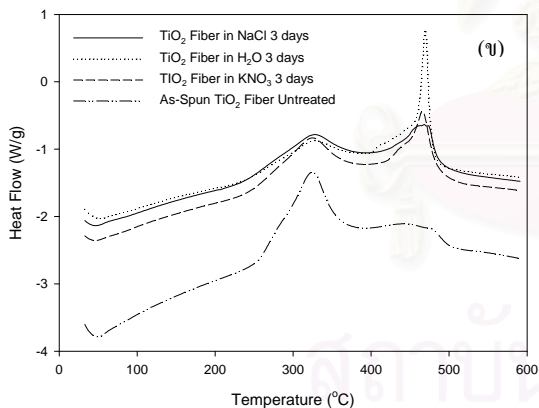
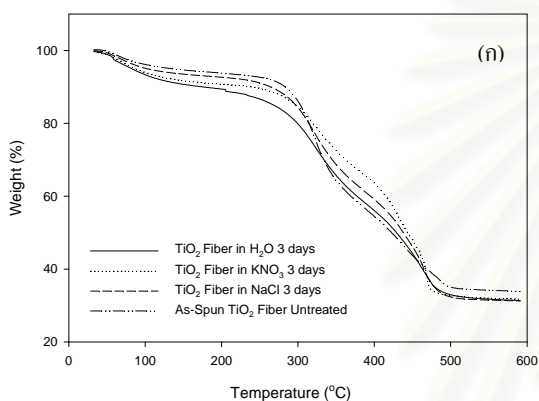
รูป 2 กราฟแสดงปริมาณของรูปผลึกรูไทล์ เมื่อนำเส้นใยไททาเนียไปบ่มในสภาวะแตกต่างกัน โดยที่ (ก) แสดงผลการบ่มเส้นใยนาน 3 วันสำหรับชั้นเส้นใยที่มีความหนาของที่ 0.1 มิลลิเมตร, (ข) แสดงผลการบ่มเส้นใยนาน 1 เดือนสำหรับชั้นเส้นใยที่มีความหนาของที่ 0.1 มิลลิเมตร, (ค) แสดงผลการบ่มเส้นใยในน้ำเป็นเวลา 1 เดือนสำหรับชั้นเส้นใยที่มีความหนา 0.03-0.05, 0.1 และ 0.3 มิลลิเมตรตามลำดับ

3.2 การศึกษาสมบัติเชิงความร้อนของเส้นใยไททาเนียด้วยเทคนิค TG-DTA

จากการวิเคราะห์สมบัติเชิงความร้อนด้วยเทคนิค TG-DTA ภายใต้การเผาด้วย O_2 ที่อุณหภูมิ $600^\circ C$ และใช้อัตราการเพิ่มอุณหภูมิที่ $10^\circ C/นาท$ จากรูปที่ (3ก) พบว่า เมื่อนำเส้นใยไททาเนียในสภาวะต่าง ๆ กัน ไปทำการเผาที่อุณหภูมิสูงจะมีแนวโน้มการลดลงของมวล

เป็นไปในทิศทางเดียวกัน โดยที่การลดลงในช่วงแรกของเส้นใยที่ทำการบ่มด้วยน้ำเป็นเวลา 3 วันจะมีการลดลงของมวลมากกว่าเส้นใยที่ทำการบ่มด้วย KNO_3 , $NaCl$ และ เส้นใยที่ไม่ได้การบ่ม ตามลำดับ ทั้งนี้อาจเกิดมาจากปริมาณของน้ำที่มีอยู่ภายในเส้นใยมีค่าไม่เท่ากันเนื่องจากสภาพความชื้นที่แตกต่างกัน รวมไปถึงการเปลี่ยนโครงสร้างของเส้นใยที่มีการรวมตัวกับพอลิเมอร์มากขึ้น แต่อย่างไรก็ตามเมื่อมีการกำจัด

พอลิเมอร์ออกไปด้วยกระบวนการคาร์บอนในเซชันพบว่าที่ อุณหภูมิ 500 °C จะมีการลดลงของมวลน้อยมาก เนื่องจากพอลิเมอร์ถูกกำจัดออกไป จากโครงสร้างของเส้นใย เหลือเพียงแต่เส้นใยไททาเนียในเฟสที่ปะปน ระหว่างอนาเทสและรูไทล์เพียงเท่านั้น และเมื่อวิเคราะห์เชิงพลังงานใน รูป (3ข) พบว่าเส้นใยไททาเนียมีช่วงการเกิดปฏิกิริยา 3 ช่วง ได้แก่ กระบวนการคาร์บอนในเซชัน, การเปลี่ยนเฟสจากรูปผลึกอสัณฐาน เป็นอนาเทส และการเปลี่ยนเฟสจากอนาเทสเป็นรูไทล์ ซึ่งเป็นปฏิกิริยา คายความร้อนทั้งสิ้น และพบว่าแนวโน้มของการเกิดปฏิกิริยาของเส้นใย ไททาเนียที่สภาวะแตกต่างกันนั้นจะเกิดที่อุณหภูมิใกล้เคียงกัน เพียงแต่ ค่าการคายพลังงานที่ได้นั้นแตกต่างกัน โดยพบว่าเส้นใยไททาเนียที่ผ่าน การบ่มด้วยน้ำจะมีการคายพลังงานค่อนข้างมากเลยทำให้เห็นตำแหน่ง การเกิดปฏิกิริยาได้อย่างชัดเจน



รูป 3 กราฟ TG-DTA ของเส้นใยไททาเนียความหนา 0.1 มิลลิเมตร ที่ทำ การบ่มในน้ำ, KNO₃ และ NaCl เป็นเวลา 3 วัน เทียบกับเส้นใยที่ยัง ไม่ได้ทำการบ่ม โดยที่ (ก) แสดงการลดลงของมวลต่ออุณหภูมิ (TG) (ข) แสดงการเปลี่ยนแปลงของพลังงานต่ออุณหภูมิ (DTA)

4. สรุปผลการทดลอง

การศึกษาปัจจัยของสภาวะการบ่มเส้นใยไททาเนียขนาดนาโน ทำให้ทราบถึงสัดส่วนของเฟสรูไทล์ต่ออนาเทสในผลิตภัณฑ์ที่ แตกต่างกัน โดยพบว่า เมื่อเส้นใยไททาเนียถูกเผาด้วยอุณหภูมิคงที่ที่ 500 องศาเซลเซียส จะได้สัดส่วนของเฟสต่างกัน ตามสภาวะการบ่ม เส้นใยก่อนการเผา โดยเส้นใยที่ทำการบ่มที่ความชื้นต่างกันจะให้ผลที่ ใกล้เคียงกัน การบ่มโดยใช้น้ำเป็นสารควบคุมความชื้นจะให้สัดส่วน ของเฟสรูไทล์ที่น้อยที่สุด แต่จะทำให้ลักษณะทางกายภาพของเส้นใย เปลี่ยนไป นอกจากนี้ยังพบว่าผลของความหนาชั้นเส้นใยยังมีผล ค่อนข้างมาก กล่าวคือ จะต้องใช้เวลานานในการบ่มมากขึ้นเมื่อความหนา ของชั้นเส้นใยมีค่ามากขึ้นเพื่อให้ได้รูปผลึกอนาเทสมากที่สุด ผลสรุปที่ ได้นี้คาดว่าน่าจะนำไปประยุกต์ใช้ในการสังเคราะห์เส้นใยไททาเนีย ขนาดนาโนที่มีรูปผลึกส่วนใหญ่เป็นอนาเทสในสัดส่วนที่สามารถ ควบคุมได้ ดังนั้นจึงเป็นประโยชน์อย่างยิ่งในการใช้เป็นตัวเร่งปฏิกิริยา ในปฏิกิริยาที่ใช้แสง หากแต่ต้องมีการศึกษาต่อไปในอนาคต

5. เอกสารอ้างอิง

- [1] Watthanarun J., Pavarajarn V. and Supaphol P., Titanium (IV) oxide nanofibers by combined sol-gel and electrospinning techniques: preliminary report on effects of preparation conditions and secondary metal dopant, *Science and Technology of Advanced Materials.*, 2005; **6(3-4)**: 240-245.
- [2] Nuansing W., Ninmuang S., Jarernboon W., Maensiri S. and Seraphin S., Structural characterization and morphology of electrospun TiO₂ nanofibers., *Material Science and Engineering B.*, 2006; **131**: 147-155
- [3] Li, D. and Xia, Y., Electrospinning of Nanofibers: Reinventing the Wheel?, *Advanced Materials.*, 2004; **16(14)**: 1151-1170.
- [4] Astrup Eva E. and Kristin E. Hovin Stub., Saturated Salt Solutions for Humidity Control of Showcases Conditions for a Successful System, *ICOM Committee for Cons., 8th Triennial Mtg*, 1994.
- [5] Vertucci C.W., Roos, E.E., Theoretical basis of protocols for seed storage II. The influence of temperature on optimal moisture levels., *Seed Science Research.*, 1993; **3**: 201-213.

VITA

Mr. Jaturon Supapol was born on October 7, 1983 in Samutsakorn, Thailand. He received the Bachelor Degree of Chemical Engineering from Faculty of Engineering, Chulalongkorn University in 2006. He continued his Master's study at Chulalongkorn University in June, 2006.



สถาบันวิทยบริการ
จุฬาลงกรณ์มหาวิทยาลัย